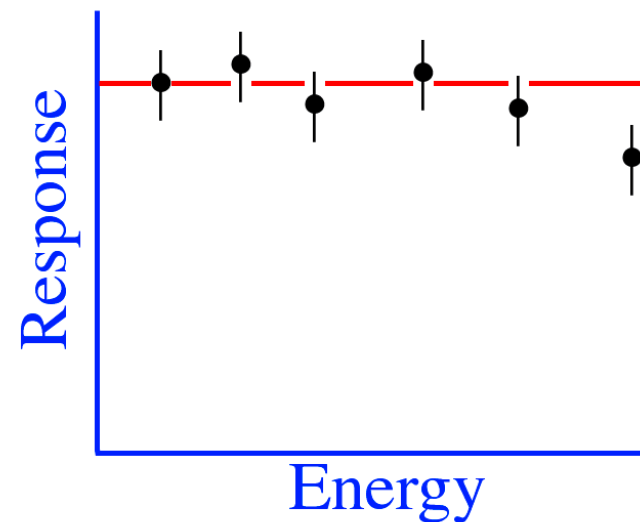
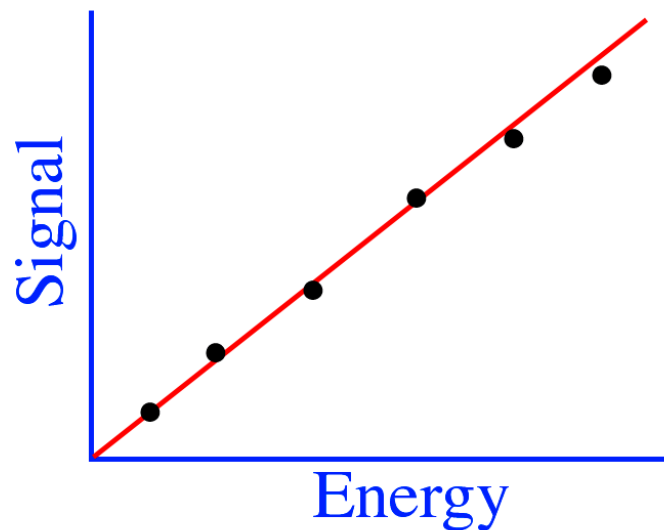


# The Calorimeter Response Function

*Response* = Average signal per unit of deposited energy

e.g. # photoelectrons/GeV, picoCoulombs/MeV, etc.

→ A *linear* calorimeter has a *constant response*



*Electromagnetic* calorimeters are in general *linear*

All energy deposited through ionization/excitation of absorber  
If *not* linear → instrumental effect (saturation, leakage,.....)

# Signal linearity for electromagnetic showers

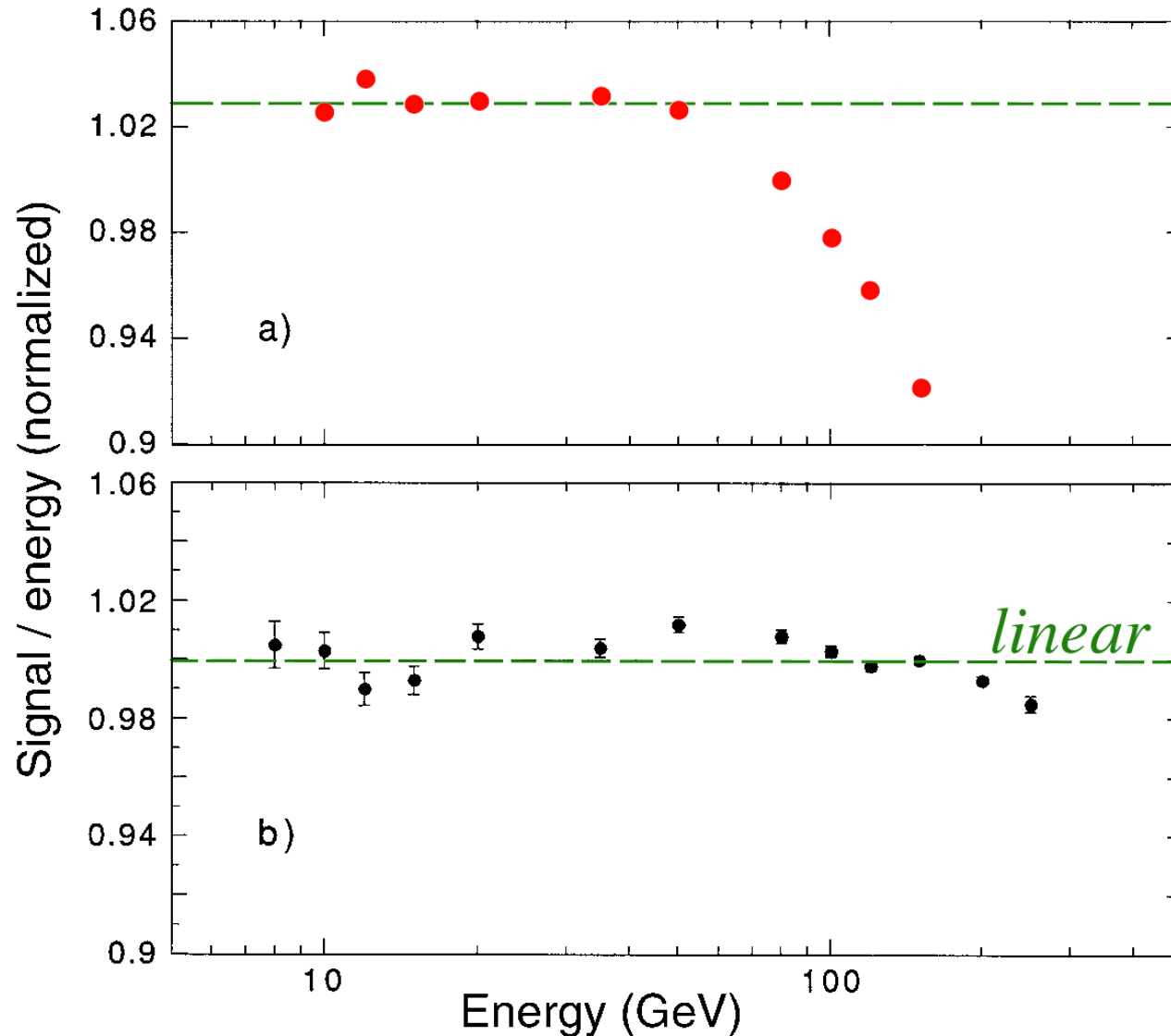


FIG. 3.1. The em calorimeter response as a function of energy, measured with the QFCAL calorimeter, before (a) and after (b) precautions were taken against PMT saturation effects. Data from [Akc 97].

# Saturation in "digital" calorimeters (wire chamber readout)

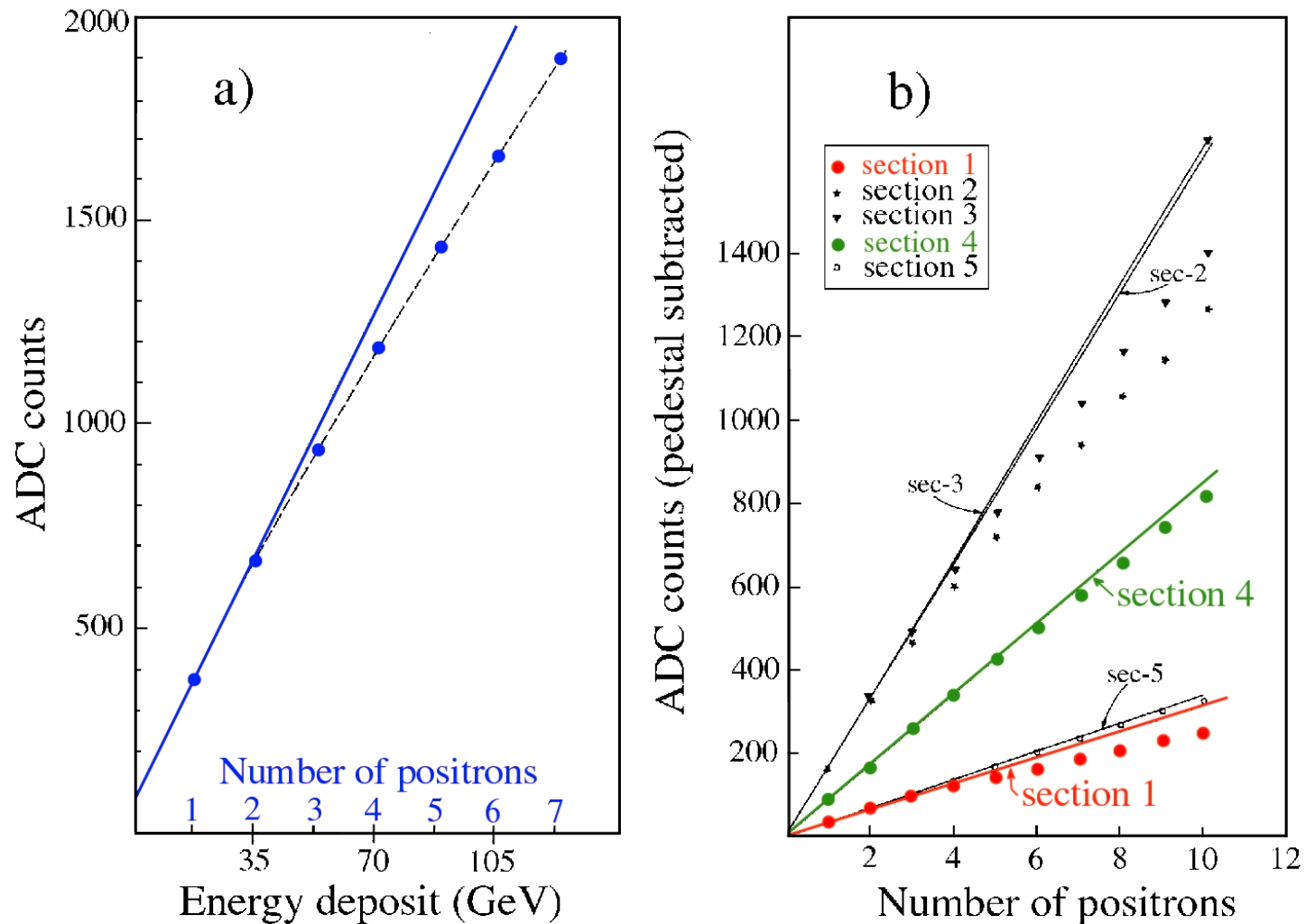


FIG. 3.2. Average em shower signal from a calorimeter read out with gas chambers operating in a "saturated avalanche" mode, as a function of energy. From: NIM 205 (1983) 113.

# Fluctuations due to instrumental effects (readout)

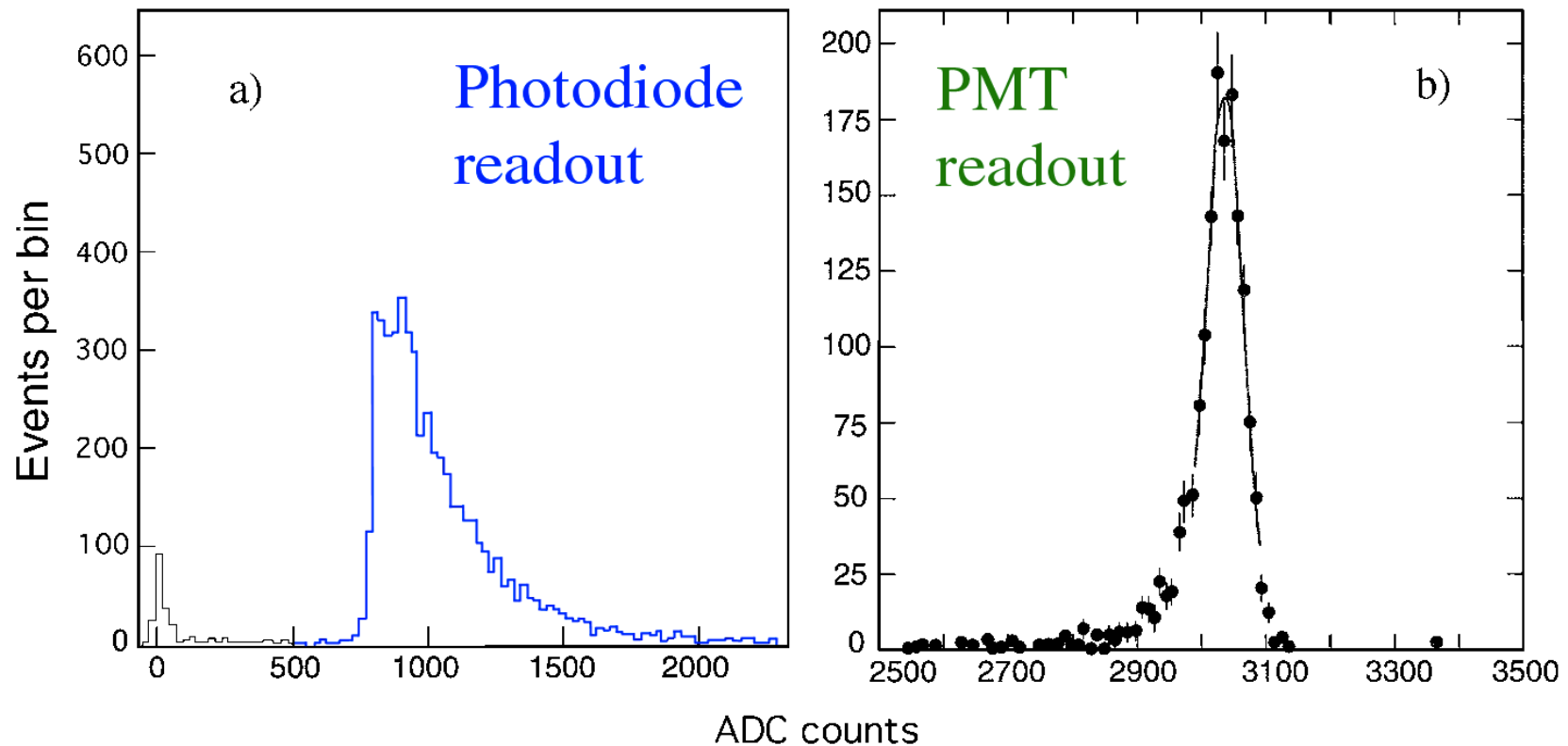


FIG. 3.3. Signal distributions for high-energy electron showers measured with a prototype  $\text{PbWO}_4$  crystal calorimeter. The calorimeter was read out either with silicon photodiodes (a) or with photomultiplier tubes (b). Data from [Pei 96].

# Sampling

- There are *homogeneous* and *sampling* calorimeters
  - Homogeneous: Absorber and active medium are the same
  - Sampling: Only part of shower energy deposited in active medium

$$\textit{Sampling fraction} (f_{\text{samp}}) = \frac{\text{energy deposited in active medium}}{\text{total energy deposited in calorimeter}}$$

- $f_{\text{samp}}$  is usually determined with a *mip* ( $dE/dx$  minimum)

N.B. *mip*'s do not exist!

*e.g.* D0 (em section):

$$\left. \begin{array}{l} 3 \text{ mm } ^{238}\text{U} \quad (dE/dx = 61.5 \text{ MeV/layer}) \\ 2 \times 2.3 \text{ mm LAr} \quad (dE/dx = 9.8 \text{ MeV/layer}) \end{array} \right\} \rightarrow f_{\text{samp}} = 13.7\%$$

# The $e/mip$ ratio

- D0:  $f_{\text{samp}} = 13.7\%$

However, for em showers, sampling fraction is only 8.2%

→  $e/mip \approx 0.6$

- $e/mip$  is a function of *shower depth*, in U/Lar it *decreases*  
 $e/mip$  increases when the *sampling frequency* becomes very high  
What is going on?

- *Photoelectric effect*:  $\sigma \propto Z^5$ ,  $(18/92)^5 = 3 \cdot 10^{-4}$

→ Soft  $\gamma$ s are very inefficiently sampled

Effects strongest at high  $Z$ , and late in the shower development

The range of the photoelectrons is typically  $< 1$  mm

→ if absorber layers are thin, they may contribute to the signals

# Sampling calorimeters: The $e/mip$ signal ratio

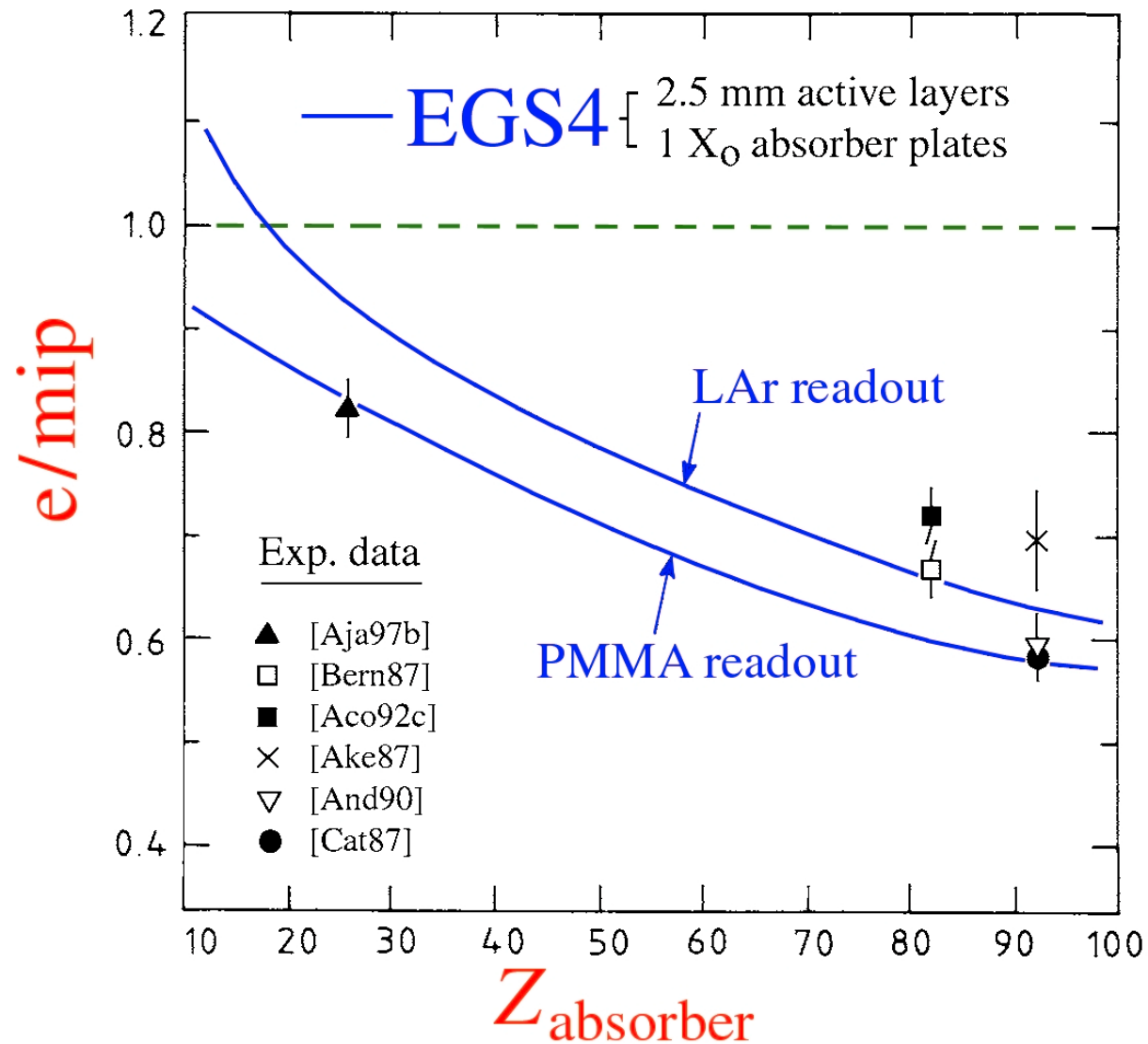


FIG. 3.7. The  $e/mip$  ratio for sampling calorimeters as a function of the  $Z$  value of the absorber material, for calorimeters with plastic scintillator or liquid argon as active material. Experimental data are compared with results of EGS4 Monte Carlo simulations [Wig 87].

# The EM sampling fraction changes with depth!

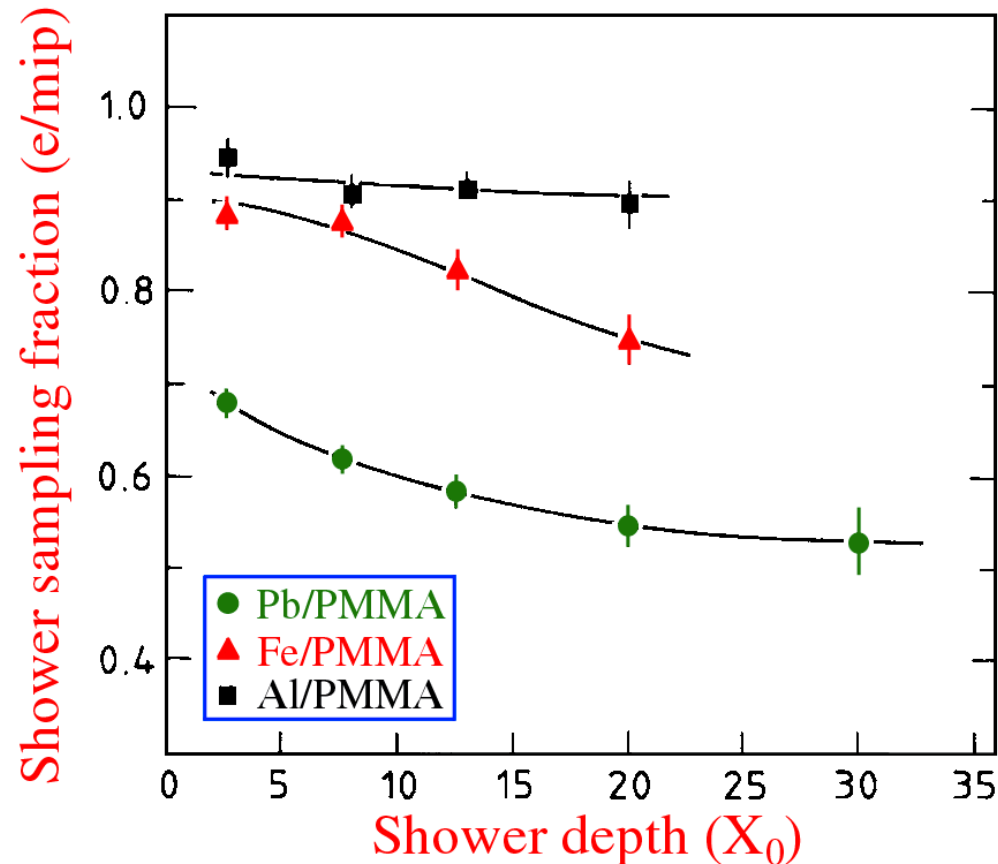


FIG. 3.8. The  $e/mip$  ratio as a function of the shower depth, or age, for 1 GeV electrons in various sampling calorimeter configurations. All calorimeters consist of 1  $X_0$  thick absorber layers, interleaved with 2.5 mm thick PMMA layers. Results from EGS4 Monte Carlo simulations [Wig 87].



# The $e/mip$ ratio: Dependence on calorimeter parameters

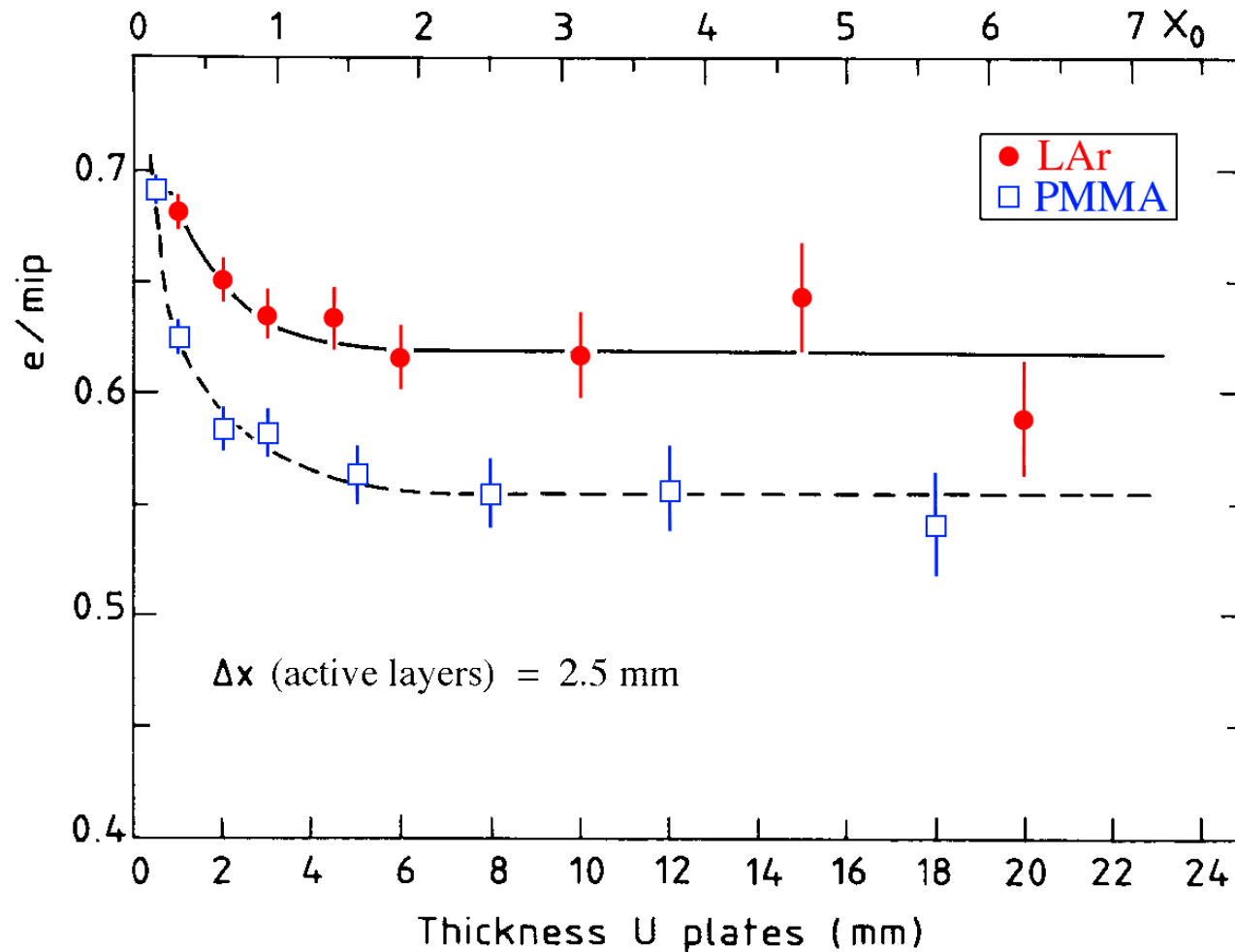


FIG. 3.9. The  $e/mip$  ratio as a function of the thickness of the absorber layers, for uranium/PMMA and uranium/LAr calorimeters. The thickness of the active layers is 2.5 mm in all cases. Results from EGS4 Monte Carlo simulations [Wig 87].

# Hadronic shower response and the $e/h$ ratio

- *The hadronic response is **not constant***

$f_{\text{em}}$ , and therefore  $e/\pi$  signal ratio is a function of energy

→ If calorimeter is linear for electrons, it is *non-linear* for hadrons

- Energy-independent way to characterize hadron calorimeters:  $e/h$

$e$  = response to the em shower component

$h$  = response to the non-em shower component

→ Response to showers initiated by pions:

$$R_{\pi} = f_{\text{em}} e + [1 - f_{\text{em}}]h \quad \rightarrow \quad e/\pi = \frac{e/h}{1 - f_{\text{em}}[1 - e/h]}$$

$e/h$  is inferred from  $e/\pi$  measured at several energies ( $f_{\text{em}}$  values)

- Calorimeters can be
  - Undercompensating* ( $e/h > 1$ )
  - Overcompensating* ( $e/h < 1$ )
  - Compensating* ( $e/h = 1$ )

# Hadron showers: Energy dependence em component

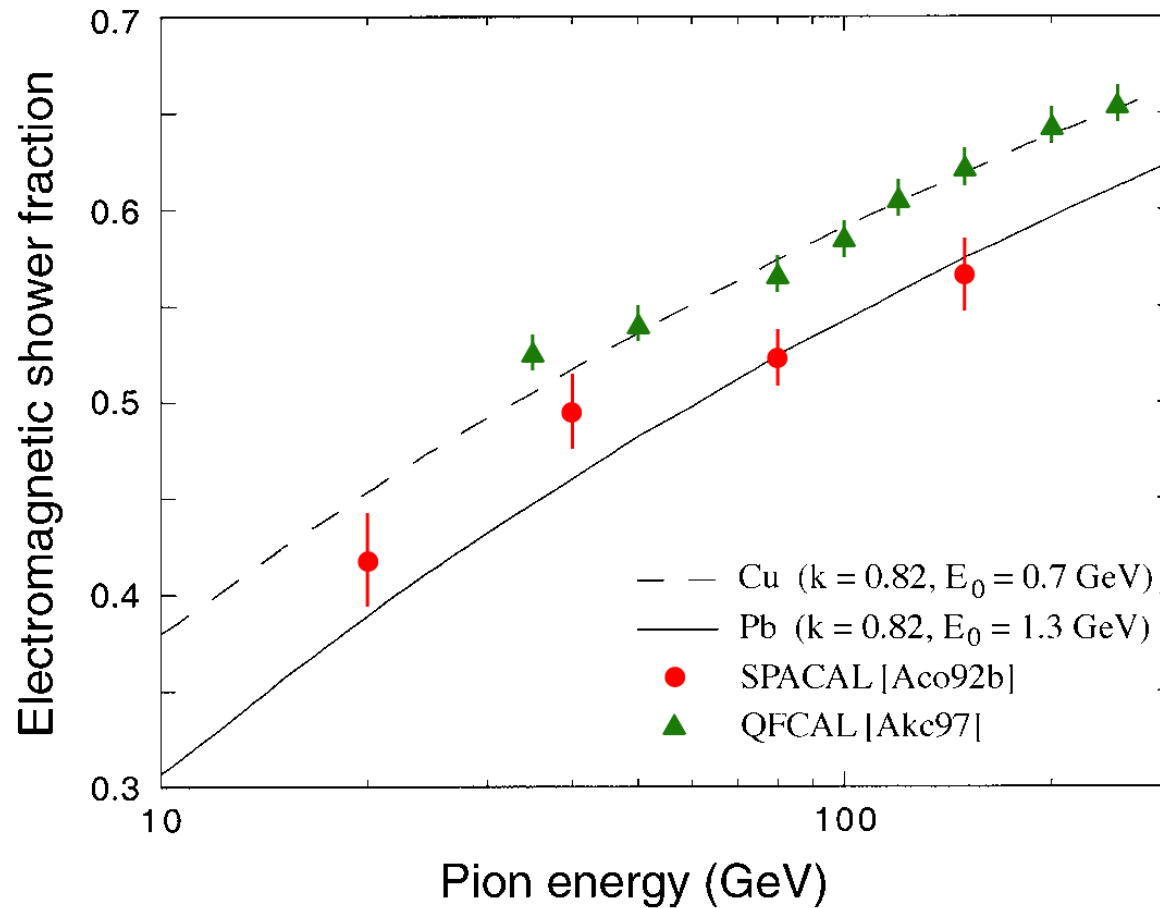


FIG. 2.22. Comparison between the experimental results on the em fraction of pion-induced showers in the (copper-based) QFCAL and (lead-based) SPACAL detectors. Data from [Akc 97] and [Aco 92b].

# Hadron showers: $e/h$ and the $e/\pi$ signal ratio

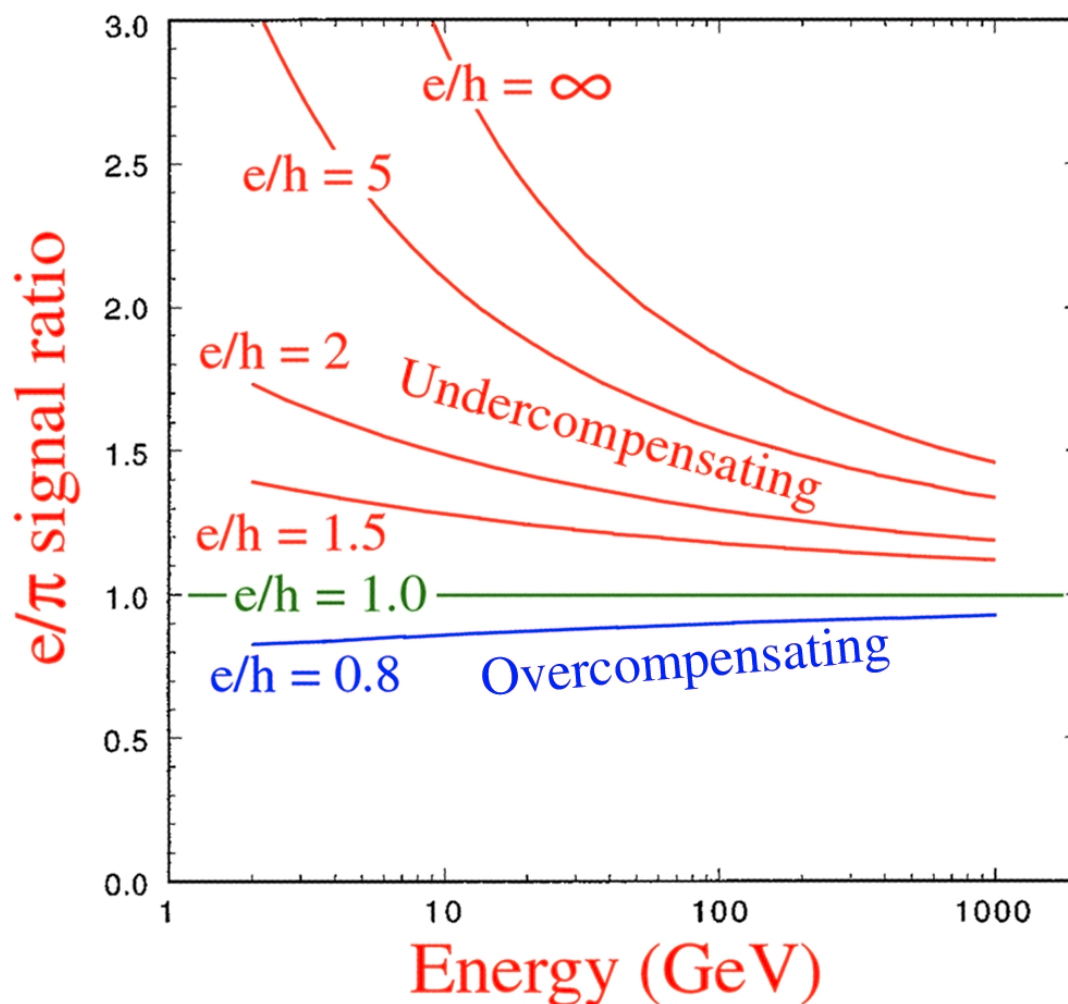


FIG. 3.4. The relation between the calorimeter response ratio to em and non-em energy deposition,  $e/h$ , and the measured  $e/\pi$  signal ratios. See text for details.

# Hadronic signal (non-)linearity: Dependence on $e/h$

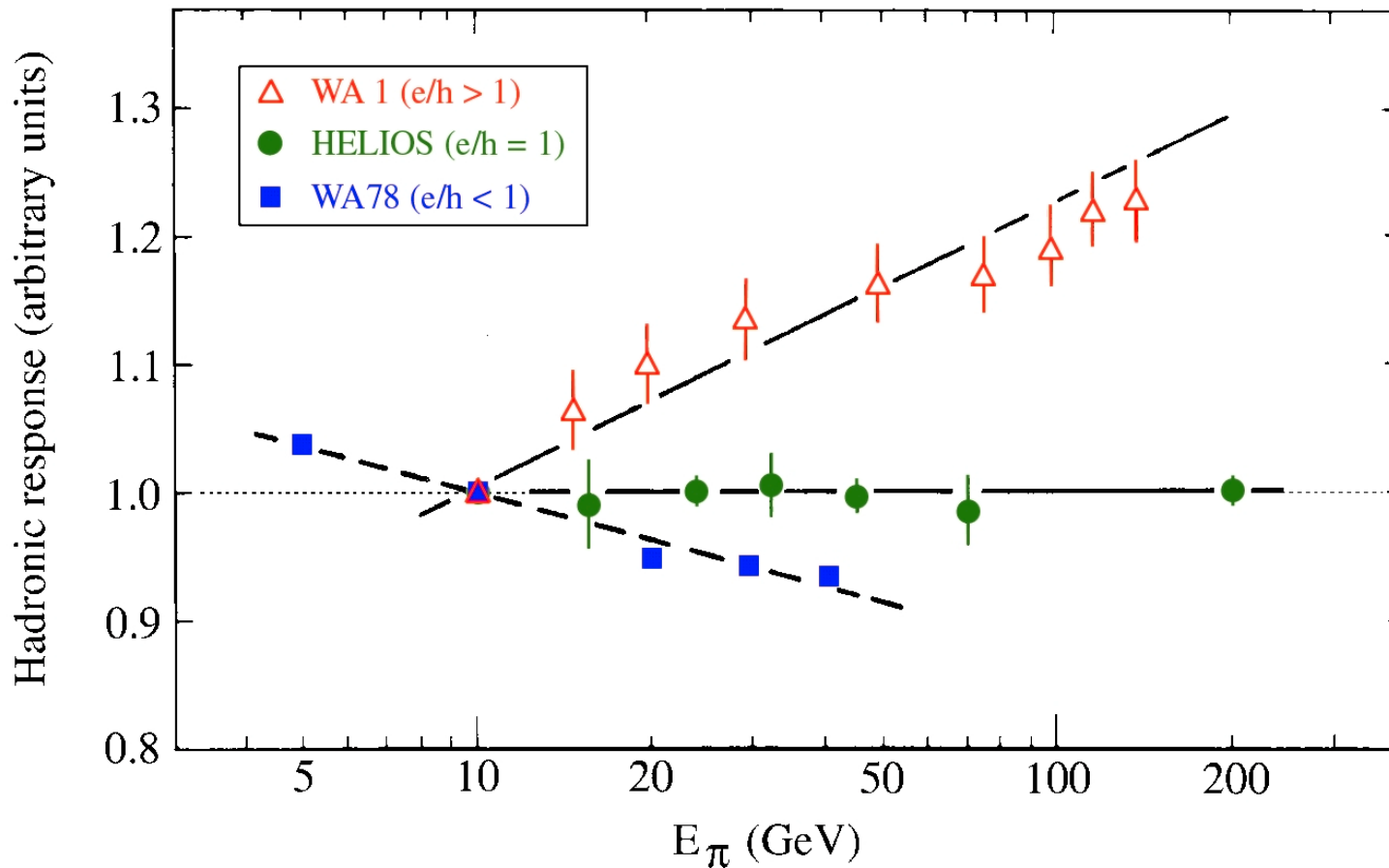


FIG. 3.14. The response to pions as a function of energy for three calorimeters with different  $e/h$  values: the WA1 calorimeter ( $e/h > 1$ , [Abr 81]), the HELIOS calorimeter ( $e/h \approx 1$ , [Ake 87]) and the WA78 calorimeter ( $e/h < 1$ , [Dev 86, Cat 87]). All data are normalized to the results for 10 GeV.

# Compensation (1)

Need to understand response to typical shower particles (relative to *mip*)

*Spallation protons* and *Neutrons*

- *Spallation protons*
  - More efficient sampling
  - Signal saturation

# Aspects of compensation: Sampling of soft shower protons

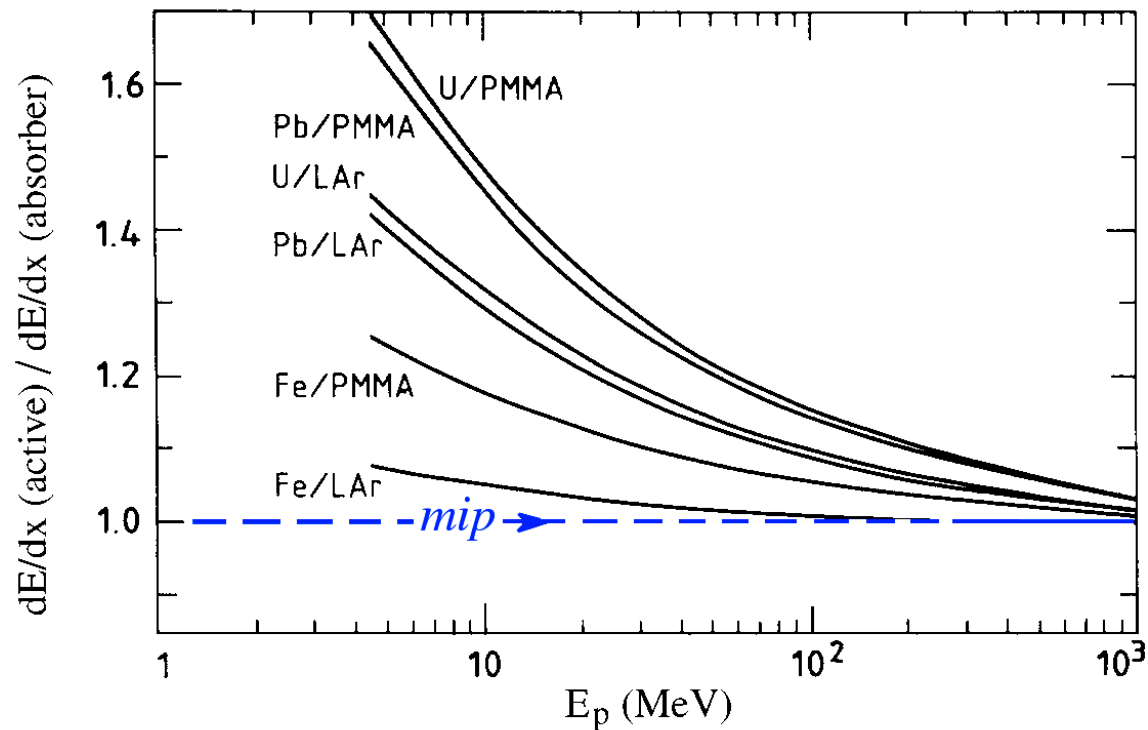


FIG. 3.15. The ratio of energy deposition by non-relativistic protons in the active and passive materials of various calorimeter structures, as a function of the proton's kinetic energy. This ratio is normalized to the one for mips. From [Wig 87].

# Aspects of compensation: Saturation effects

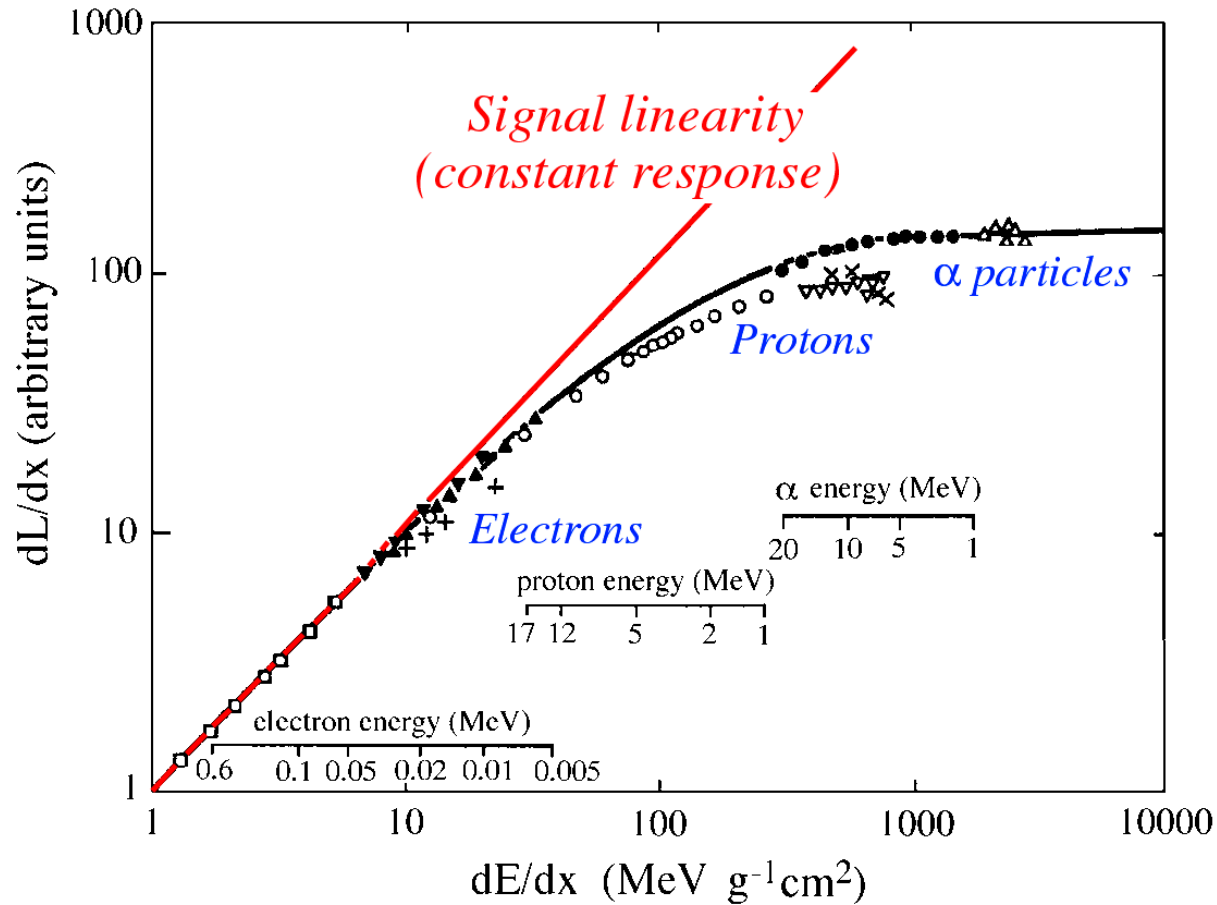


FIG. 3.25. Variation of the specific fluorescence,  $dL/dx$ , with the specific ionization loss,  $dE/dx$ , in anthracene crystals. The solid curve represents Equation 3.13 with  $k_B = 6.6 \text{ mg cm}^{-2} \text{ MeV}^{-1}$ .



# Compensation: The spallation proton/mip signal ratio

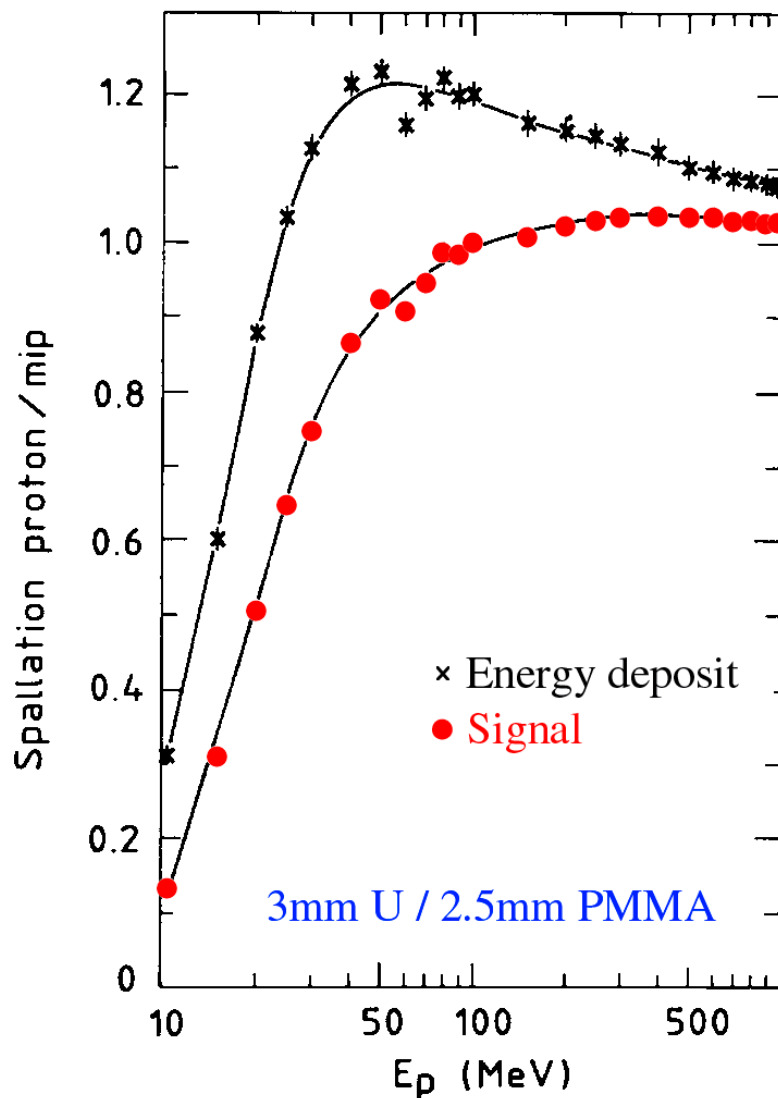



FIG. 3.16. The energy deposit in the active layers (upper curve) and the calorimeter signal (lower curve) for stopping protons, relative to mips, as a function of the kinetic proton energy, in a 3 mm U/2.5 mm PMMA sampling calorimeter. See text for details. Results from Monte Carlo simulations [Wig 87].

## Compensation (2)

Need to understand response to typical shower particles (relative to *mip*)

### *Spallation protons* and *Neutrons*

- *Neutrons*

- $(n, n'\gamma)$  *inelastic* scattering: not very important
- $(n, n')$  *elastic* scattering: most interesting 
- $(n, \gamma)$  *capture* (thermal): lots of energy, but process is slow ( $\mu\text{s}$ )

# Compensation (3) – The role of neutrons

- **Elastic scattering**  $f_{\text{elastic}} = 2A/(A + 1)^2$   
Hydrogen  $f_{\text{elastic}} = 0.5$ , Lead  $f_{\text{elastic}} = 0.005$   
Pb/H<sub>2</sub> calorimeter structure (50/50)  
1 MeV  $n$  deposits 98.3% in H<sub>2</sub>  
 $mip$  deposits 2.2% in H<sub>2</sub>  $\left. \vphantom{\begin{array}{l} 1 \text{ MeV } n \text{ deposits } 98.3\% \text{ in H}_2 \\ mip \text{ deposits } 2.2\% \text{ in H}_2 \end{array}} \right\} \rightarrow n/mip = 45$
- **Recoil protons can be measured!**  
→ Neutrons have an enormous potential to amplify hadronic shower signals, and thus **compensate** for losses in invisible energy
- **Tune the  $e/h$  value through the sampling fraction!**  
*e.g.* 90% Pb/10% H<sub>2</sub> calorimeter structure  
1 MeV  $n$  deposits 86.6% in H<sub>2</sub>  
 $mip$  deposits 0.25% in H<sub>2</sub>  $\left. \vphantom{\begin{array}{l} 1 \text{ MeV } n \text{ deposits } 86.6\% \text{ in H}_2 \\ mip \text{ deposits } 0.25\% \text{ in H}_2 \end{array}} \right\} \rightarrow n/mip = 350$

# Compensation in a Uranium/gas calorimeter

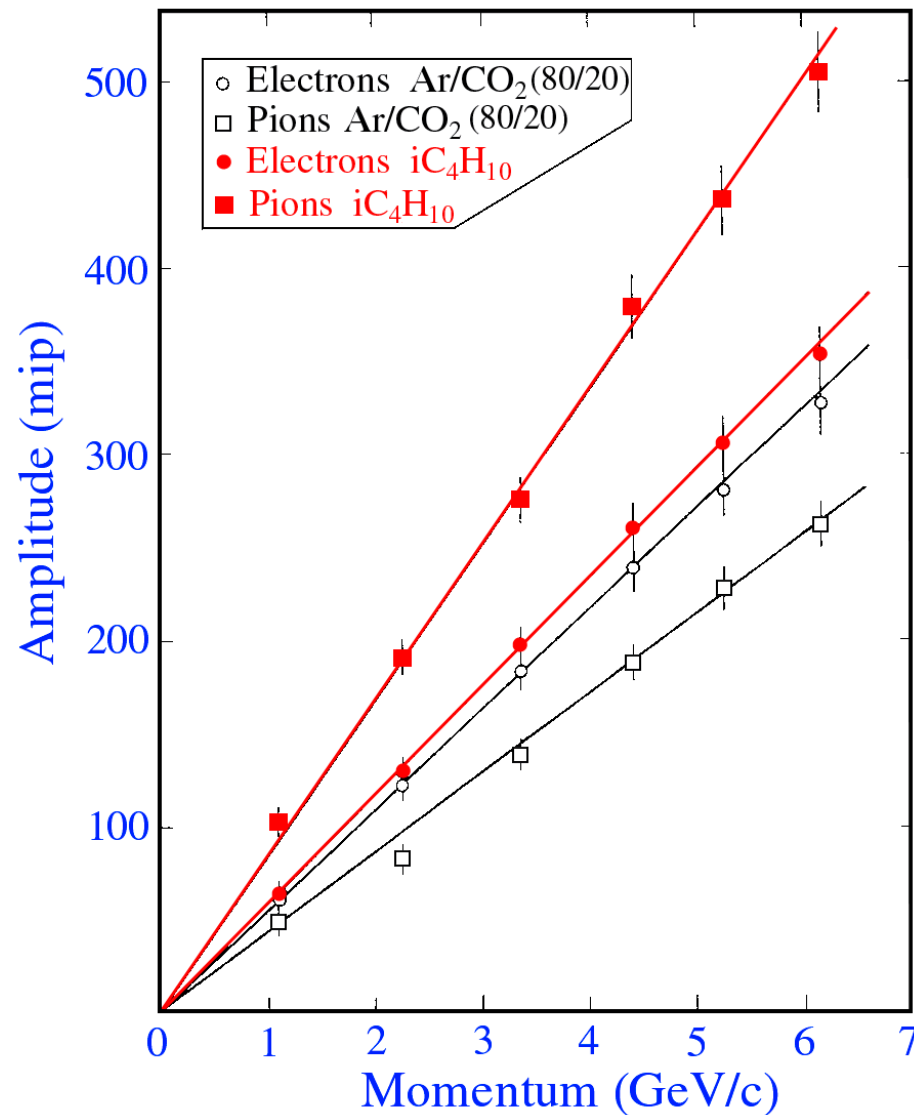


FIG. 3.31. The average signals for electrons and pions, measured with the uranium/gas calorimeter of the L3 Collaboration, for two different choices of gas with which the proportional wire chambers were operated. From: NIM A251 (1986) 258.

# Compensation: The importance of soft neutrons

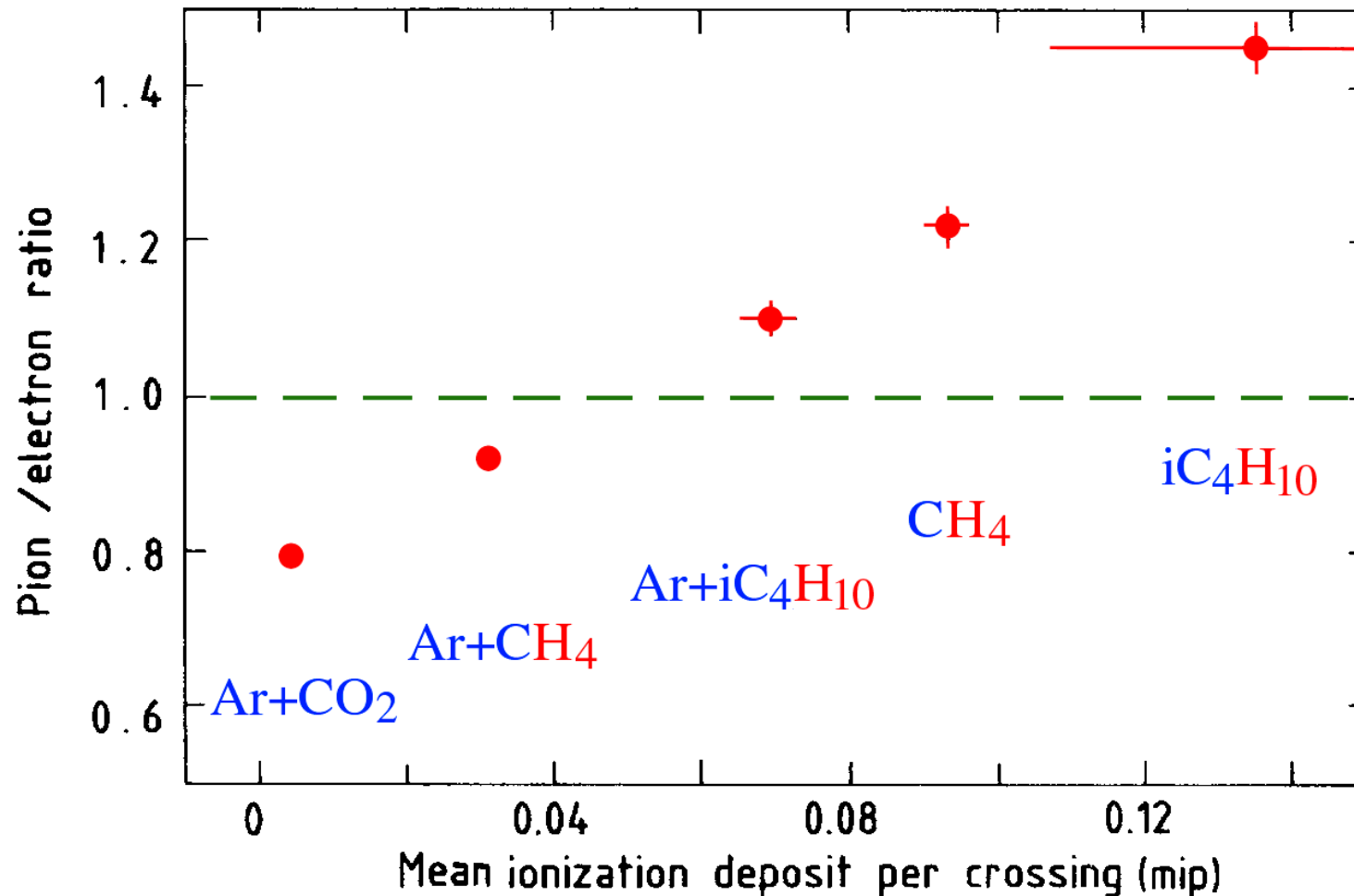


FIG. 3.32. The pion/electron signal ratio, averaged over the energy range 1.5 GeV, measured for different gas mixtures with the uranium/gas calorimeter of the L3 Collaboration. The horizontal scale gives the (calculated) average energy deposit in a chamber gap by slow neutrons [Gal 86].

# Compensation (3) – The role of neutrons

- **Elastic scattering**  $f_{\text{elastic}} = 2A/(A + 1)^2$   
Hydrogen  $f_{\text{elastic}} = 0.5$ , Lead  $f_{\text{elastic}} = 0.005$   
Pb/H<sub>2</sub> calorimeter structure (50/50)  
1 MeV  $n$  deposits 98.3% in H<sub>2</sub>  
 $mip$  deposits 2.2% in H<sub>2</sub>  $\rightarrow n/mip = 45$
- **Recoil protons can be measured!**  
→ Neutrons have an enormous potential to amplify hadronic shower signals, and thus **compensate** for losses in invisible energy
- **Tune the  $e/h$  value through the sampling fraction!**  
*e.g.* 90% Pb/10% H<sub>2</sub> calorimeter structure  
1 MeV  $n$  deposits 86.6% in H<sub>2</sub>  
 $mip$  deposits 0.25% in H<sub>2</sub>  $\rightarrow n/mip = 350$

# Compensation: The crucial role of the sampling fraction

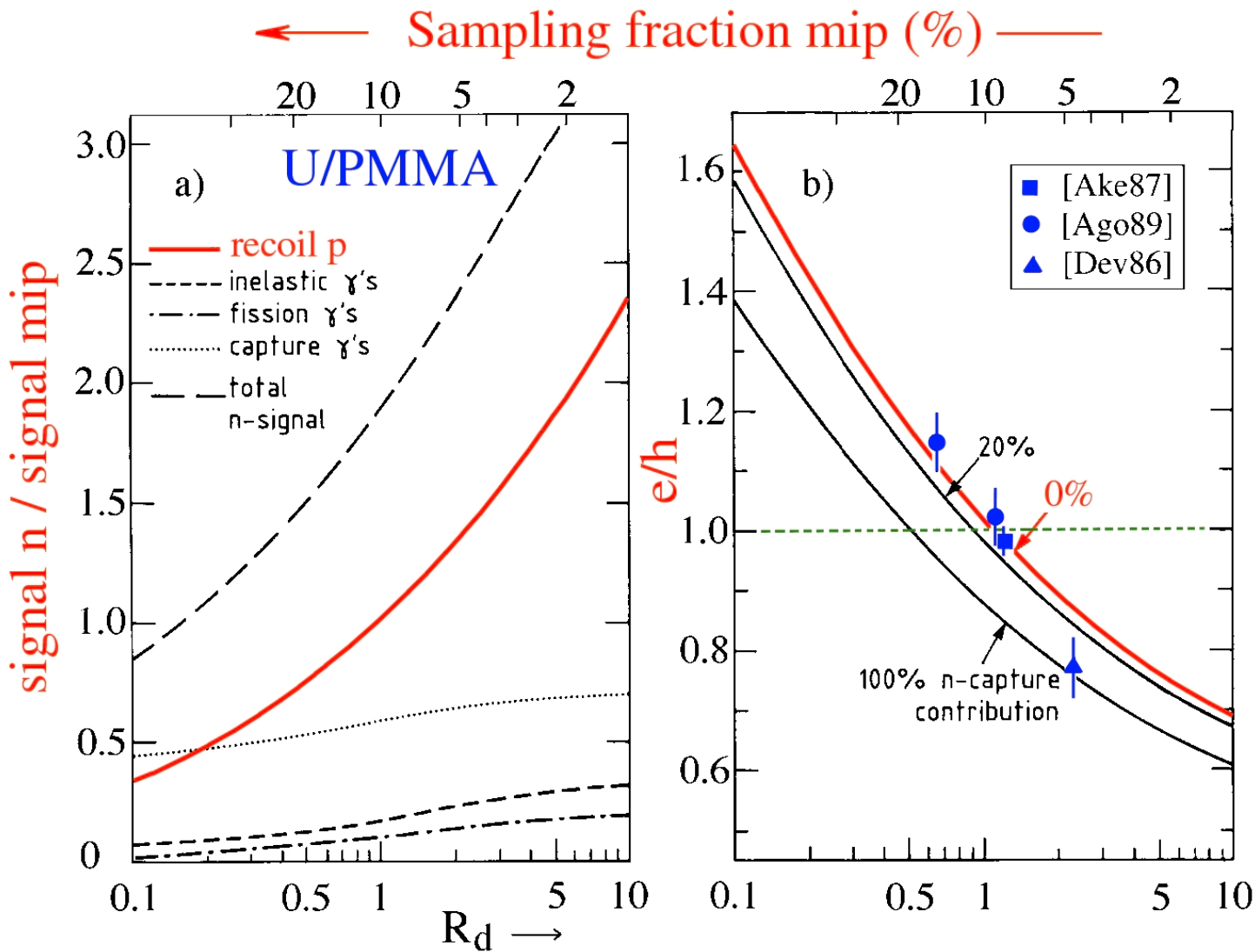


FIG. 3.33. The  $n/mip$  response ratio, split up into its components, for  $^{238}\text{U}/\text{PMMA}$  calorimeters, as a function of  $R_d$ , the ratio of the thicknesses of the passive and active calorimeter layers (a). The  $e/h$  ratio as a function of  $R_d$ , assuming that 0%, 20% or 100% of the  $\gamma$ s released in thermal neutron capture contribute to the calorimeter signals (b). The top axis of both graphs indicates the sampling fraction for mips. From [Wig 88].

# Compensation in practice: Pb/scintillator calorimeters

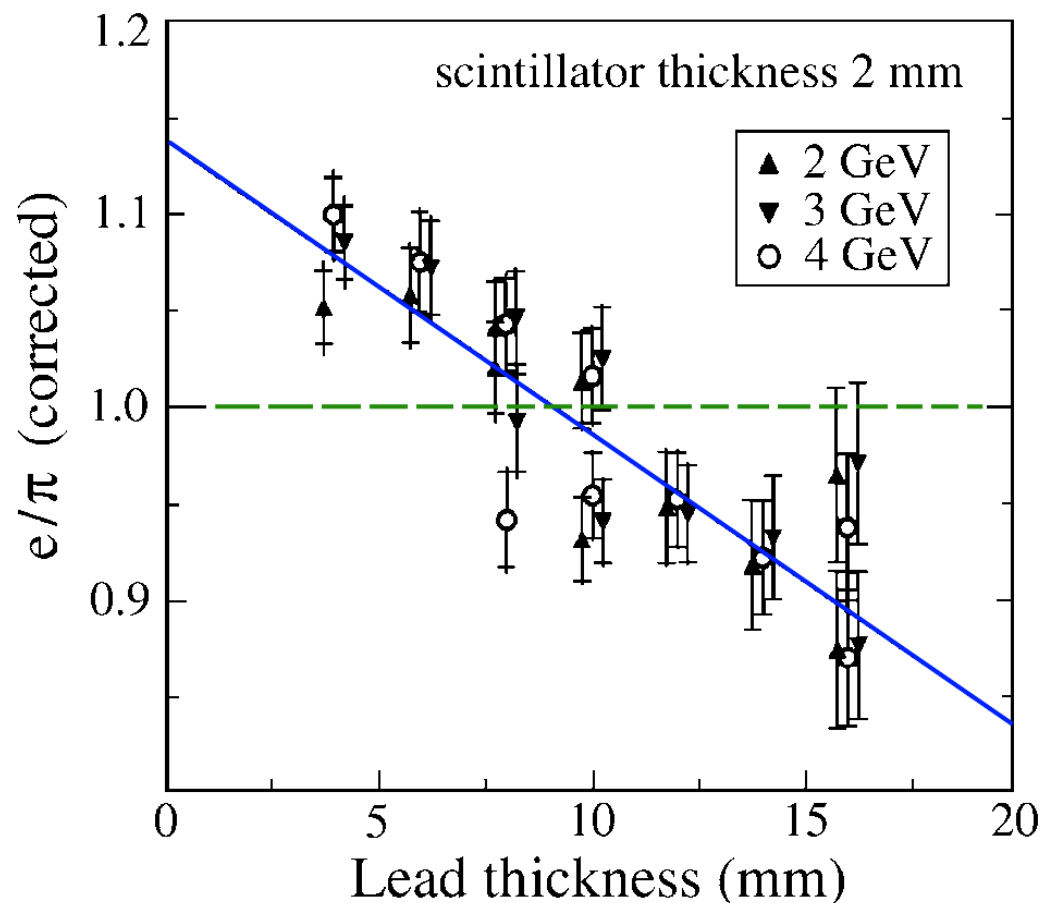


FIG. 3.35. The  $e/\pi$  signal ratio, corrected for the effects of shower leakage, for lead/polystyrene-scintillator calorimeters, as a function of the thickness of the lead plates, for 2 mm thick scintillator plates. The inner (outer) error bars show the combined systematic and statistical uncertainty without (with) the shower leakage corrections. The line in the plot is a result of a linear fit to the experimental data [Suz 99].



# Compensation in Fe/scintillator calorimeters?

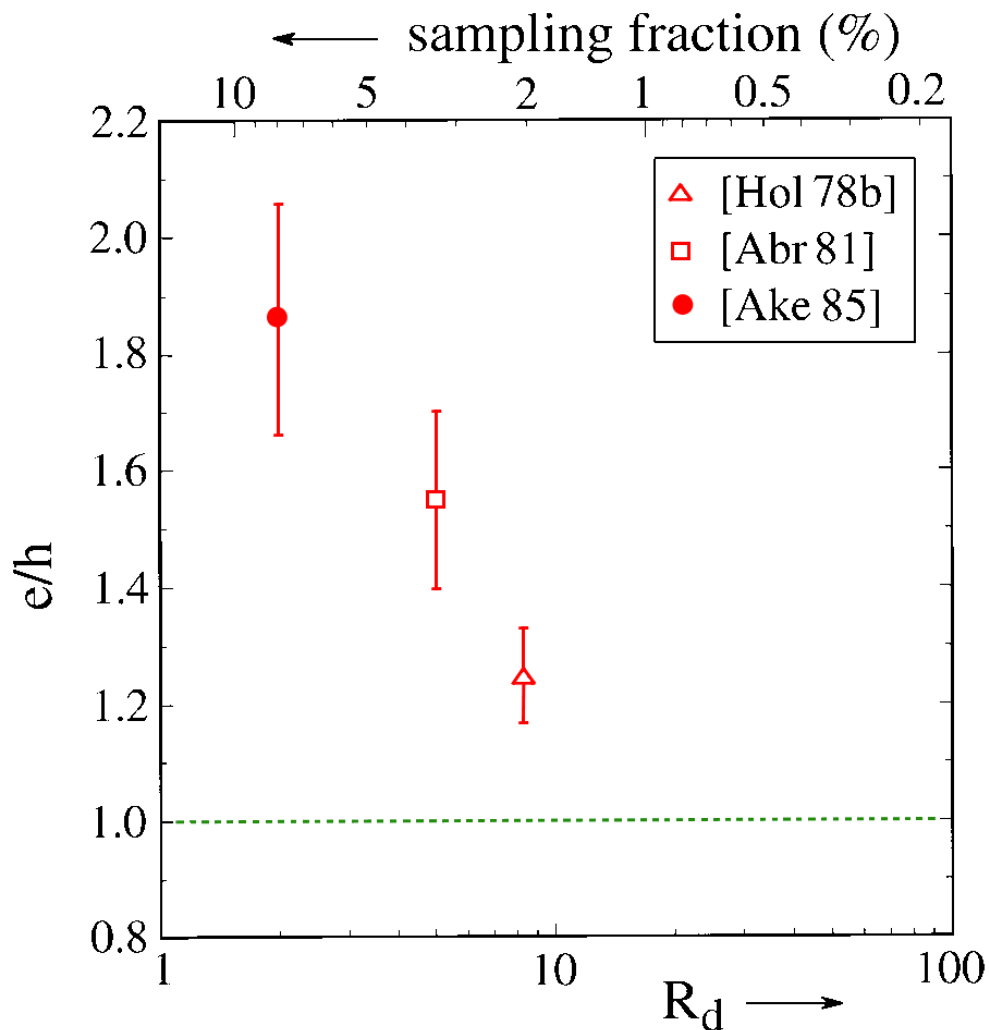


FIG. 3.36. The  $e/h$  value for iron/plastic-scintillator calorimeters, as a function of the sampling fraction for mips (top horizontal scale), or the volume ratio of the amounts of passive and active material (bottom horizontal scale).

# Compensation: Slow neutrons and the signal's time structure

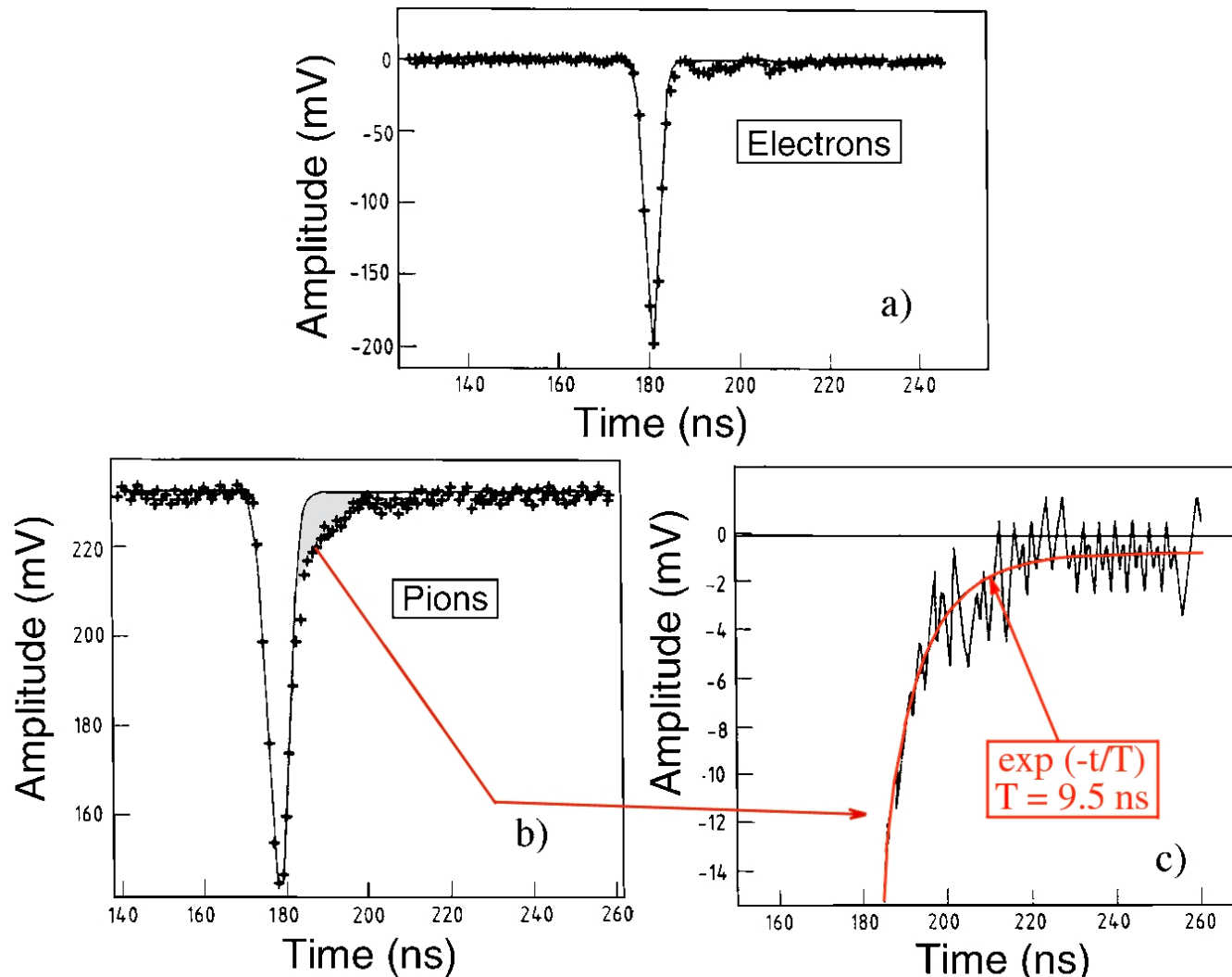


FIG. 3.24. Typical calorimeter signals for 150 GeV electrons (a) and pions (b) measured with the SPACAL calorimeter. The pion signal exhibits a clear exponential tail with a time constant of  $\sim 10$  ns (c). The  $t = 0$  point is arbitrary and the bin size is 1 ns. Data from [Aco 91a].

# Compensation: Effect of slow neutrons on the signals

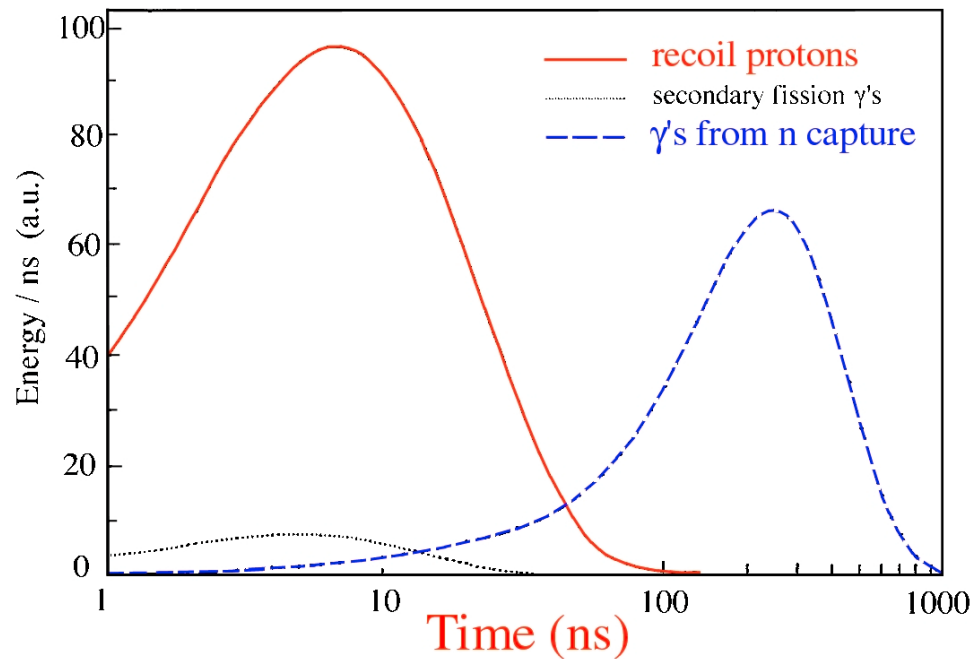


FIG. 3.22. Time structure of various contributions from neutron-induced processes to the hadronic signals of the ZEUS uranium/plastic-scintillator calorimeter [Bru 88].

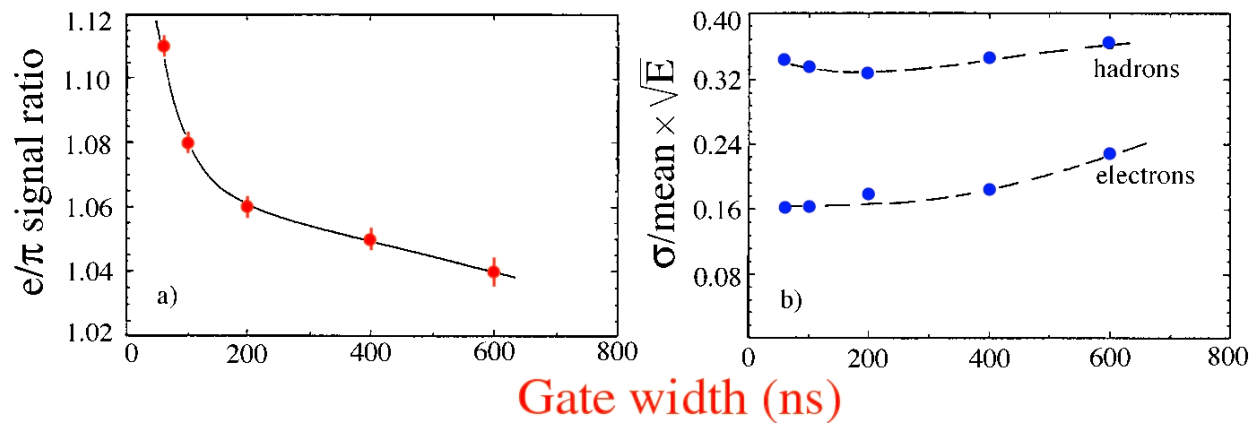


FIG. 3.23. The ratio of the average ZEUS calorimeter signals from 5 GeV/ $c$  electrons and pions (a) and the energy resolutions for detecting these particles (b), as a function of the charge integration time [Kru 92].

# Compensation (4)

All compensating calorimeters rely on the contribution of *neutrons* to the signals

- *Ingredients* for compensating calorimeters:
  - *Sampling* calorimeter
  - *Hydrogenous* active medium (recoil  $p!$ )
  - Precisely tuned *sampling fraction*  
*e.g.* 10% for U/scintillator, 3% for Pb/scintillator,.....
- *Uranium* absorber
  - Helpful*, but neither *essential* nor *sufficient*

# Fluctuations

- Calorimeter's **energy resolution is determined by *fluctuations***  
→ applying overall weighting factors (“*offline compensation*”) has **no merit** in this context
- **Many sources** of fluctuations may play a role, for example:
  - Signal **quantum** fluctuations (*e.g.*, photoelectron statistics)
  - **Sampling** fluctuations
  - Shower **leakage**
  - **Instrumental** effects (*e.g.*, electronic noise, light attenuation, structural non-uniformity)

but usually one source dominates.

Improve performance → work on that source

- **Poissonian** fluctuations:

Energy  $E$  gives  $N$  signal quanta, with  $\sigma = \sqrt{N}$

$$\rightarrow \sigma \sqrt{E} \propto \sqrt{N} \sqrt{N} = cE$$

$$\rightarrow \frac{\sigma}{E} = \frac{c}{\sqrt{E}}$$

# What excellent energy resolution does for you

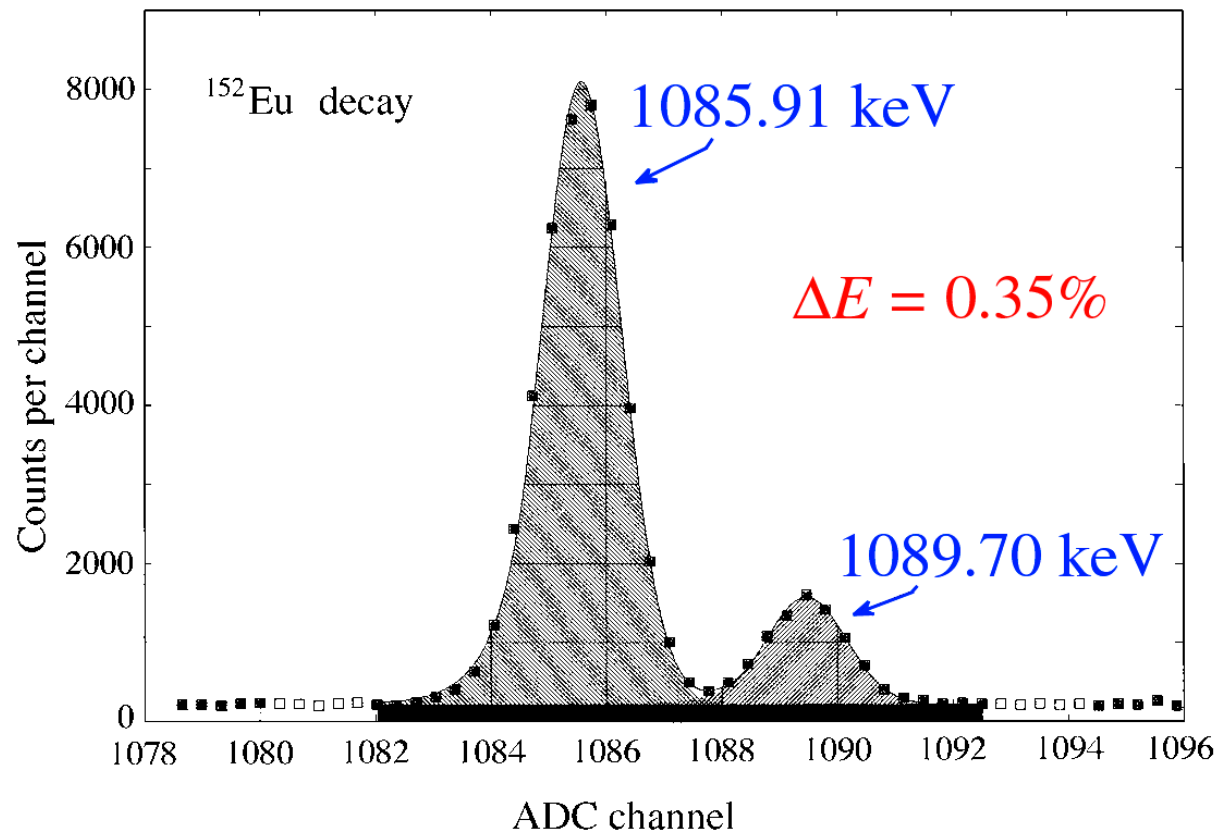


FIG. 4.1. Detection of nuclear  $\gamma$ -rays, from the decay of  $^{152}\text{Eu}$ , with a high-purity germanium crystal. The energy resolution of this calorimeter is about 0.1% at 1 MeV. Courtesy of G. Roubaud, CERN.

## Fluctuations (2)

- *Signal quantum fluctuations*

- **Ge** detectors for nuclear  $\gamma$  ray spectroscopy: 1 eV/quantum

- If  $E = 1$  MeV:  $10^6$  quanta, therefore  $\sigma/E = 0.1\%$

- Usually  $E$  expressed in GeV →  $\sigma/E = 0.003\%/\sqrt{E}$

- **Quartz fiber** calorimeters: Typical light yield  $\sim 1$  photoelectron/GeV

- $\sigma/E = 100\%/\sqrt{E}$ . If  $E = 100$  GeV,  $\sigma/E = 10\%$

# Signal quantum fluctuations dominate (1)

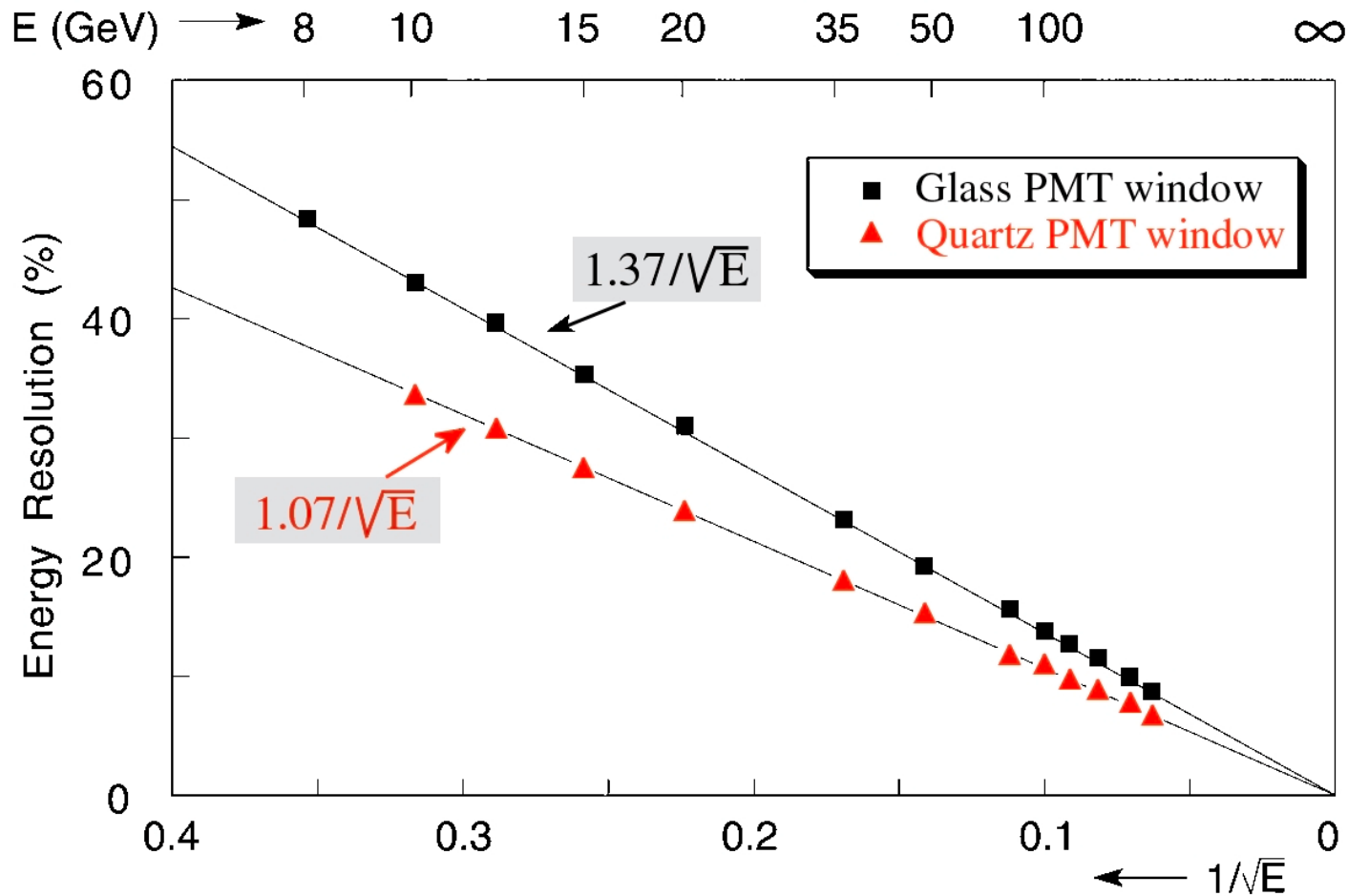


FIG. 4.2. The energy resolution for electron detection with the QFCAL prototype detector, as a function of energy. Results are given for measurements in which photomultiplier tubes with a glass window were used and for measurements in which the same type of PMTs were equipped with a quartz window [Akc 97].



## Signal quantum fluctuations dominate also here (2)

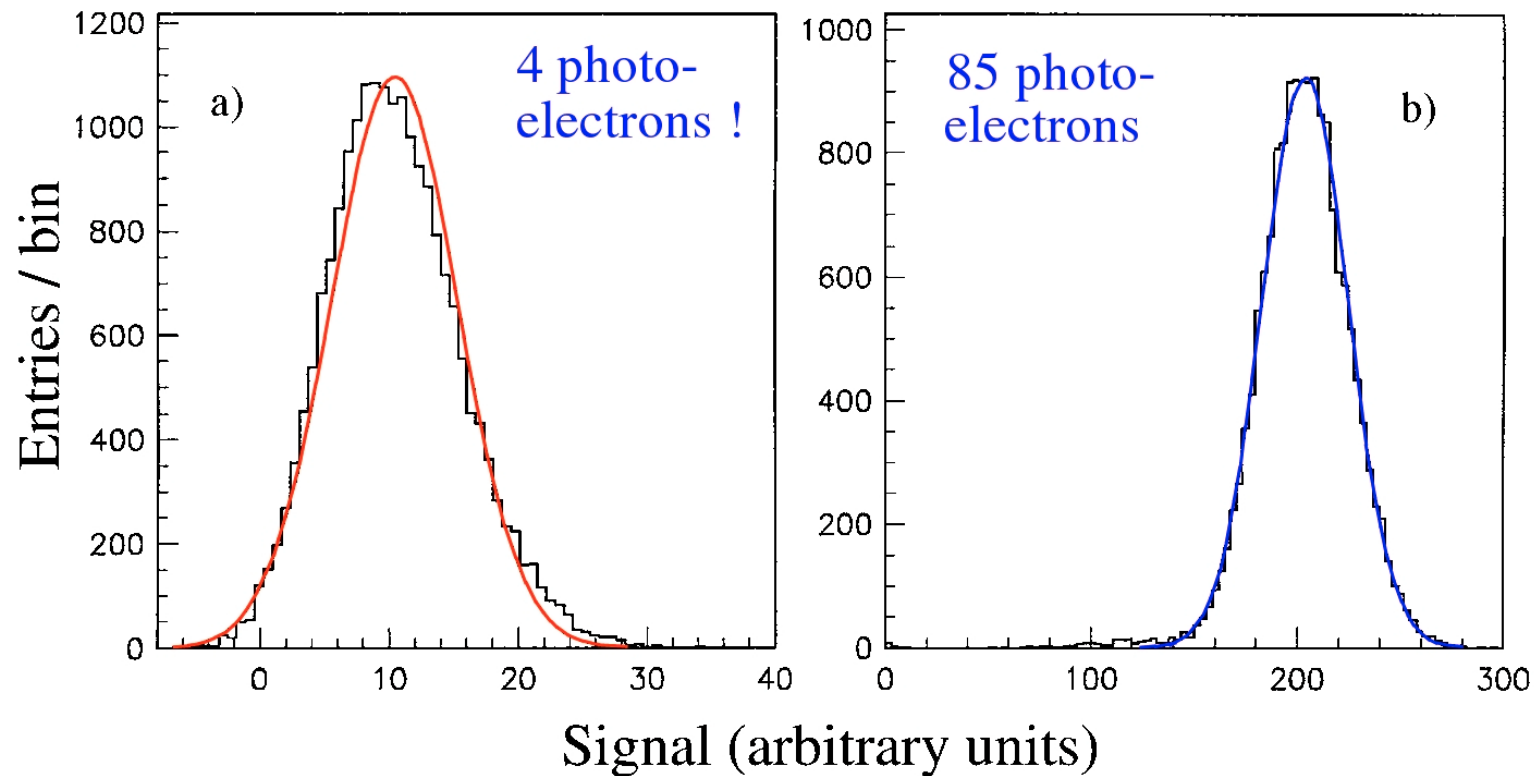


FIG. 4.3. Signal distributions for 10 GeV (a) and 200 GeV (b) electrons showering in the CMS Quartz-Fiber calorimeter, measured with a PMT with a glass window. The curves represent Gaussian fits to the experimental data [Akc 97].

## Fluctuations (3)

- *Sampling fluctuations*

Determined by fluctuations in the **number of different shower particles** contributing to the signals

Both the sampling *fraction* and the sampling *frequency* are important

ZEUS: **No correlation** between particles contributing to signals in neighboring sampling layers → range of shower particles is very small

# Sampling fluctuations in em calorimeters

## Determined by sampling fraction and sampling frequency

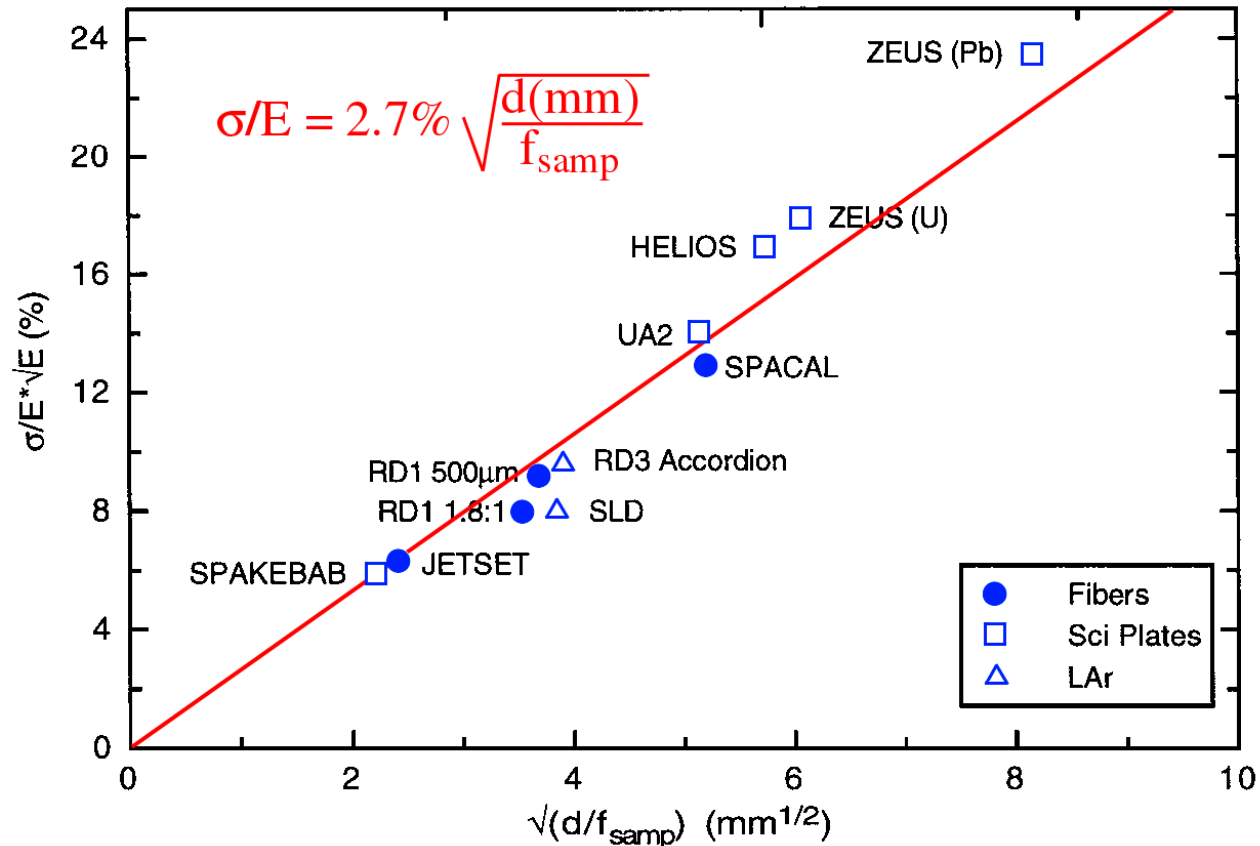


FIG. 4.8. The em energy resolution of sampling calorimeters as a function of the parameter  $(d/f_{\text{samp}})^{1/2}$ , in which  $d$  is the thickness of an active sampling layer (*e.g.* the diameter of a fiber or the thickness of a scintillator plate or a liquid-argon gap), and  $f_{\text{samp}}$  is the sampling fraction for mips [Liv 95].

# How to measure the effects of sampling fluctuations

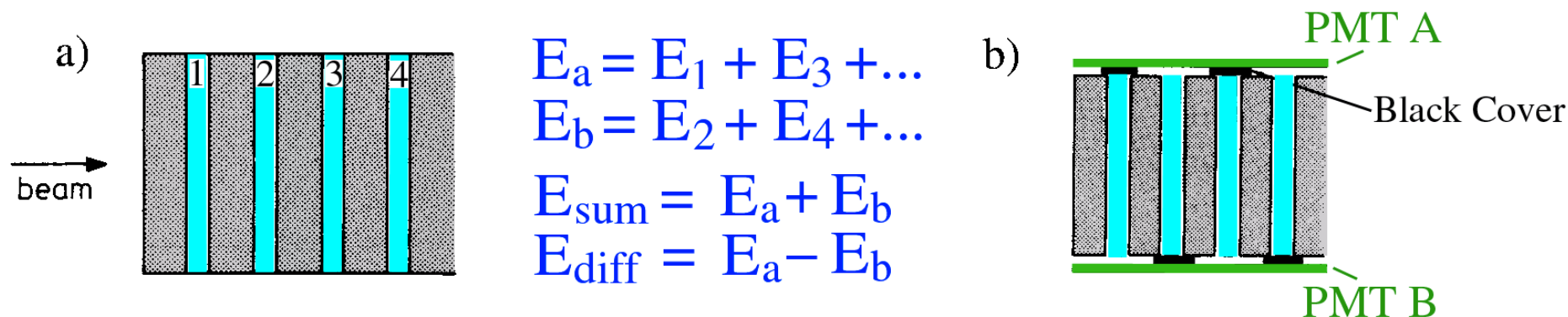


FIG. 4.13. Schematic structure of the ZEUS calorimeter (a) and the configuration used to measure the contribution of sampling fluctuations to the energy resolutions for em and hadronic showers (b).

| Fluctuations (%)       | 3 mm uranium / 2.5 mm plastic |                | 10 mm lead / 2.5 mm plastic |                |
|------------------------|-------------------------------|----------------|-----------------------------|----------------|
|                        | Electrons                     | Pions          | Electrons                   | Pions          |
| $\sigma_A, \sigma_B$   | $26.6 \pm 1.0$                | $49.5 \pm 1.0$ | $36.0 \pm 1.0$              | $60.5 \pm 1.0$ |
| $\sigma_{\text{sum}}$  | $18.5 \pm 1.0$                | $37.3 \pm 1.0$ | $24.5 \pm 1.0$              | $43.5 \pm 1.0$ |
| $\sigma_{\text{diff}}$ | $19.2 \pm 1.0$                | $32.6 \pm 1.0$ | $25.8 \pm 1.0$              | $42.3 \pm 1.0$ |
| $\sigma_{\text{samp}}$ | $16.5 \pm 0.5$                | $31.1 \pm 0.9$ | $23.5 \pm 0.5$              | $41.2 \pm 0.9$ |
| $\sigma_{\text{intr}}$ | $2.2 \pm 4.8$                 | $20.4 \pm 2.4$ | $0.3 \pm 5.1$               | $13.4 \pm 4.7$ |

**Table 4.1** The contributions of sampling fluctuations and intrinsic fluctuations to the energy resolutions for electrons and pions in compensating uranium/plastic-scintillator and lead/plastic-scintillator calorimeters. Listed are the values of the coefficient  $a$  (Equation 4.1), expressed in %. Data from [Dre 90].

# How to measure the effects of sampling fluctuations (2)

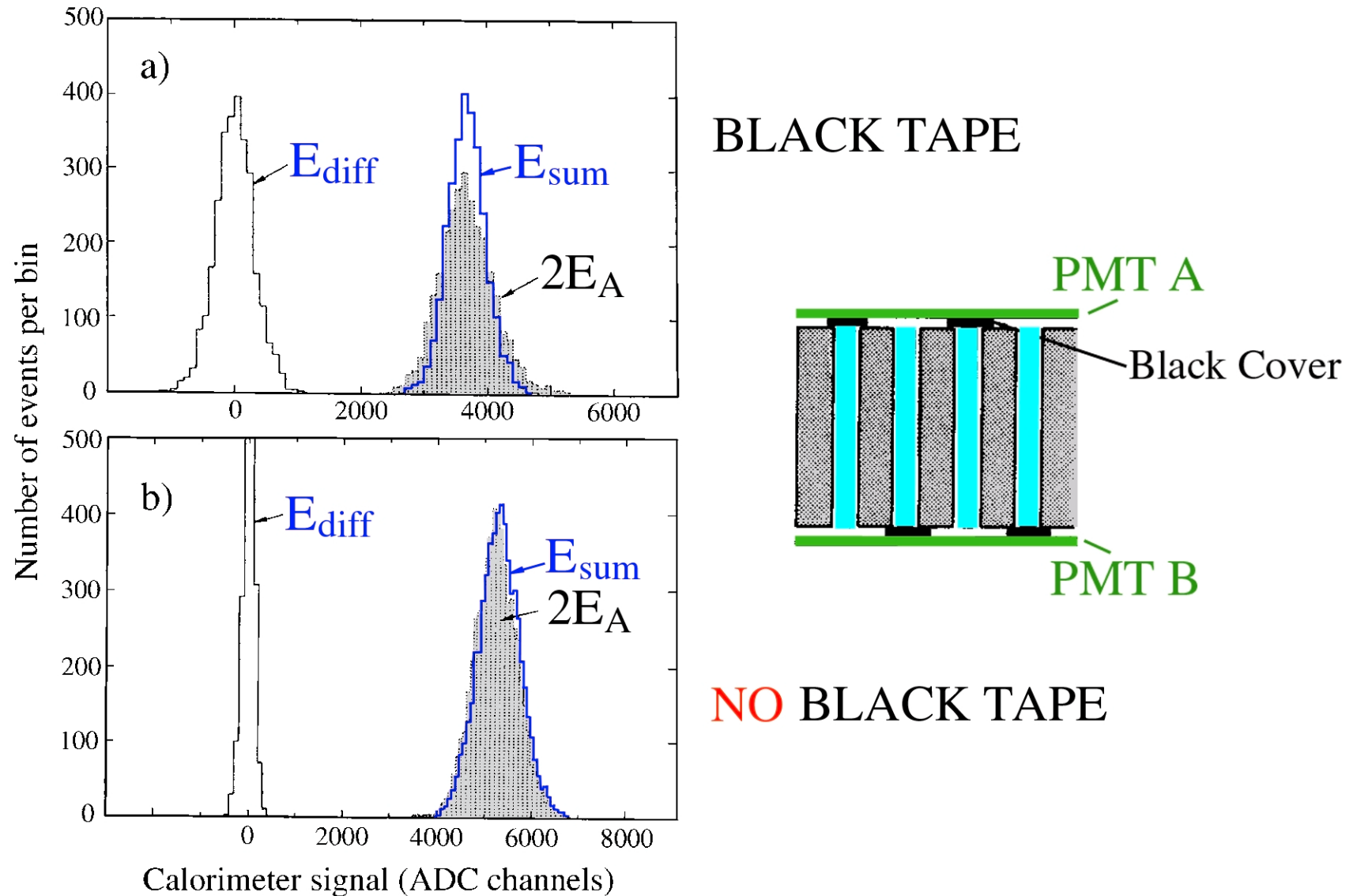


FIG. 4.14. Pulse height distributions for 30 GeV hadrons obtained with the ZEUS lead/plastic-scintillator prototype calorimeter. Diagram *a*) shows the distributions of  $E_{sum}$ ,  $E_{diff}$  and  $2E_A$ , measured in the configuration depicted in Figure 4.13b. Diagram *b*) shows the same distributions measured in the same configuration, but with the black tape removed. See text for details. From [Dre 90].

## Fluctuations (4)

- *Shower leakage fluctuations*

- These fluctuations are *non-Poissonian*
- For a given average containment, *longitudinal* fluctuations are *larger than lateral* ones.

Difference comes from # of particles responsible for leakage.

*e.g.* Differences between  $e, \gamma$  induced showers

# Contribution of leakage fluctuations to energy resolution

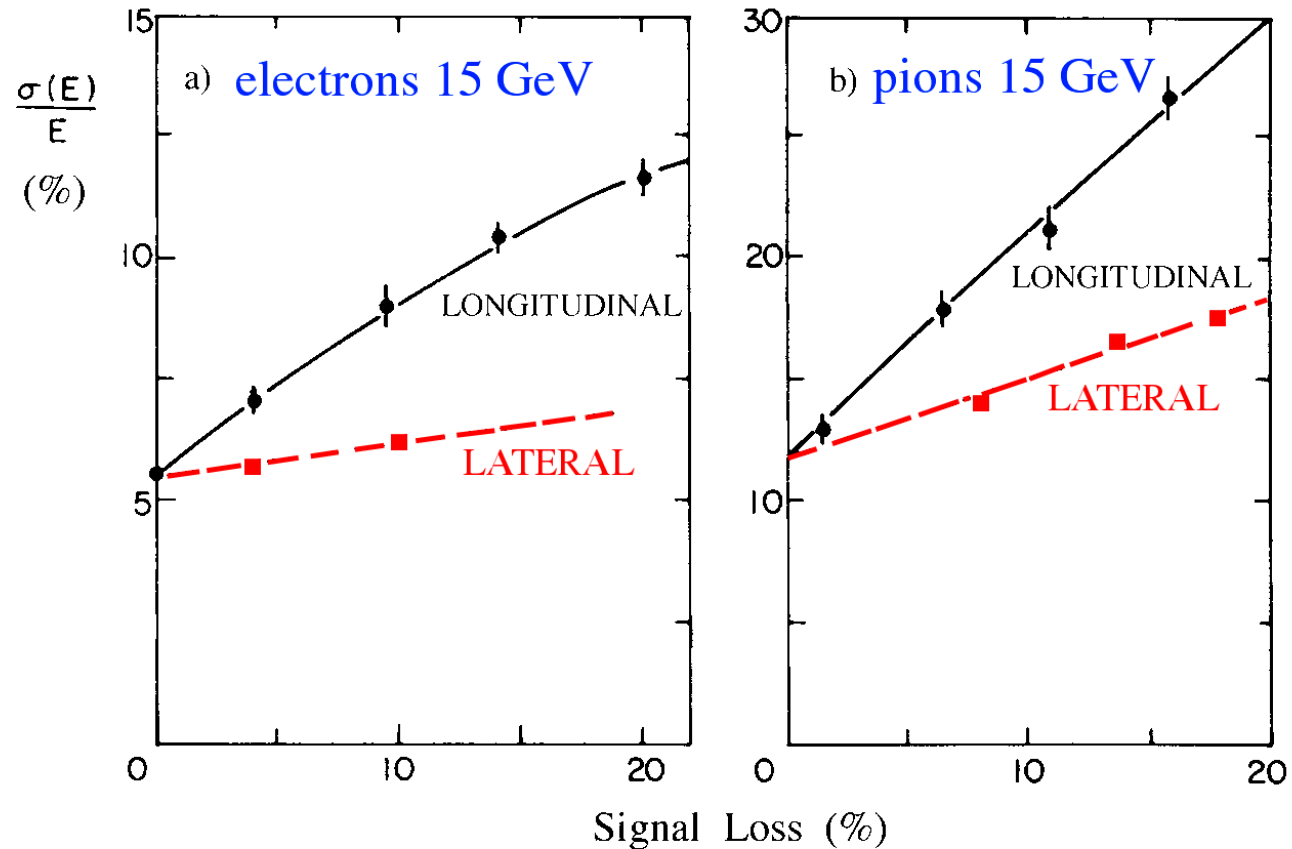


FIG. 4.28. The effects of longitudinal and lateral shower leakage on the energy resolution, as measured for 15 GeV electrons (a) and pions (b) by the CHARM Collaboration in a low- $Z$  calorimeter [Did 80, Amal 81].

# Effects back-, front-, and side leakage on em energy resolution

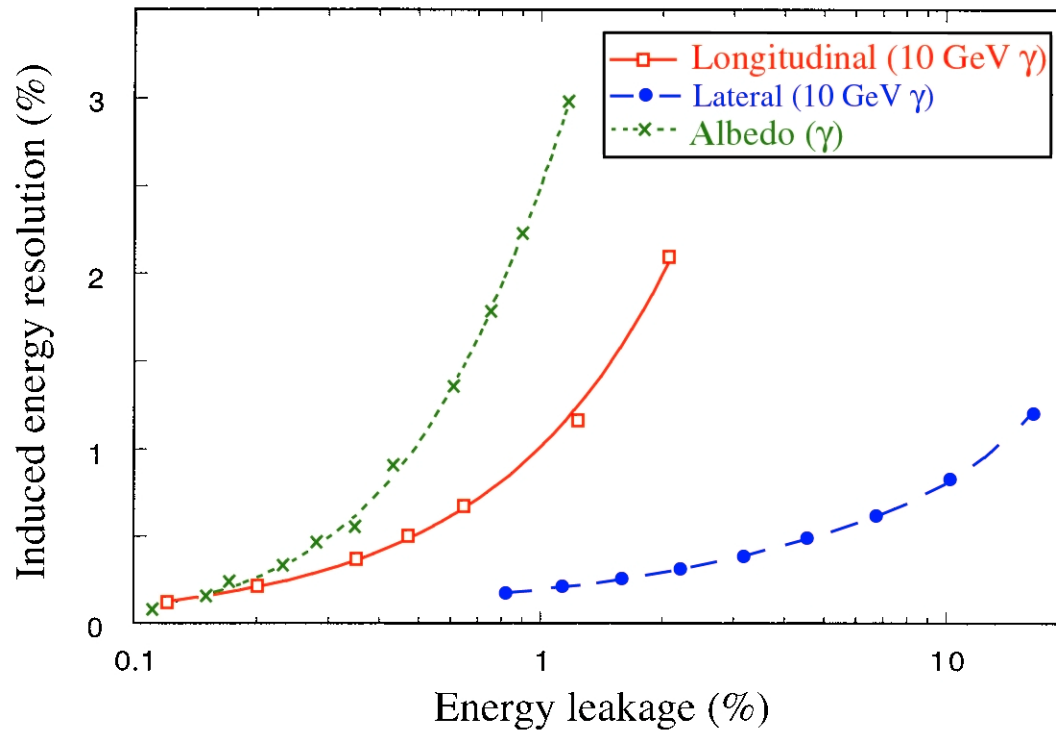


FIG. 4.37. A comparison of the effects caused by different types of shower leakage. Shown are the induced energy resolutions resulting from albedo, longitudinal and lateral leakage as a function of the average energy fraction carried by particles escaping from the detector. The longitudinal and lateral leakage data concern 10 GeV  $\gamma$ s, the albedo data are for  $\gamma$ -induced showers of different energies. Results from EGS4 Monte Carlo calculations.



# Leakage and leakage fluctuations in electron / $\gamma$ induced showers

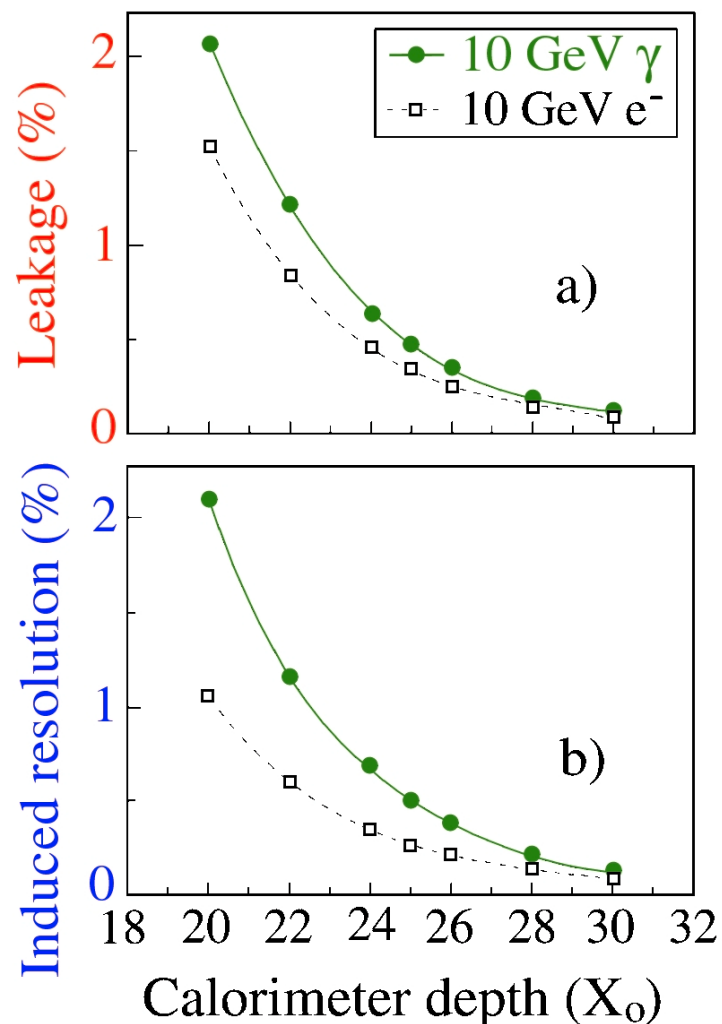


Figure 5: The average fraction of the shower energy carried by particles escaping the calorimeter through the back plane (a) and the relative increase in the energy resolution caused by this effect (b), for showers induced by 10 GeV electrons and 10 GeV  $\gamma$ s developing in blocks of tin with different thicknesses, ranging from  $20X_0$  to  $30X_0$ . Results from EGS4 Monte Carlo calculations.

## Fluctuations (5)

- *Instrumental effects*

- Structural differences in sampling fraction
- “Channeling” effects
- Electronic noise, light attenuation,.....

# Instrumental effects: Channeling in fiber calorimeters

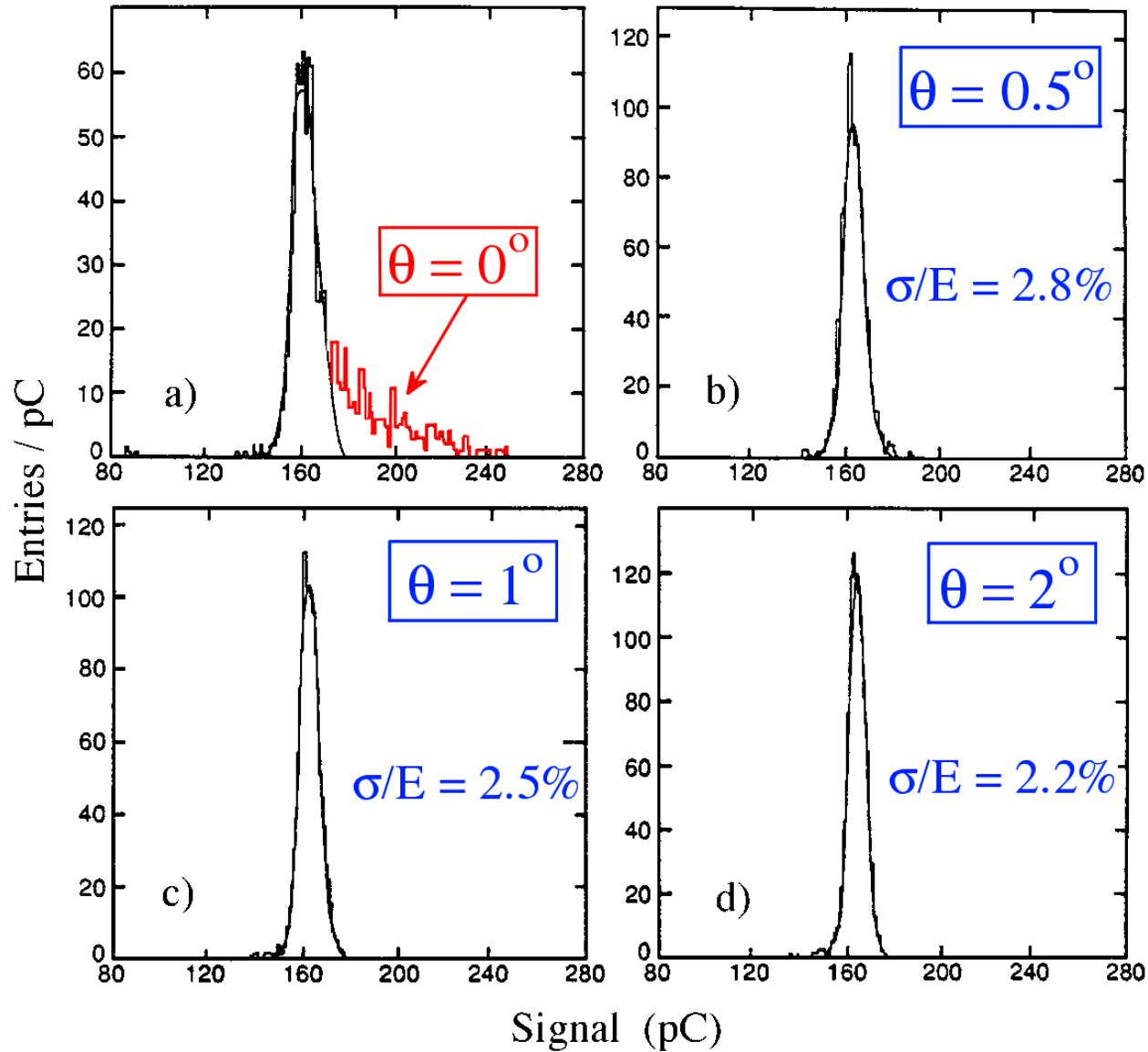


FIG. 4.22. Signal distributions for 40 GeV electron showers measured with the RD1 0.5 mm fiber calorimeter, for different angles between the particle s direction and the fiber [Bad 94a].

# Fluctuations (6)

- Different effects have *different energy dependence*
  - quantum, sampling fluctuations:  $\sigma/E \sim E^{-1/2}$
  - shower leakage  $\sigma/E \sim E^{-1/4}$
  - electronic noise  $\sigma/E \sim E^{-1}$
  - structural non-uniformities  $\sigma/E = \text{constant}$

Add in quadrature:  $\sigma_{\text{tot}}^2 = \sigma_1^2 + \sigma_2^2 + \sigma_3^2 + \sigma_4^2 \dots$

# The em energy resolution of the ATLAS calorimeter

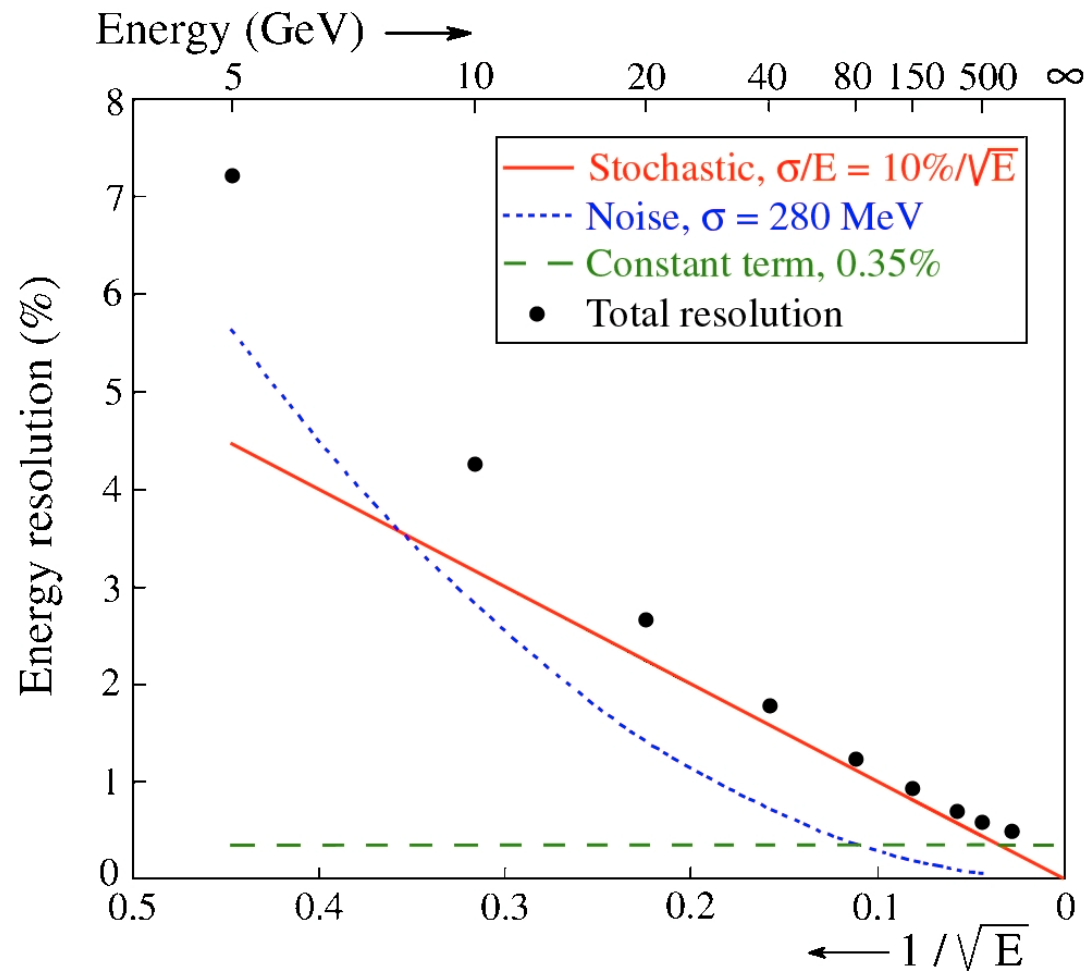


FIG. 9.30. The em energy resolution and the separate contributions to it, for the em barrel calorimeter, at  $\eta = 0.28$  [Gin 95].

# Fluctuations in Hadron Showers

Same types of fluctuations as in em showers, *plus*

- Fluctuations in *visible energy*  
(ultimate limit of hadronic energy resolution)
- Fluctuations in the *em shower fraction*,  $f_{\text{em}}$ 
  - *Dominating effect* in most hadron calorimeters ( $e/h \neq 1$ )
  - Fluctuations are *asymmetric* in pion showers (one-way street)
  - *Differences* between  $p, \pi$  induced showers
    - No leading  $\pi^0$  in proton showers (baryon # conservation)

# Hadron showers: Fluctuations in nuclear binding energy losses

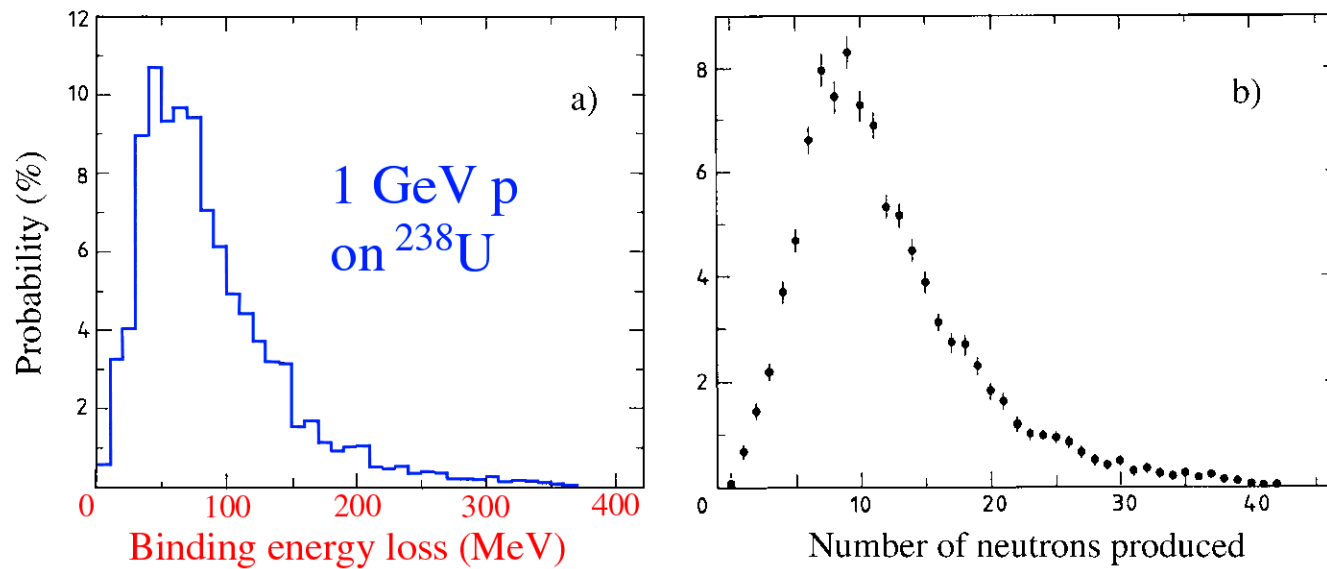


FIG. 4.43. The nuclear binding energy lost in spallation reactions induced by 1 GeV protons on  $^{238}\text{U}$  nuclei (a), and the number of neutrons produced in such reactions (b). From [Wig 87].

# Fluctuations in Hadron Showers

Same types of fluctuations as in em showers, *plus*

- Fluctuations in *visible energy*  
(ultimate limit of hadronic energy resolution)
- Fluctuations in the *em shower fraction*,  $f_{\text{em}}$ 
  - *Dominating effect* in most hadron calorimeters ( $e/h \neq 1$ )
  - Fluctuations are *asymmetric* in pion showers (one-way street)
  - *Differences* between  $p, \pi$  induced showers
    - No leading  $\pi^0$  in proton showers (baryon # conservation)



# Hadron showers: Fluctuations in em shower fraction ( $f_{em}$ )

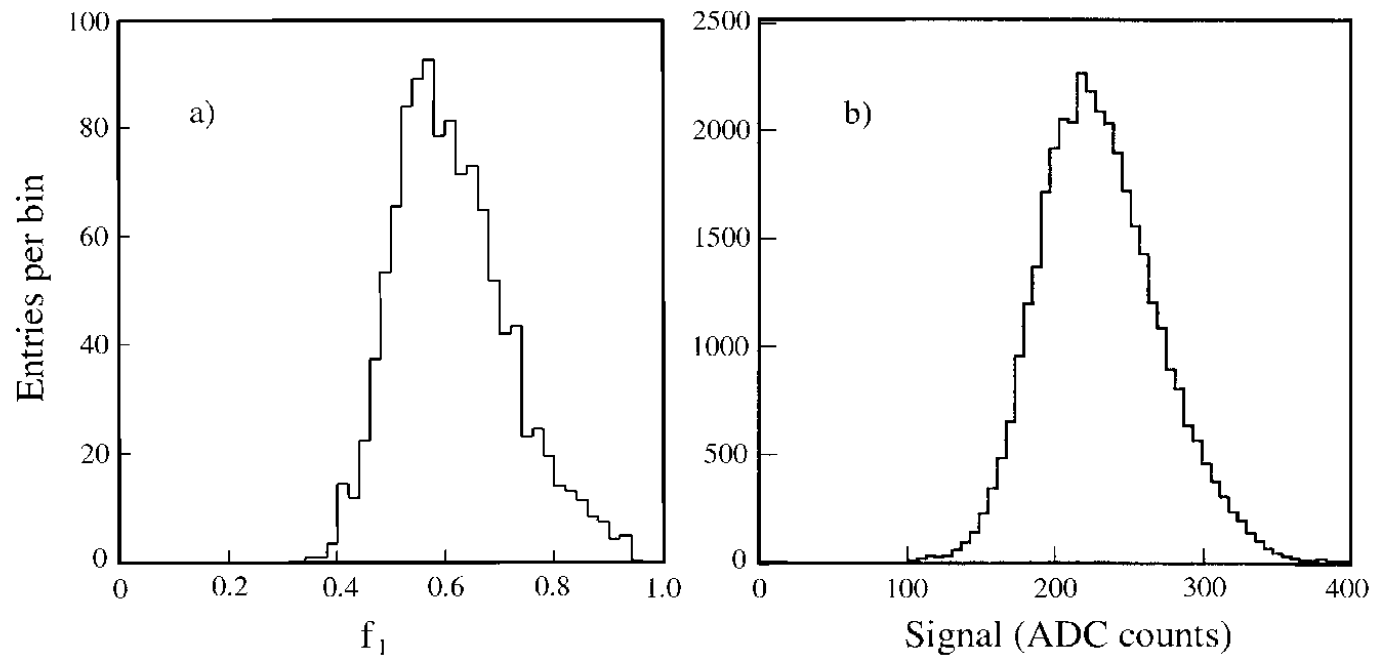


FIG. 4.44. The distribution of the fraction of the energy of 150 GeV  $\pi^-$  showers contained in the em shower core, as measured with the SPACAL detector (a) [Aco 92b] and the signal distribution for 300 GeV  $\pi^-$  showers in the CMS Quartz-Fiber calorimeter (b) [Akc 98].

# Hadronic response function: Effect of $e/h$

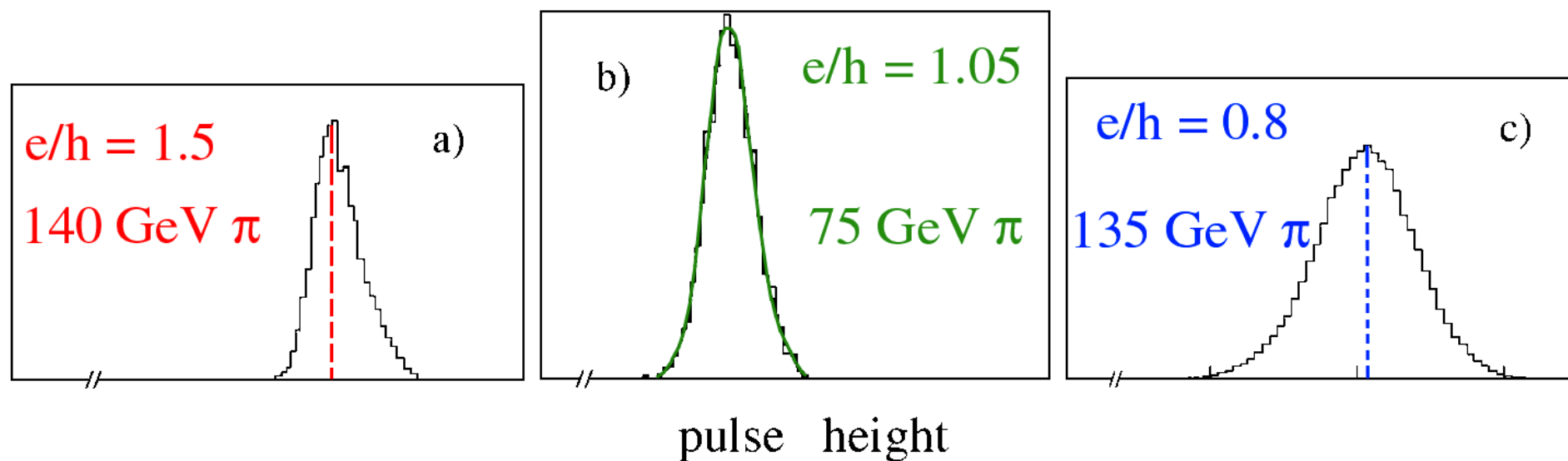
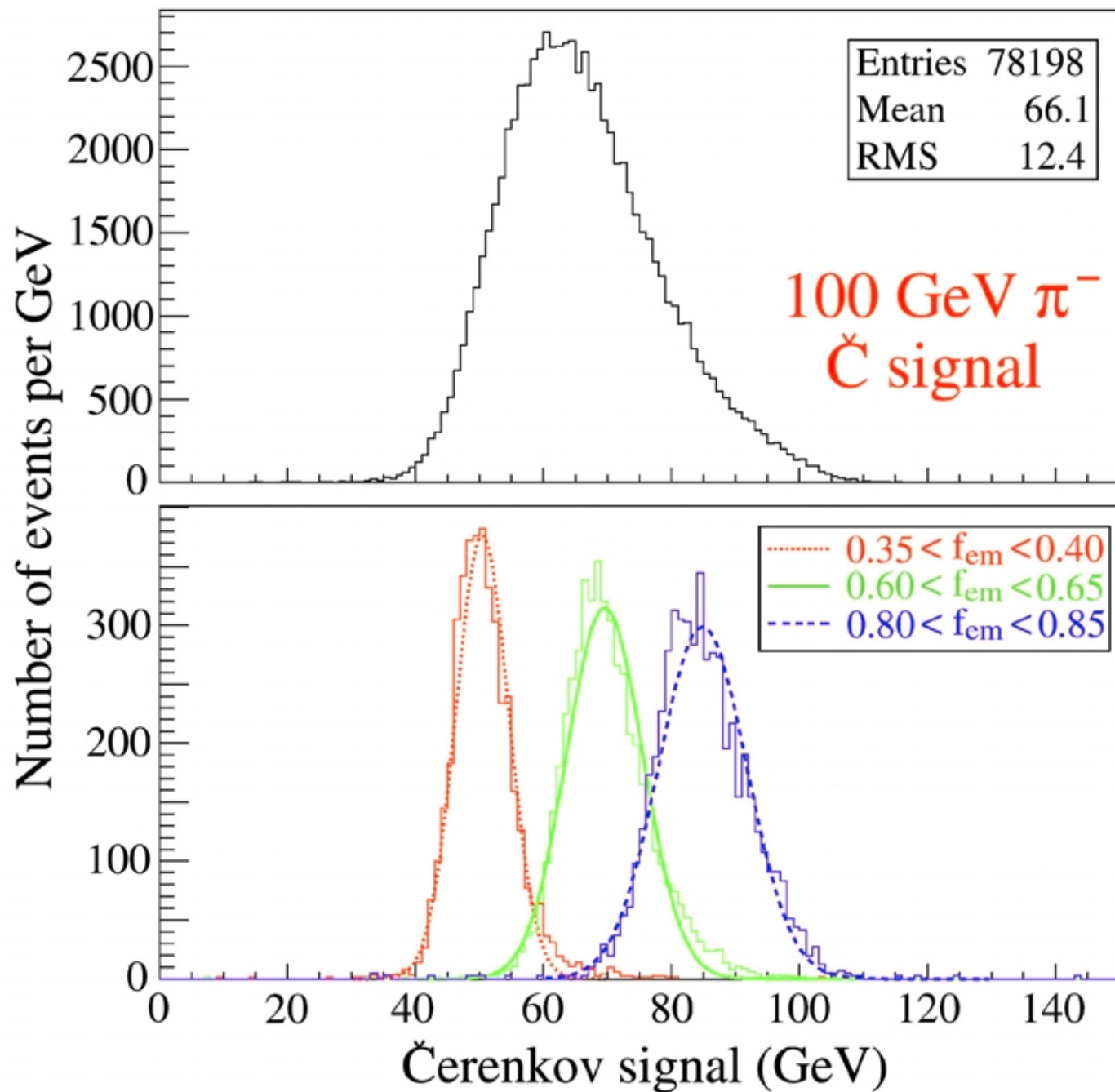


FIG. 7.24. Signal distributions for mono-energetic pions in calorimeters with different  $e/h$  values. Data from WA1 [Abr 81], ZEUS [Beh 90] and WA78 [Dev 86].

# DREAM: Effect of event selection based on $f_{em}$



# Fluctuations in $f_{em}$ : Differences $p/\pi$ induced showers

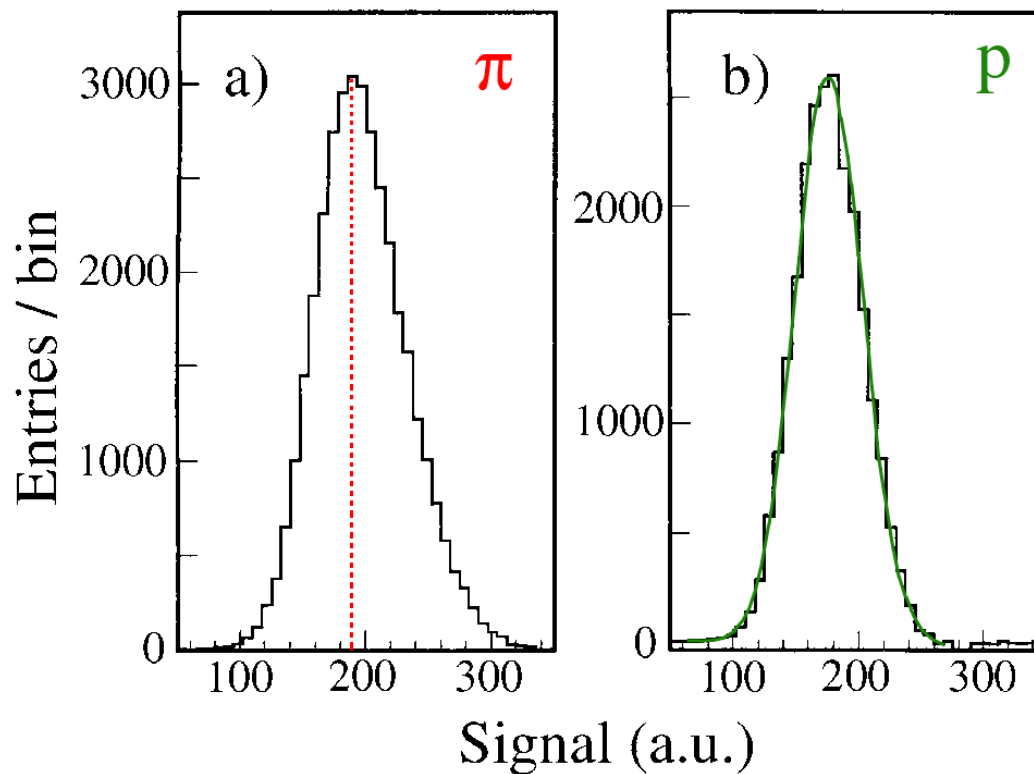


FIG. 4.49. Signal distributions for 300 GeV pions (*a*) and protons (*b*) detected with a quartz-fiber calorimeter. The curve represents the result of a Gaussian fit to the proton distribution [Akc 98].

## Fluctuations in Hadron Showers (2)

- Effect of **non-compensation** on  $\sigma/E$  is ***not*** a constant term

In practice,

$$\frac{\sigma}{E} = \frac{a}{\sqrt{E}} + b$$

is a good approximation

# Hadronic resolution of non-compensating calorimeters

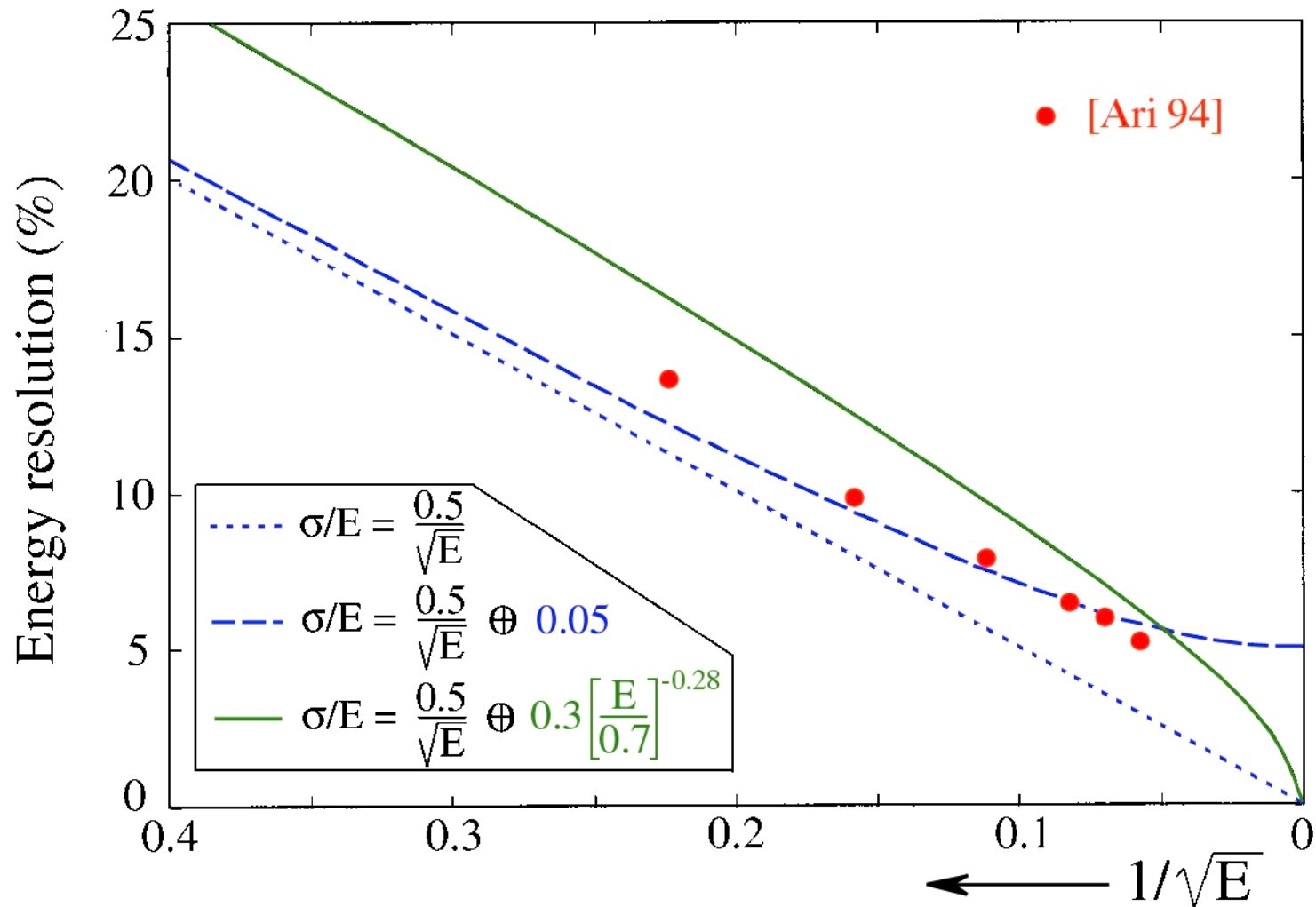


FIG. 4.47. Comparison between Equations 4.28 (the dashed curve) and 4.29 (the solid curve). The dotted line represents the stochastic term in these equations. The experimental data were taken from [Ari 94]. See text for details.

# Hadronic resolution of non-compensating calorimeters

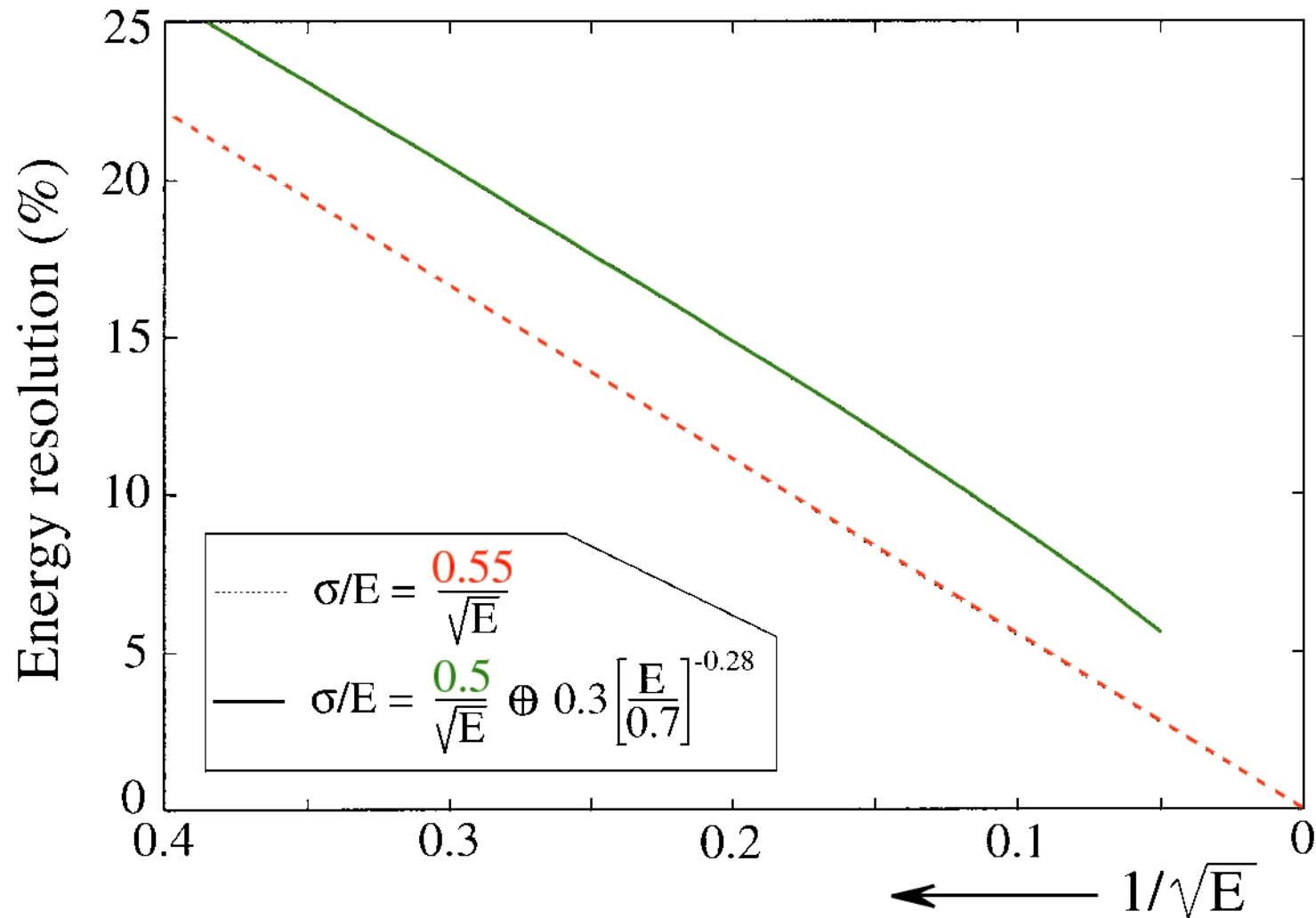


FIG. 4.48. The energy resolution calculated with Equation 4.29 for energies up to 400 GeV (the solid line), and calculated with a sole stochastic term with a slightly larger  $a_1$  value (the dotted line). See text for details.

## Fluctuations in Hadron Showers (3)

- The *ultimate limit* on hadronic energy resolution is determined by the correlation between  $\Sigma E_n$  and nuclear binding energy loss

**Better in Pb** than in Uranium ( $13\%/\sqrt{E}$  vs.  $20\%/\sqrt{E}$ )



# The ultimate limit on hadronic energy resolution

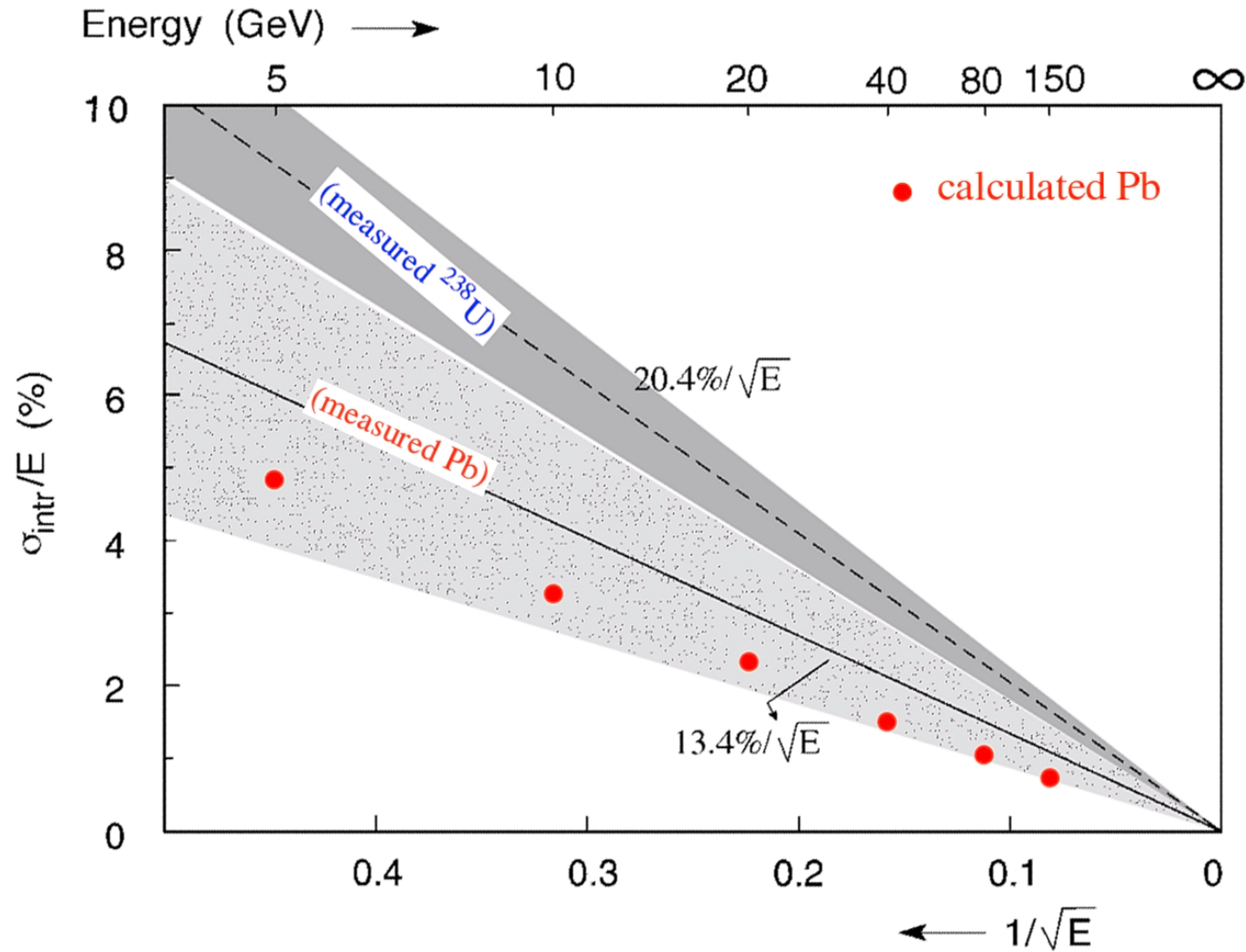


FIG. 4.55. The (calculated) contribution of fluctuations in the total kinetic energy carried by neutrons to the hadronic energy resolution of a compensating Pb/plastic-scintillator calorimeter, as a function of energy (the black dots). The measured value of the irreducible fluctuations in such a calorimeter is indicated by the shaded area. The dashed line represents the measured value of the irreducible fluctuations in a compensating <sup>238</sup>U/plastic-scintillator calorimeter.

## Lessons for calorimeter design (1)

- *Improve* resolution  $\rightarrow$  work on fluctuations that *dominate*

Example: 60 ton (**liquid**) scintillator does not make good hadron calorimeter

**All** fluctuations eliminated, except non-compensation:  $\sigma/E > 10\%$  at all energies!

SPACAL ( $e/h \approx 1.0$ , but other sources of fluctuation present):

$\sigma/E \approx 2\%$  at  $E = 300$  GeV

# Hadron calorimeters: Effects $f_{em}$ fluctuations on resolution

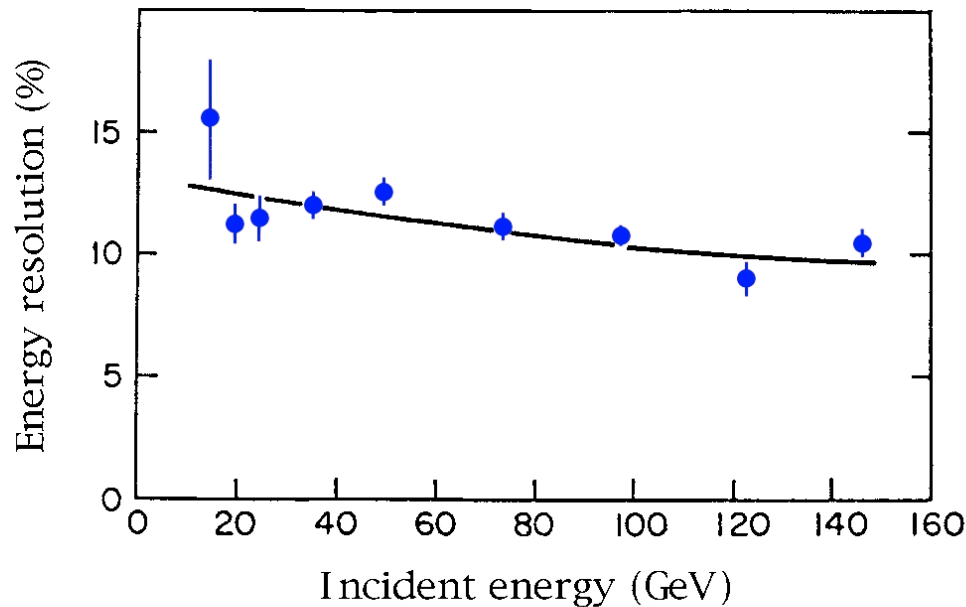


Figure 9: The hadronic energy resolution as a function of energy, for a homogeneous calorimeter consisting of *60 tonnes of liquid scintillator*

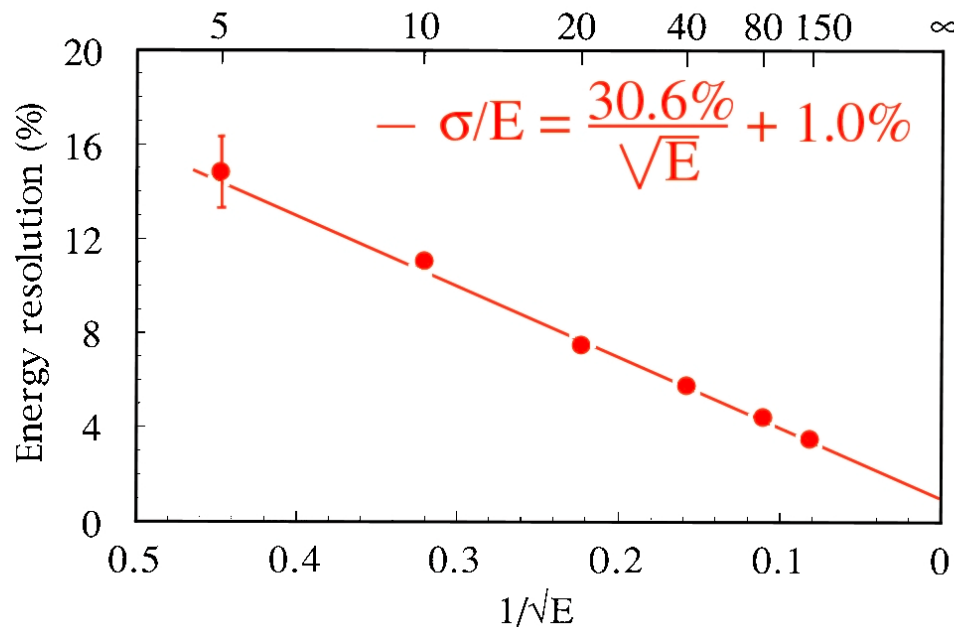


Figure 10: The hadronic energy resolution as a function of energy, for the compensating SPACAL *lead/plastic-scintillator calorimeter (sampling fraction 2%)*

## Lessons for calorimeter design (2)

- Do not spend your money reducing fluctuations that do *not* dominate

### *Practical examples:*

- A  $2\lambda_{\text{int}}$  deep calorimeter for extraterrestrial detection of high energy cosmic hadrons is dominated by *shower leakage*
- ➔ A high-quality crystal calorimeter is as good (bad) as a crudely sampling one
- A calorimeter system with a crystal em section will have poor performance for hadron detection, *no matter what* you choose as the hadronic section, because of the large  $e/h$  value of homogeneous devices
- ➔ *Don't waste your money on the hadronic section*

# Dominating fluctuations dominate

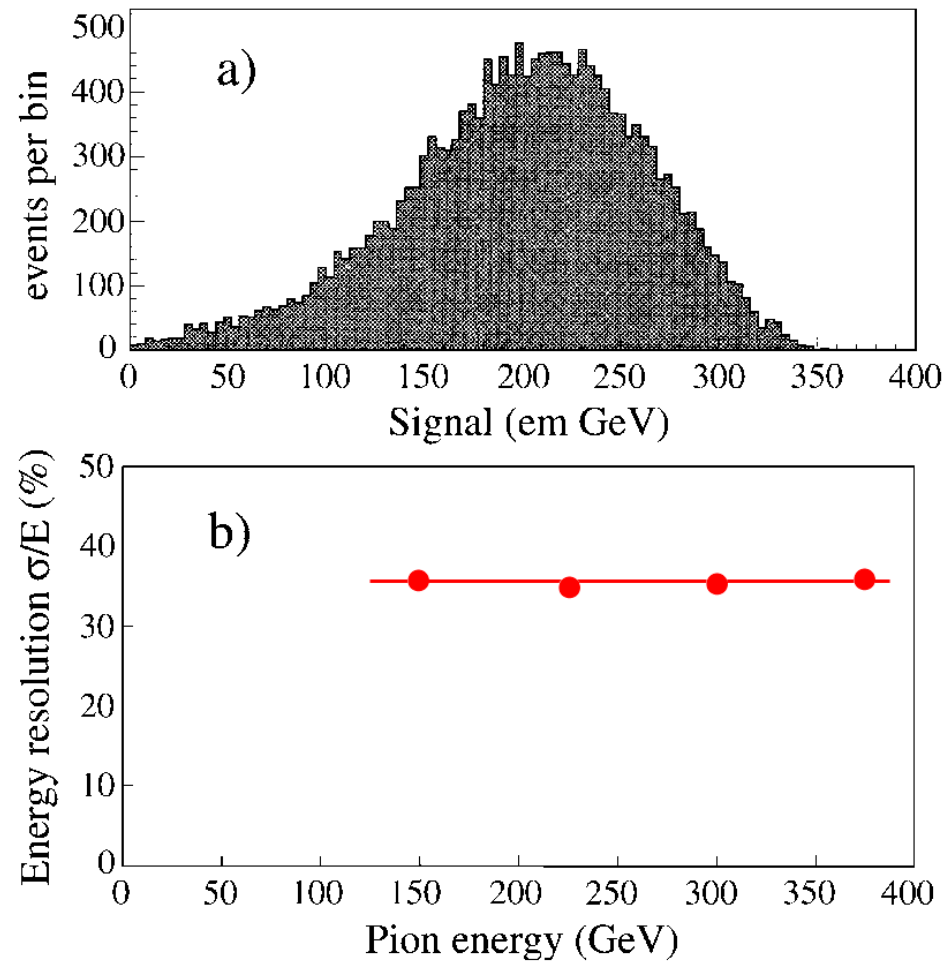


Figure 4: Signal distribution for 375 GeV  $\pi^-$  in a  $1.4\lambda_{\text{int}}$  deep calorimeter (a) and the energy resolution of this detector as a function of the pion energy (b).

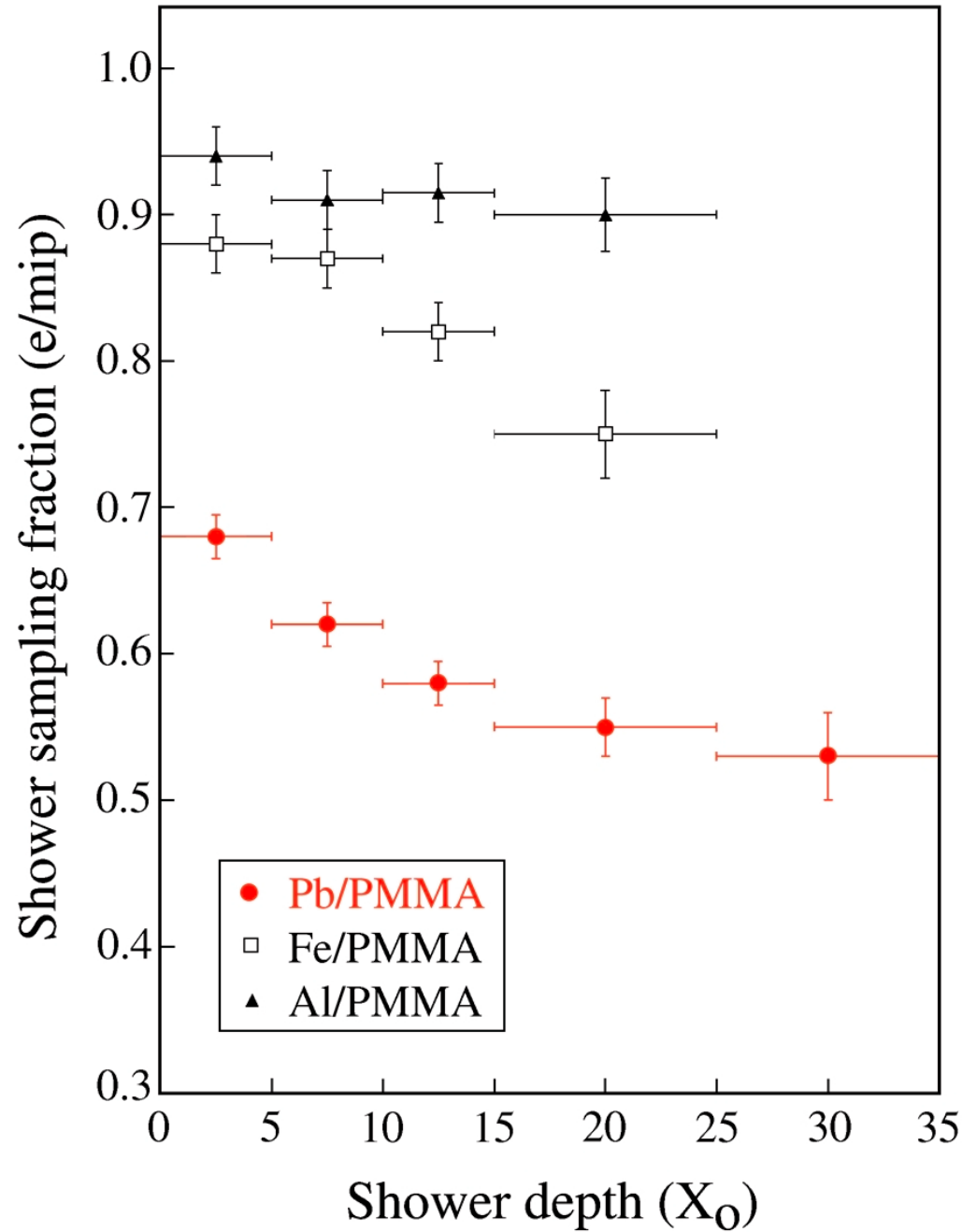
# Practical Issues

*(student / postdoc jobs)*

# CALIBRATION

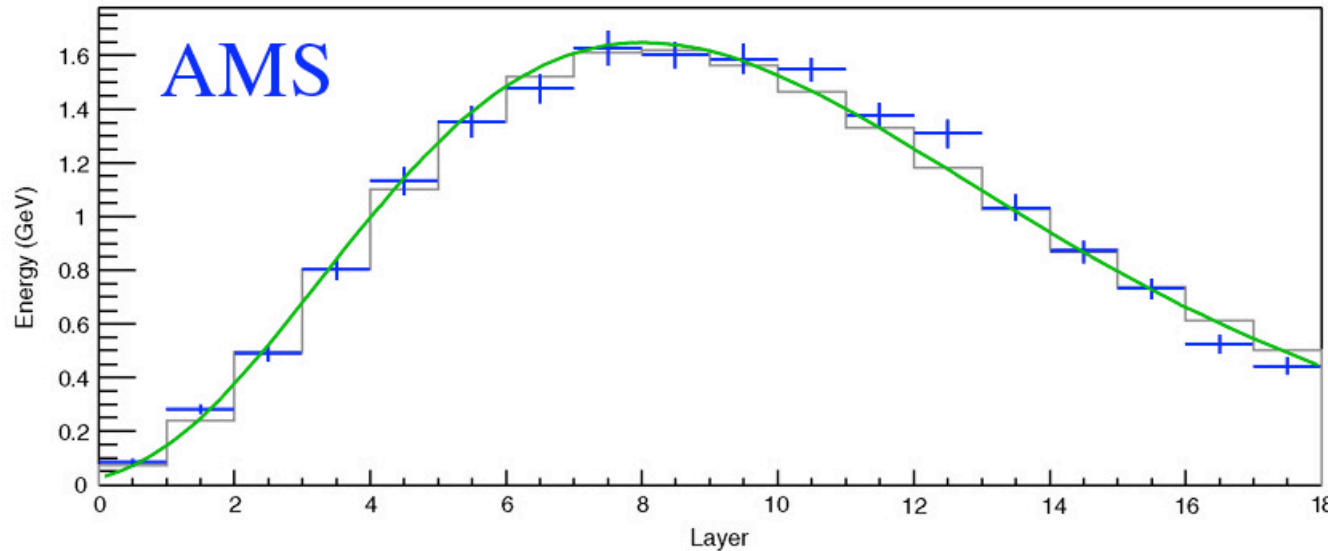
- Performance of calorimeters determined by processes that take place in the last stages of the shower development (**MeV/keV/eV level**)
- This has important consequences for calibration of *longitudinally segmented* devices
- The sampling fraction is a function of *depth* (or shower *age*).  
Example: in em showers, soft  $\gamma$ s are sampled differently than mips.  
→ Ratio (energy deposit/resulting signal) is function of depth.  
Effect is *energy dependent* as well.

The sampling fraction changes with depth!





# Consequences of depth dependence sampling fraction

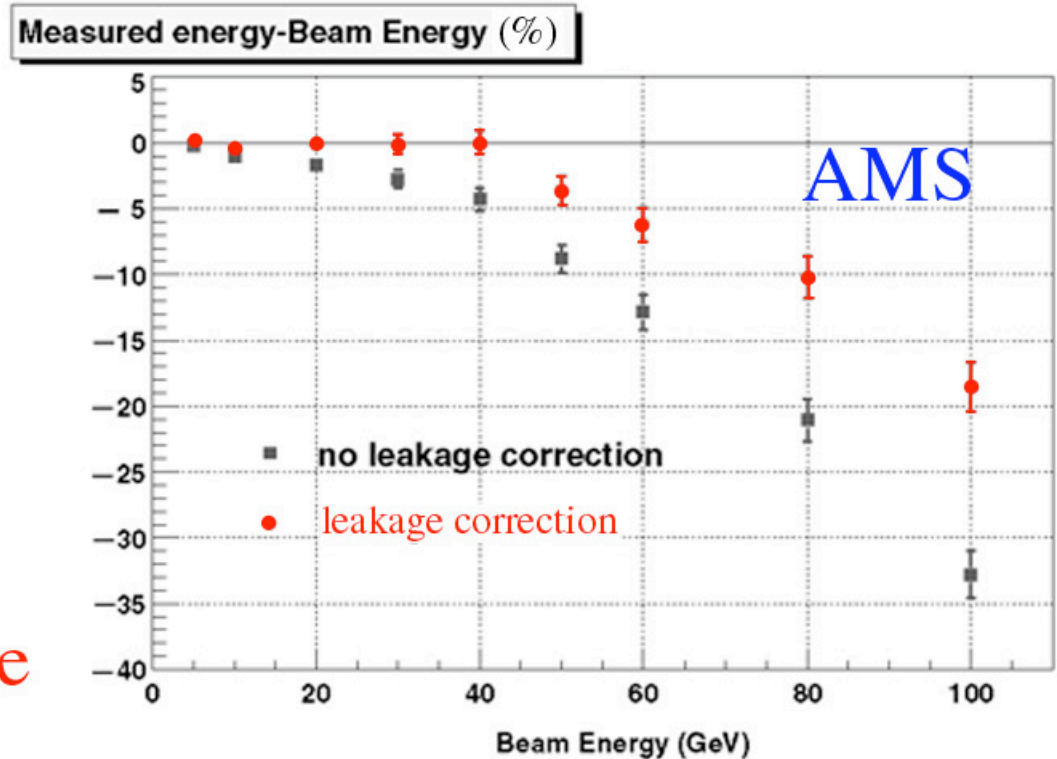


NIM A490, 132  
(2002)

Pb/scintillating fiber  
18 layers ( $17 X_0$ )

Calibrated with mip's:  
11.7 MeV/layer

Shower leakage:  
(under)estimated on basis  
of fit to longitudinal profile



# Effects of depth dependence sampling fraction

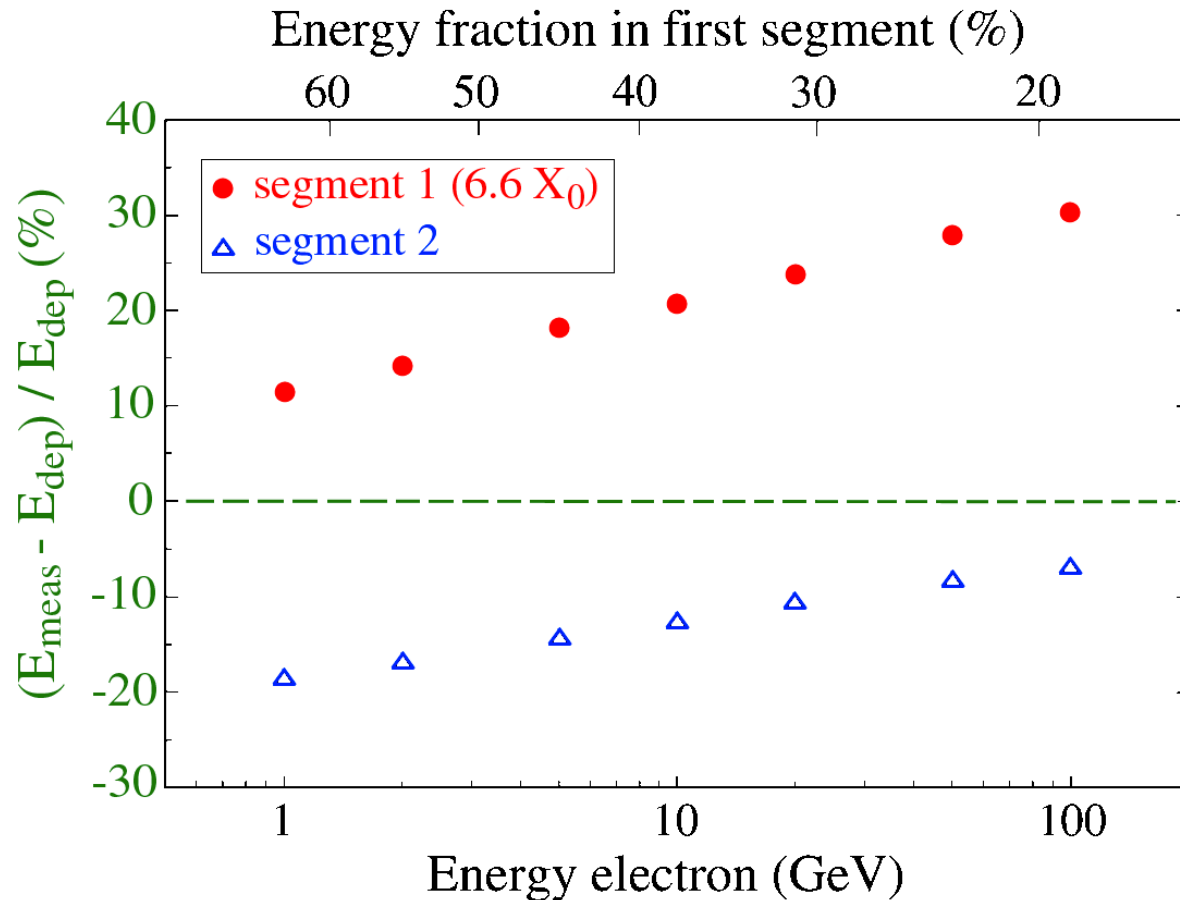
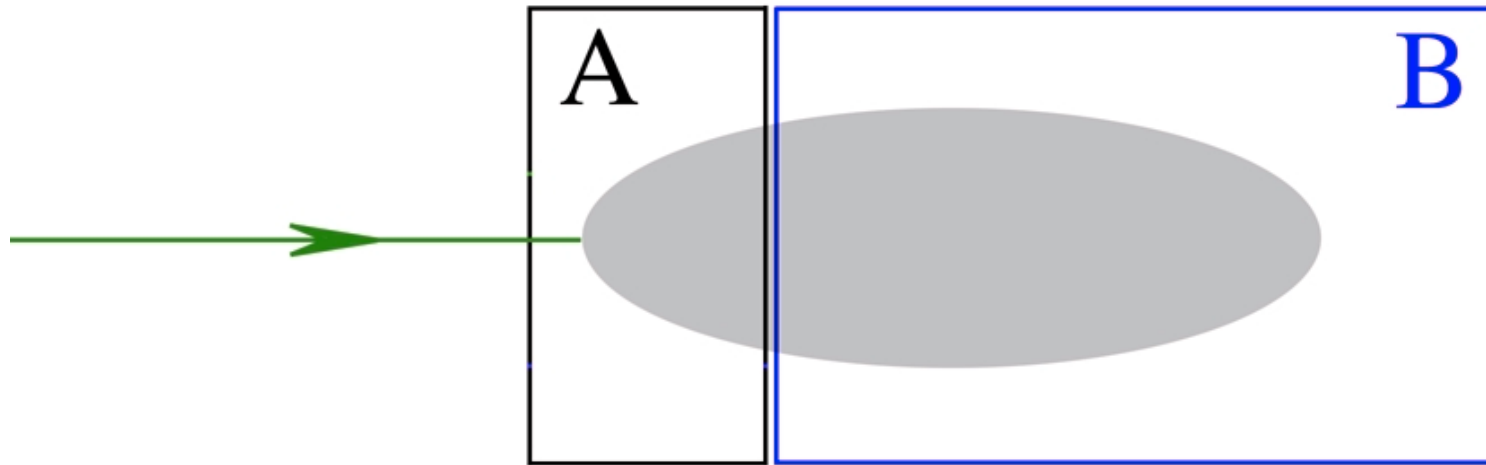


FIG. 6.3. Fractional mismeasurement of the energy deposited in the individual sections of a longitudinally segmented uranium/plastic-scintillator calorimeter, as a function of the energy of the showering electrons (bottom axis) or the energy sharing between the two calorimeter sections (top axis). The energy in the first,  $6.6X_0$  deep section is systematically overestimated, the energy in the second segment is systematically underestimated, when the scintillator signals are considered a measure for the deposited energy.

# Calibration of longitudinally segmented device



**Minimize** 
$$Q = \sum_{j=1}^N \left[ E - A \sum_{i=1}^n S_{ij}^A - B \sum_{i=1}^n S_{ij}^B \right]^2$$

**→ Determine A,B**

## Calibration by Minimizing Total Width

- Calibration methods based on minimizing total width are affected:
  - **Calibration** constants are **energy dependent**
  - Response **non-linearity** is introduced
  - Systematic **mismeasurement** of energy  
(*e.g.*,  $\pi^0$ ,  $e$  and  $\gamma$  of same energy give different measurement results)

# Calibrating longitudinally segmented calorimeters

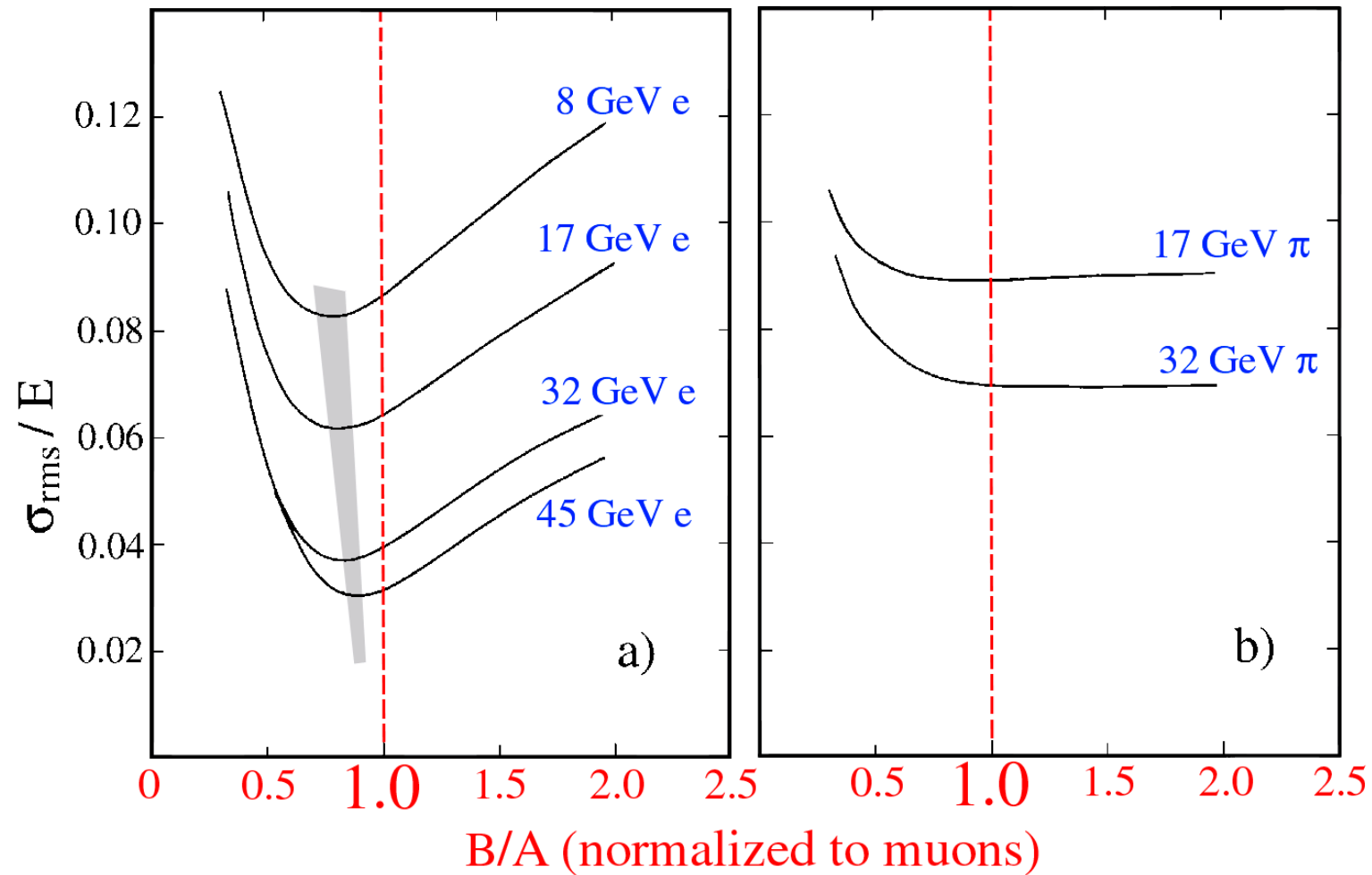


FIG. 6.2. The fractional width  $\sigma/E$  of the signal distributions for electrons (a) and pions (b) of different energies, as a function of the value of the intercalibration constant  $B/A$  of the HELIOS calorimeter system. The dashed line corresponds to the intercalibration constant derived from muon measurements [Ake 87].

# Results of miscalibration: Non-linearity

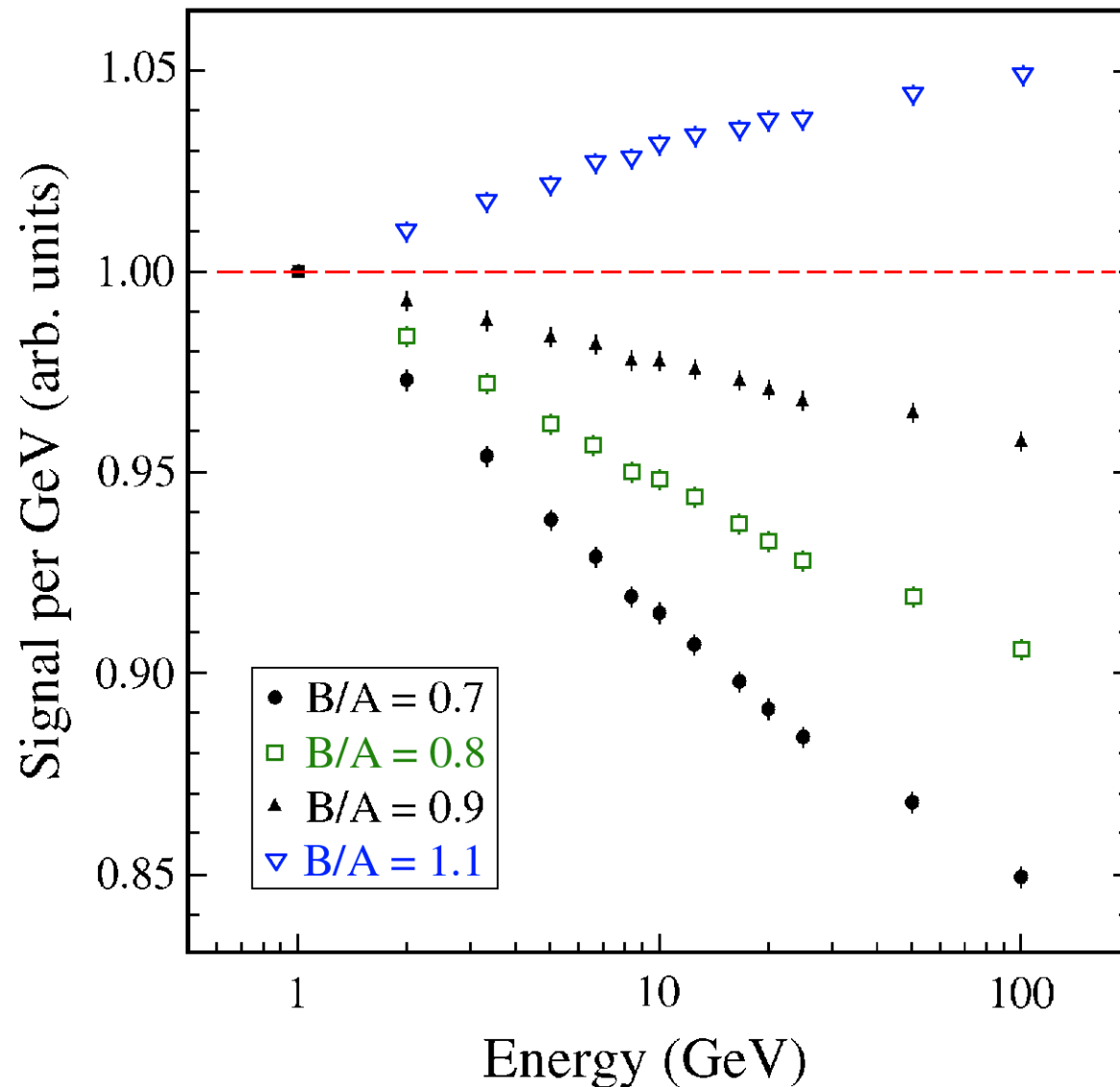


Figure 12: Signal nonlinearity for electrons resulting from miscalibration of a longitudinally segmented calorimeter. The total calorimeter response (average signal per unit of energy) is given for 3 different values of the ratio of the calibration constants for the 2 longitudinal segments,  $B/A$ . See text for details.

# Results of miscalibration: Mass dependence

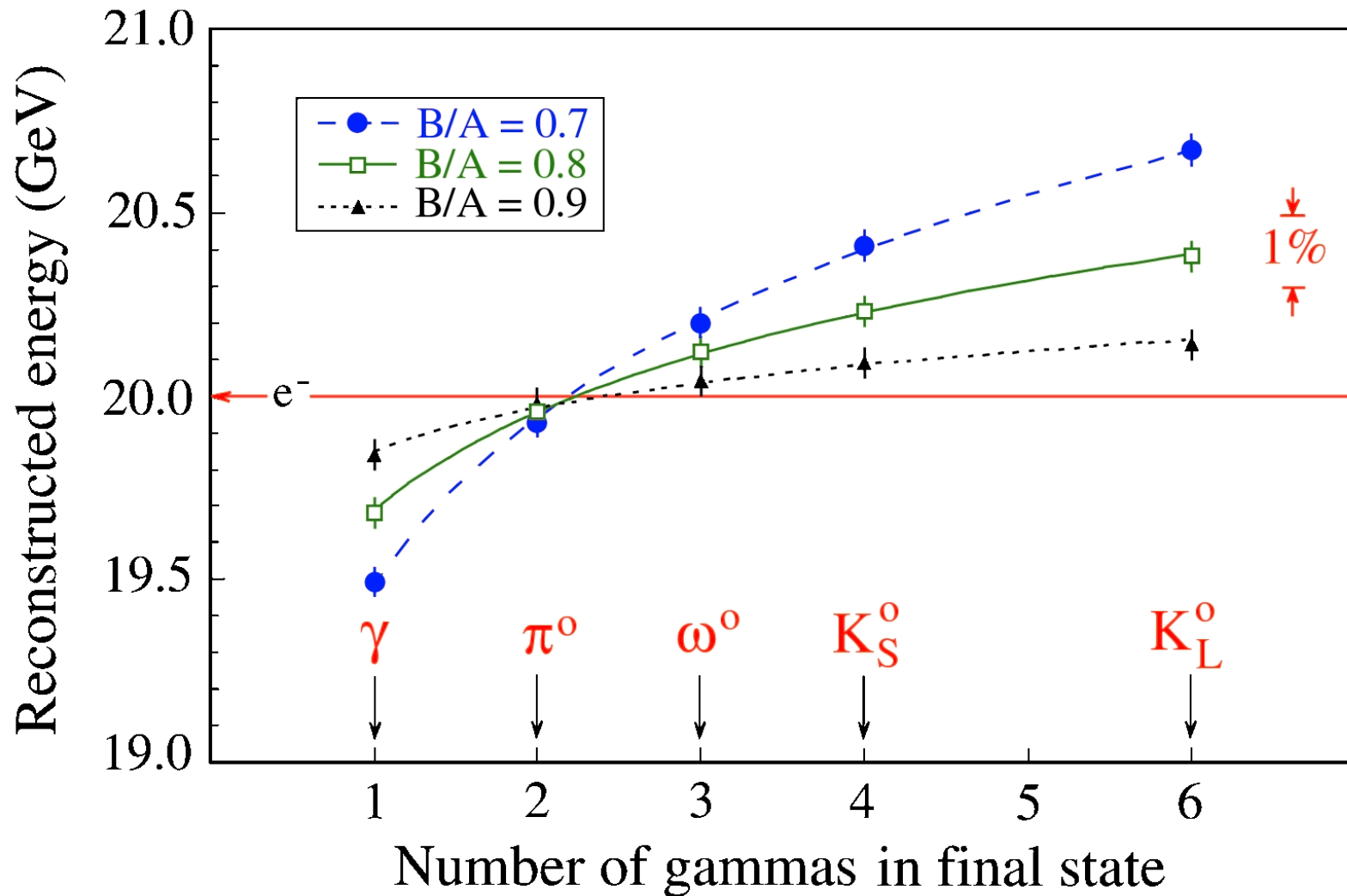


Figure 13: The average reconstructed energy for 20 GeV  $\gamma$ s and for 20 GeV particles decaying into multiple  $\gamma$ s in a longitudinally segmented Pb/scintillator calorimeter that was calibrated with 20 GeV electrons, for different values of the ratio of the calibration constants for the 2 longitudinal segments,  $B/A$ . See text for details.

# Results of miscalibration: Mass dependence

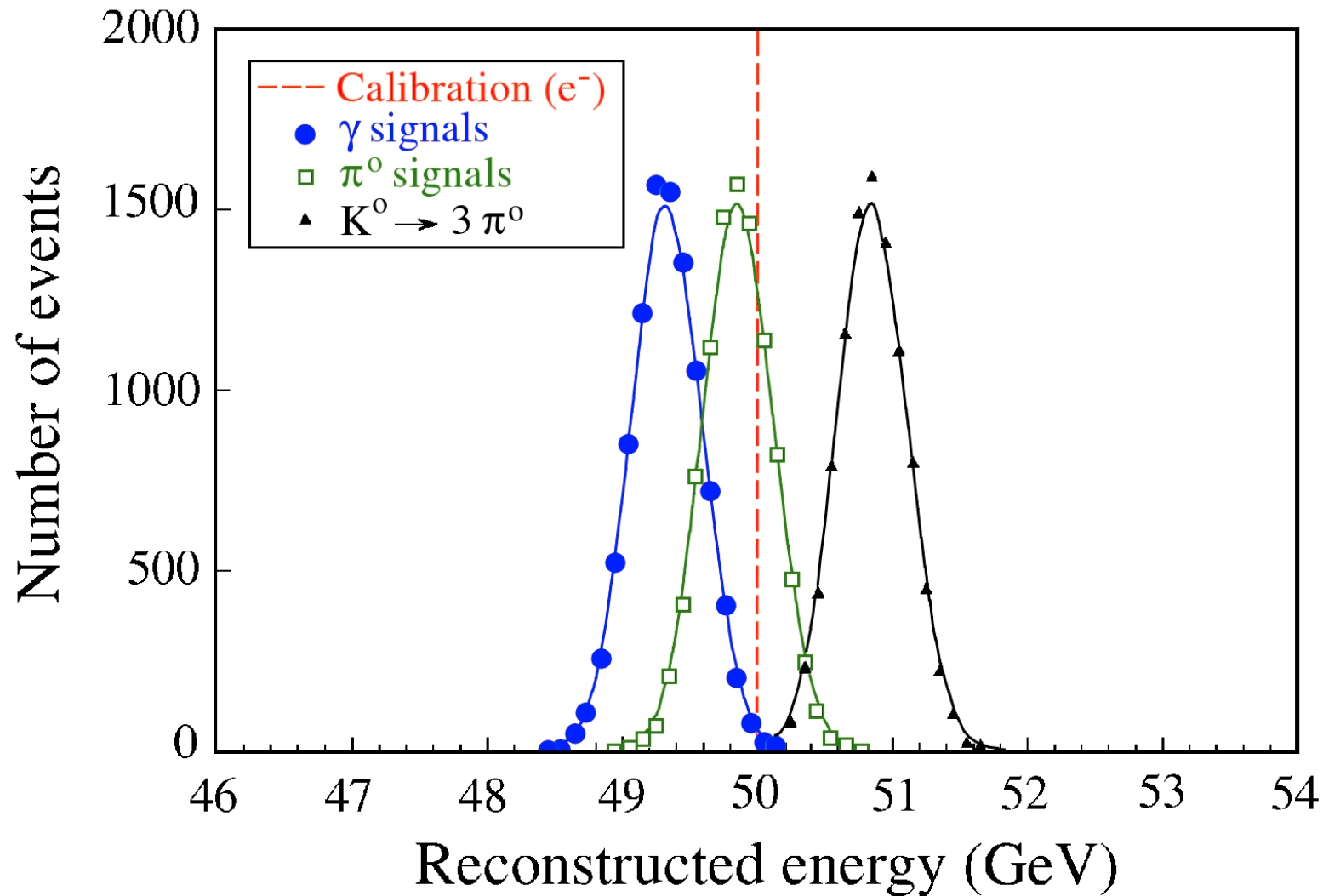


Figure 14: Signal distributions for  $\gamma$ s and various hadrons decaying into all- $\gamma$  final states. All particles have the same nominal energy and the detector, which has an intrinsic resolution of 0.5% for em showers of this energy, was calibrated with electrons using  $B/A = 0.8$ . See text for details.



## Calibration (hadrons)

- Effects are even *worse for hadrons*
  - Reconstructed energy depends on starting point of shower
  - If calorimeter is calibrated with pions, jet energies are systematically mismeasured
- Resolution is not only determined by the width of a signal distribution, it is also necessary that the distribution is centered around the correct value

# Calibration of hadron calorimeters

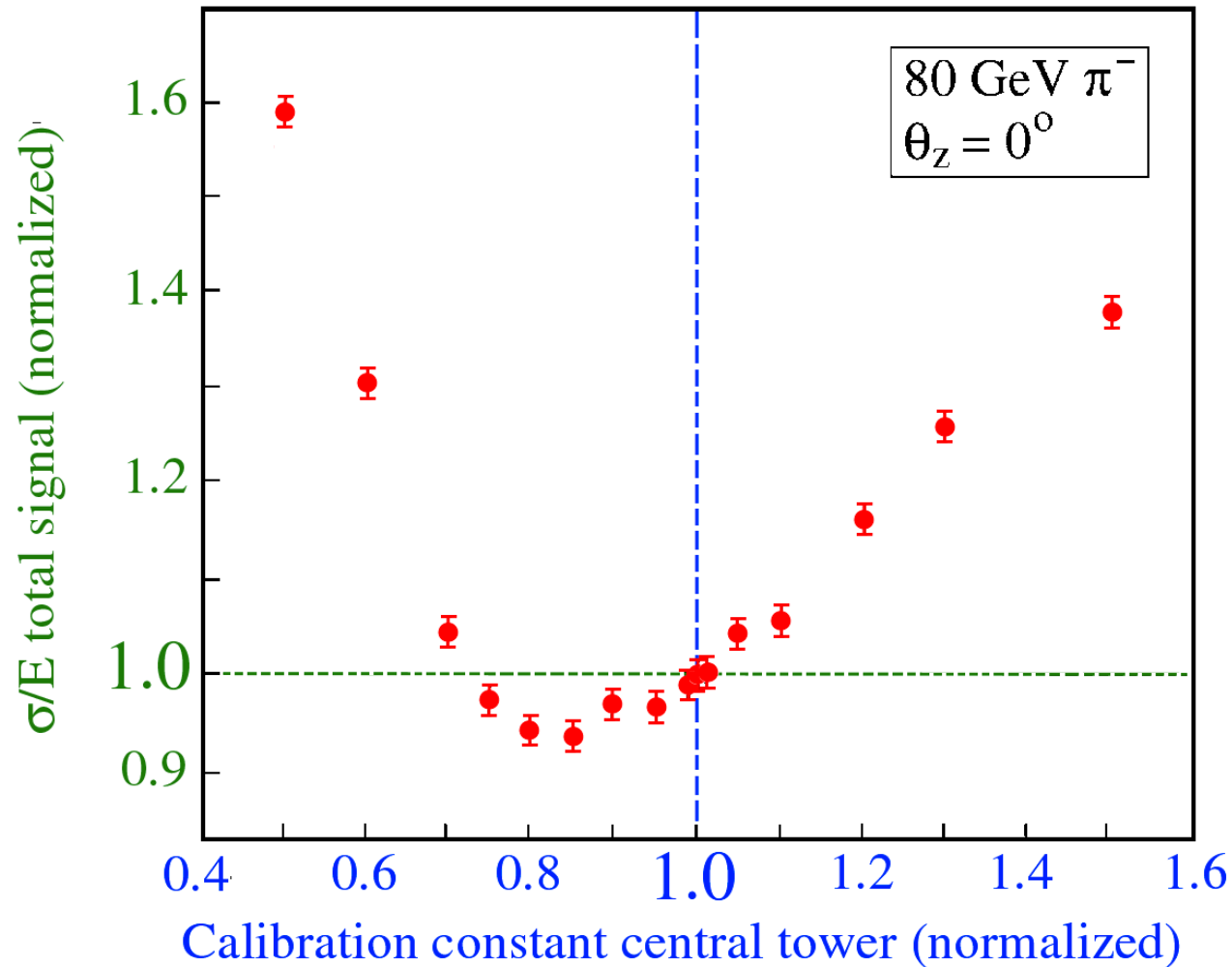
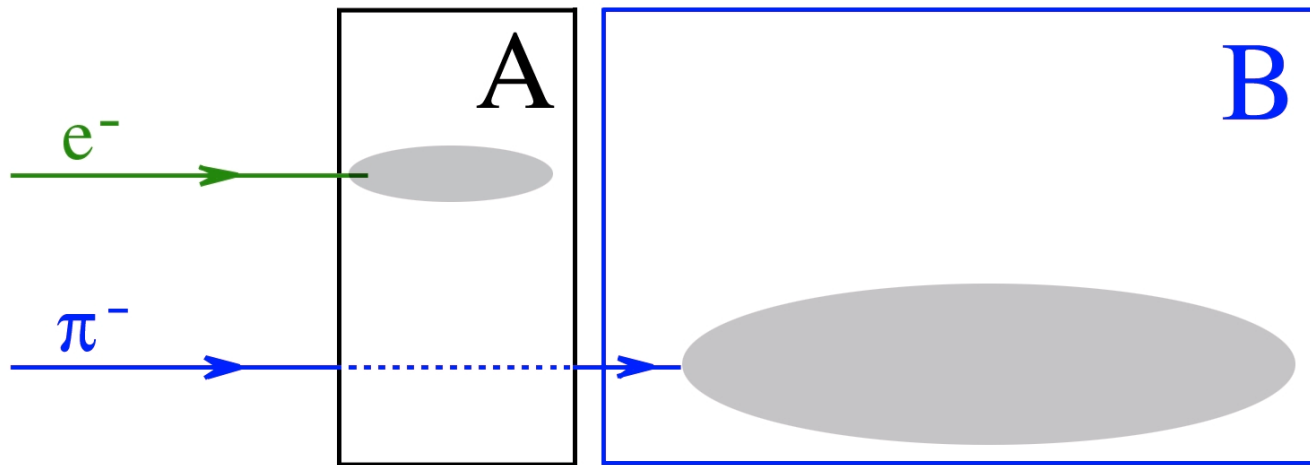


Figure 11: The fractional width,  $\sigma/E$ , of the signal distribution for 80 GeV  $\pi^-$  in the SPACAL detector as a function of the weighting factor applied to signals from the central calorimeter tower into which the pion beam was steered. The calorimeter towers were calibrated with high-energy electrons [7].

## Alternative method: Each section its own particles



- **Problem:** How about hadrons that start shower in section A?
  - **Energy** systematically **mismeasured** depending on  $e/h$  values of sections A,B
  - Reconstructed **energy depends on starting point** of shower

# Wrong B/A: Response depends on starting point

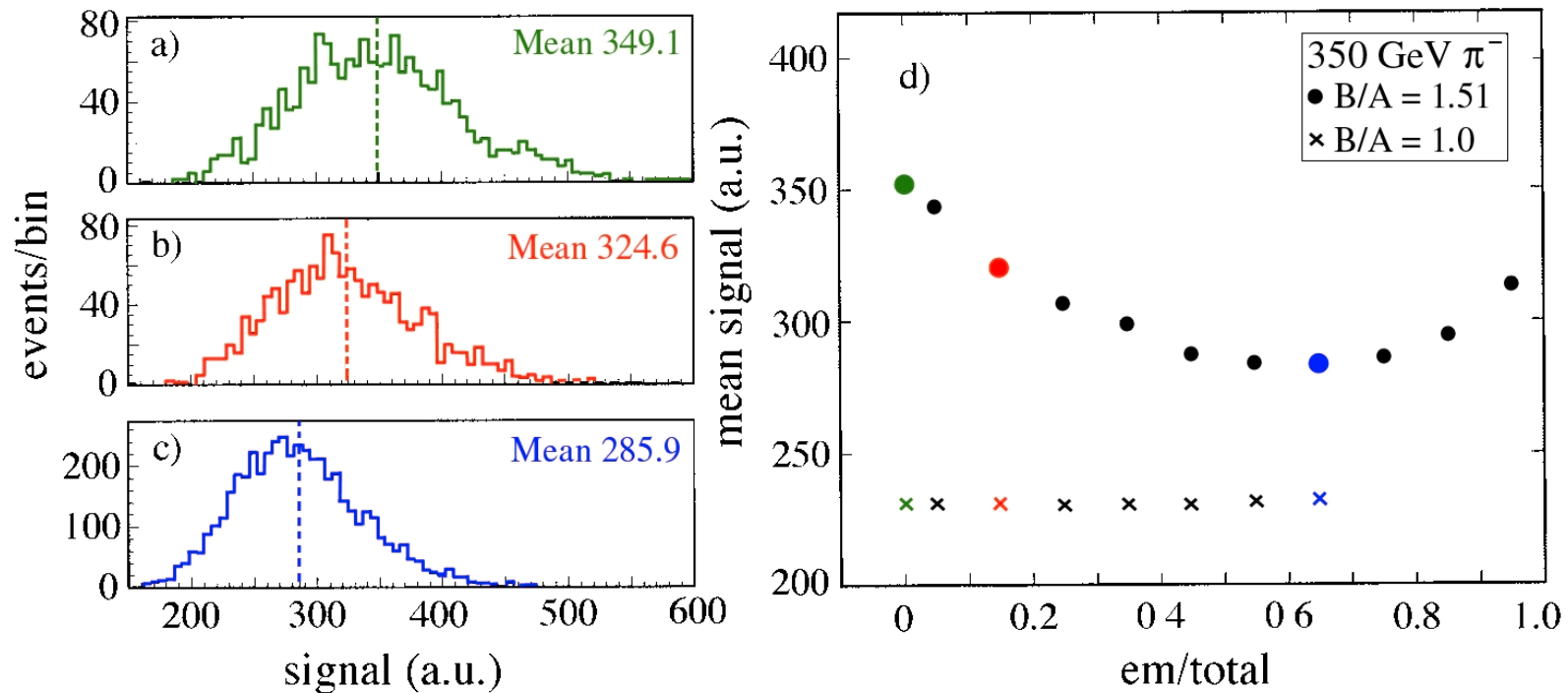


FIG. 6.10. Signal distributions for 350 GeV pion showers in a longitudinally segmented quartz-fiber calorimeter, for events in which different fractions of the (unweighted) shower energy were recorded in the em calorimeter section. Shown are distributions for which this fraction was compatible to zero (a), 10–20% (b), or 60–80% (c). The average calorimeter signal for 350 GeV pions, as a function of this fraction, is shown in diagram (d). The calorimeter was calibrated on the basis of  $B/A = 1.51$  in all these cases, as required for reconstructing the energy of 350 GeV pions that penetrated the em compartment without undergoing a strong interaction. Diagram (d) also contains results (the crosses) obtained for a calorimeter calibration on the basis of  $B/A = 1$ . From [Gan 98].

# Effects of miscalibration: Mass reconstruction

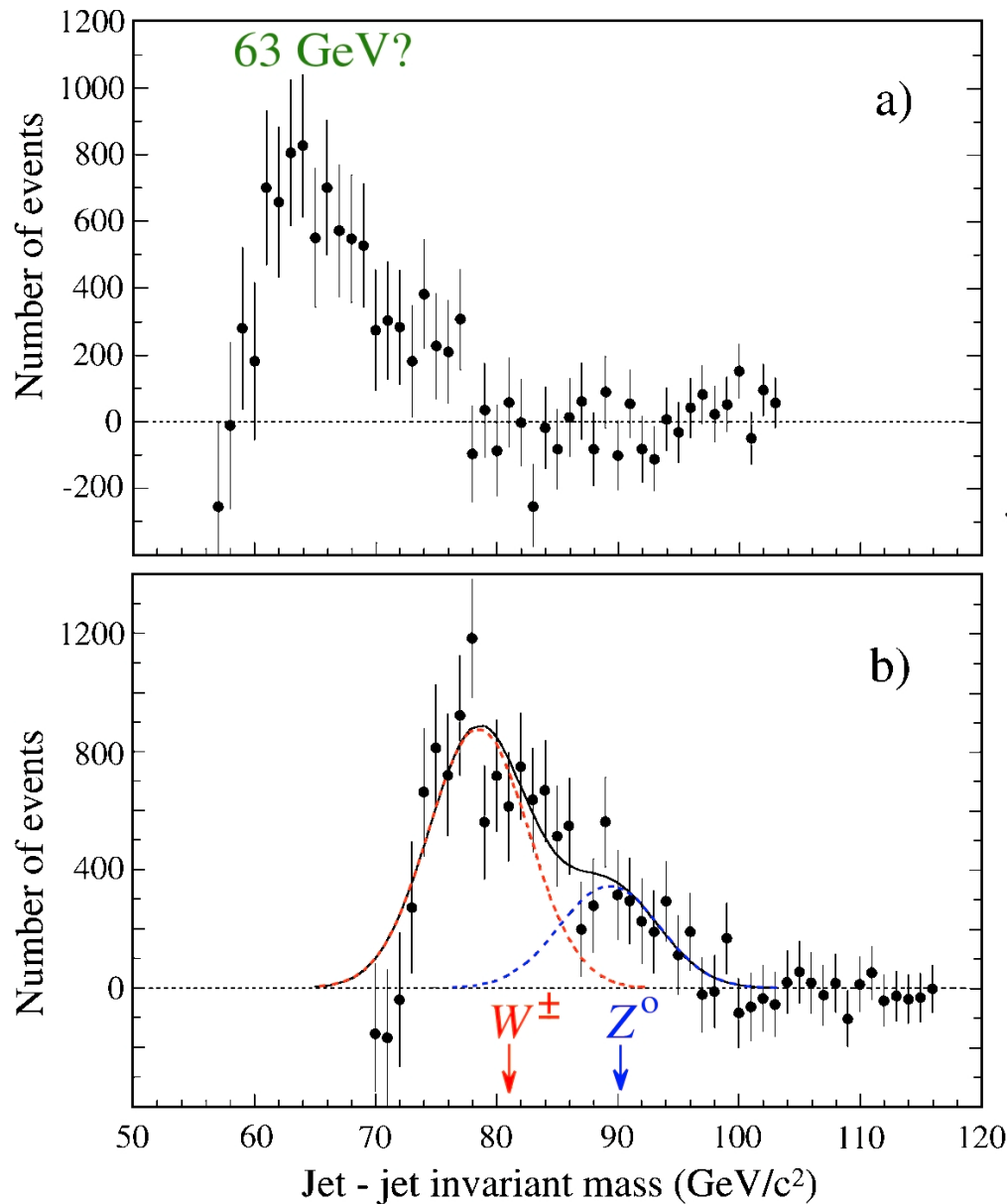


Figure 2.27: The jet-jet invariant mass distribution for CDF Run Ic. The background has been subtracted. Results are shown for the standard CDF calibration constants (a) and for our alternative calibration scheme (b).

# Conclusions (calibration)

- Calibration is a **very delicate** issue
- Discussed strategies (and several others used in practice) only work for a **subset of events**  
(electrons of certain energy, pions penetrating em section, ...)
- **Negative consequences** for the rest of the events
  - Systematic mismeasurement of energy
  - Reconstructed energy depends on starting point shower
  - Signal non-linearity, .....
- Correct method:  **$B/A = 1$**   
i.e. calibrate all calorimeter sections in the same way
- For purposes of energy measurement, a **non-segmented** calorimeter is preferable

# Monte Carlo simulations and calorimetry

- *Electromagnetic calorimetry*

EGS4 highly reliable → learned a lot of important things

- Origin of  $e/mip \neq 1$ ,  $Z$ -dependence of effect
- Detailed understanding of sampling fluctuations
- Cause of depth dependence of sampling fraction
- Angular response dependence of fiber calorimeters
- *etc.*

# Sampling calorimeters: The $e/mip$ signal ratio

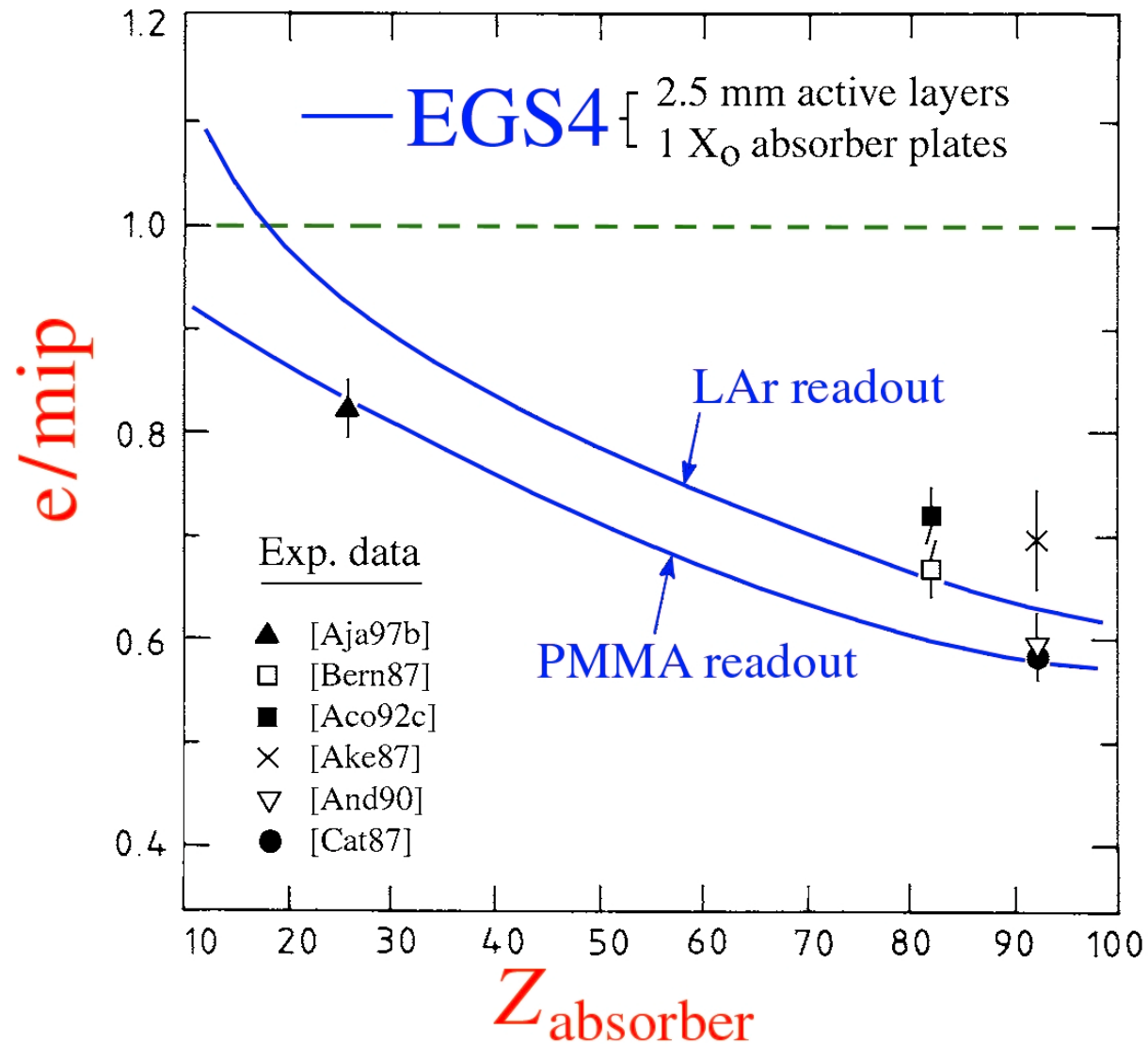


FIG. 3.7. The  $e/mip$  ratio for sampling calorimeters as a function of the  $Z$  value of the absorber material, for calorimeters with plastic scintillator or liquid argon as active material. Experimental data are compared with results of EGS4 Monte Carlo simulations [Wig 87].



# Sampling fluctuations in em calorimeters

## Determined by sampling fraction and sampling frequency

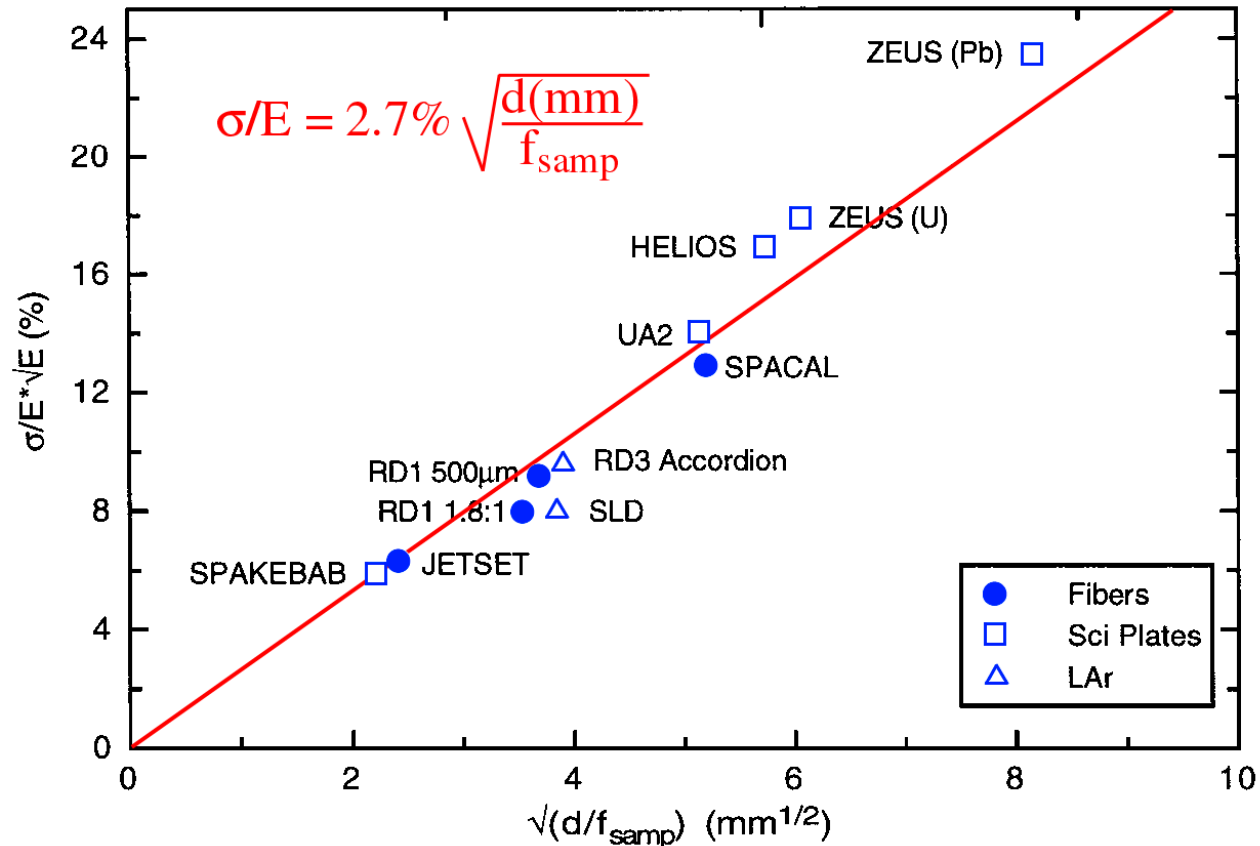


FIG. 4.8. The em energy resolution of sampling calorimeters as a function of the parameter  $(d/f_{\text{samp}})^{1/2}$ , in which  $d$  is the thickness of an active sampling layer (*e.g.* the diameter of a fiber or the thickness of a scintillator plate or a liquid-argon gap), and  $f_{\text{samp}}$  is the sampling fraction for mips [Liv 95].

# The $e/mip$ ratio: Dependence on calorimeter parameters

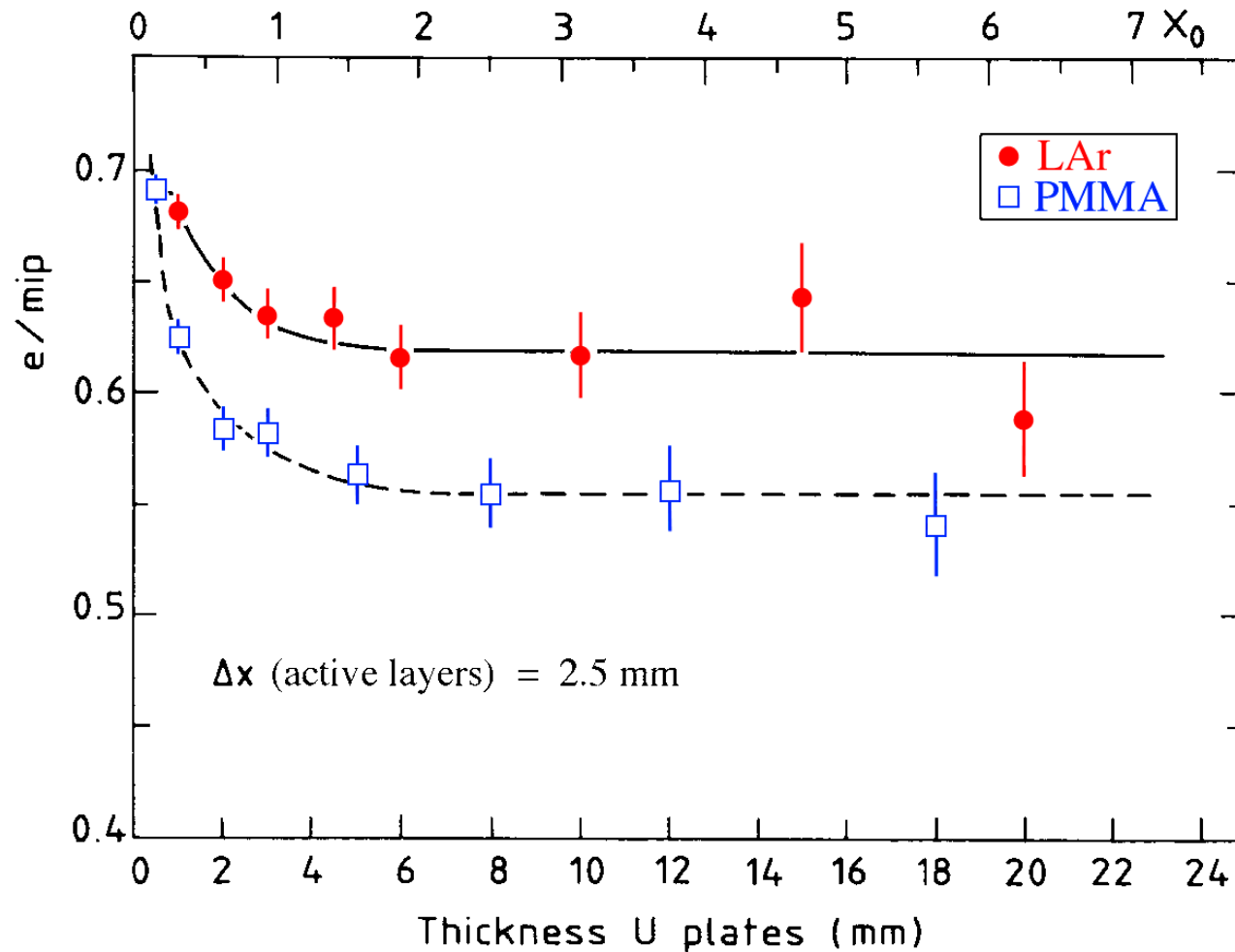
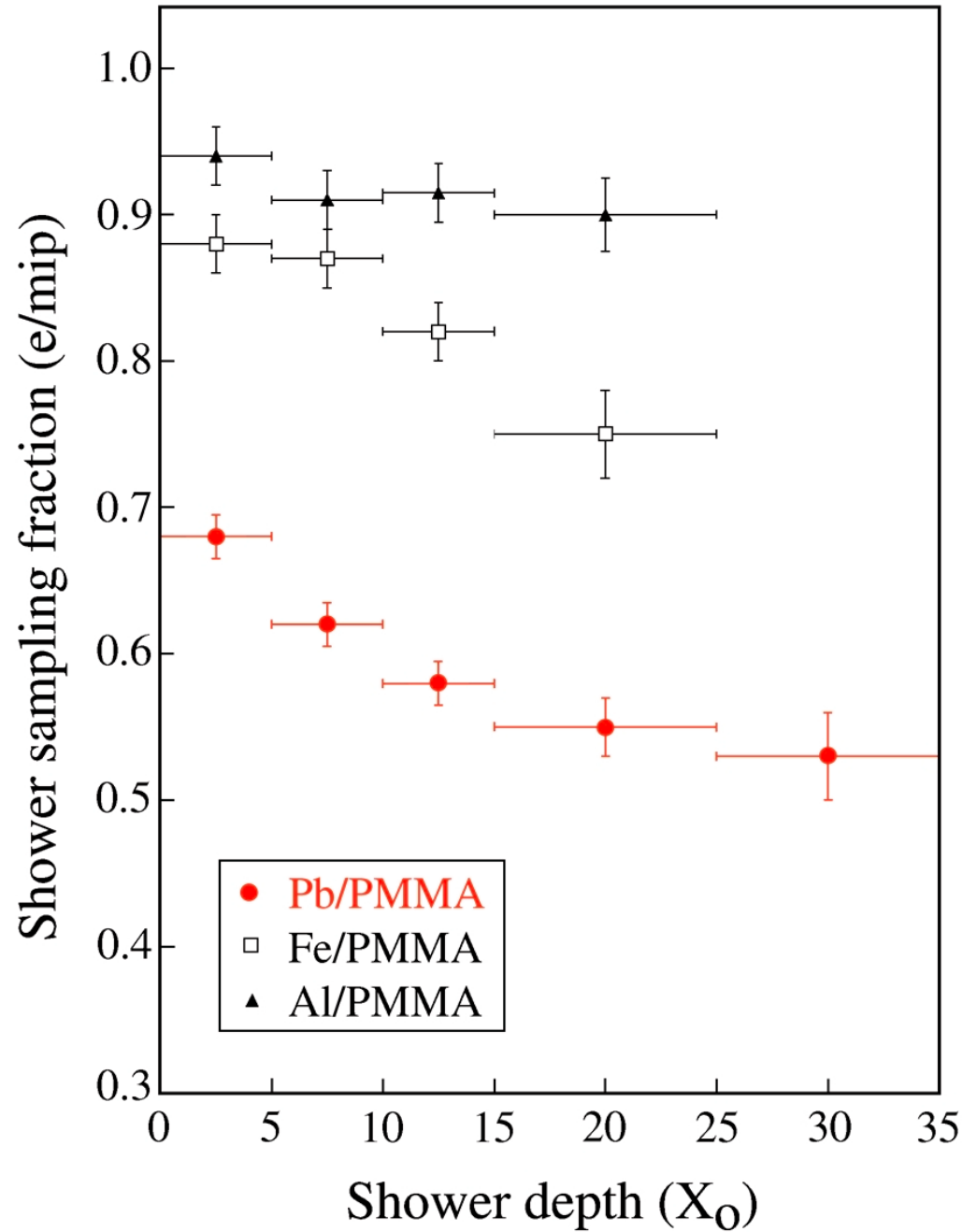


FIG. 3.9. The  $e/mip$  ratio as a function of the thickness of the absorber layers, for uranium/PMMA and uranium/LAr calorimeters. The thickness of the active layers is 2.5 mm in all cases. Results from EGS4 Monte Carlo simulations [Wig 87].

The sampling fraction changes with depth!



# Instrumental effects: Channeling in fiber calorimeters

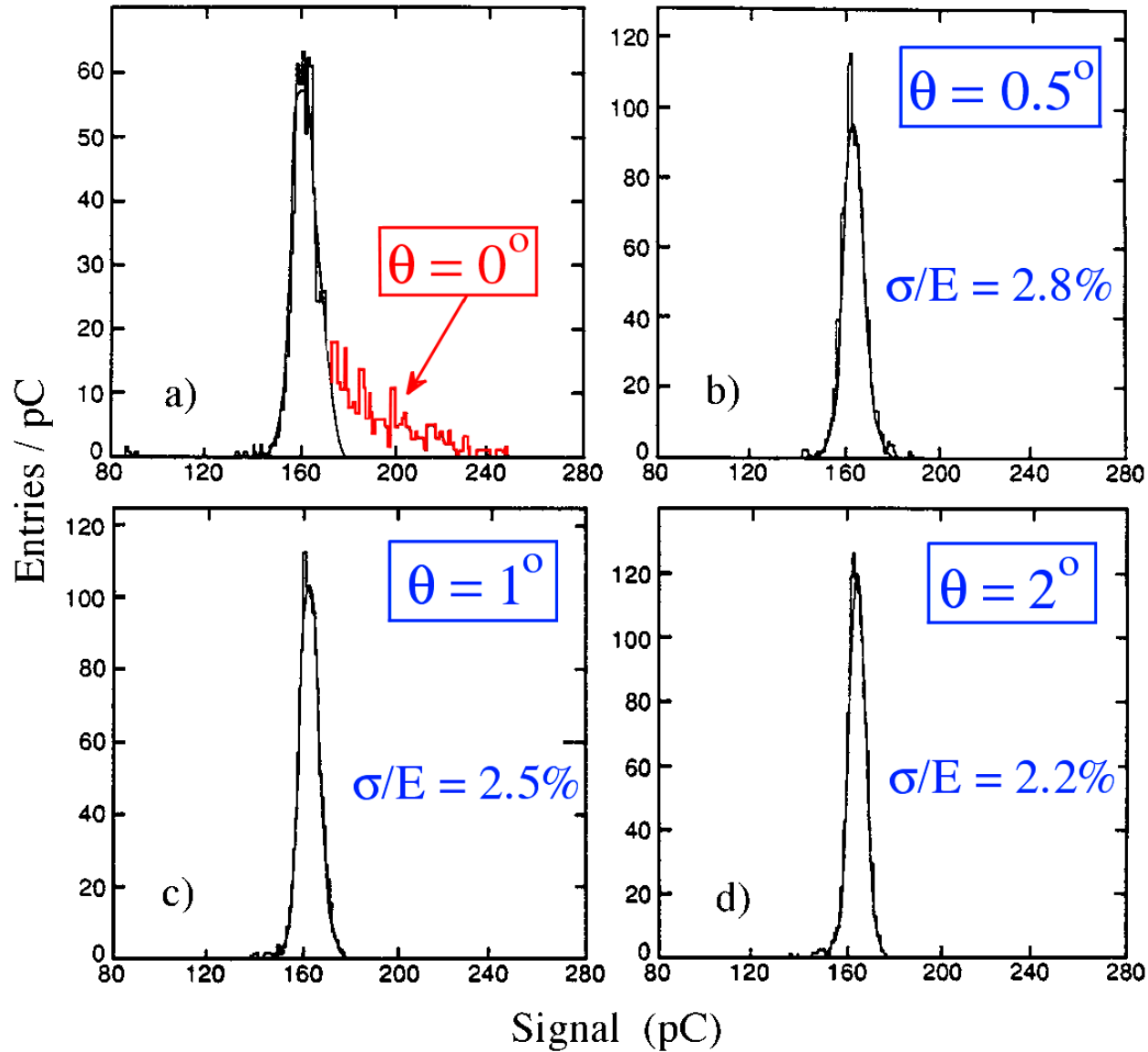


FIG. 4.22. Signal distributions for 40 GeV electron showers measured with the RD1 0.5 mm fiber calorimeter, for different angles between the particle s direction and the fiber [Bad 94a].

# Monte Carlo simulations and hadron calorimetry

- *Hadron calorimetry*

GEANT/GEISHA/FLUKA .... *have not contributed anything* to our fundamental understanding of hadron calorimetry

Progress in understanding has been made *despite* these programs

Simulations are *flawed at fundamental levels*, e.g.  $\pi^0$  production and neutron contributions to the signals, which are crucial for understanding hadron calorimetry

**Benchmark** data for tests of MC simulations:

- E. Bernardi *et al.*, NIM **A262** (1987) 229
- G. d'Agostini *et al.*, NIM **A274** (1989) 134
- N. Akchurin *et al.*, NIM **A408** (1998) 380.

# Benchmark data for hadronic Monte Carlo

## Test of $\pi^0$ production modelling

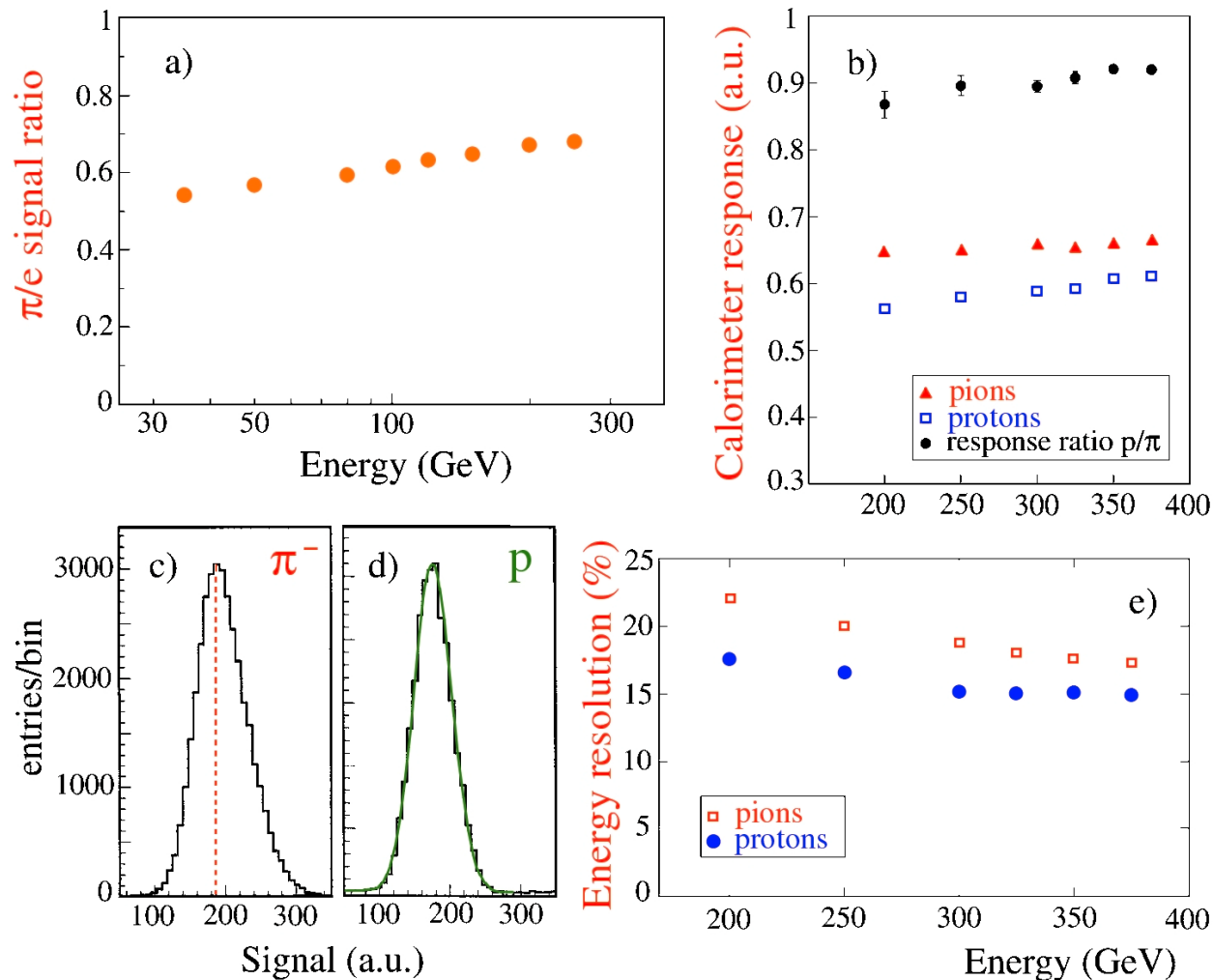


FIG. 8.27. Calorimeter benchmark data for testing the correct implementation of  $\pi^0$  production in Monte Carlo simulations of hadronic shower development. Experimental data from a copper/quartz-fiber calorimeter, showing the  $\pi/e$  signal ratio as a function of energy (a), the response to protons and pions, as well as the ratio of these responses, as a function of energy (b), the response functions to 300 GeV pions (c) and protons (d), and the energy resolutions for pions and protons as a function of energy (e) [Akc 97].

# Benchmark data for hadronic Monte Carlo

## Test of description neutron effects

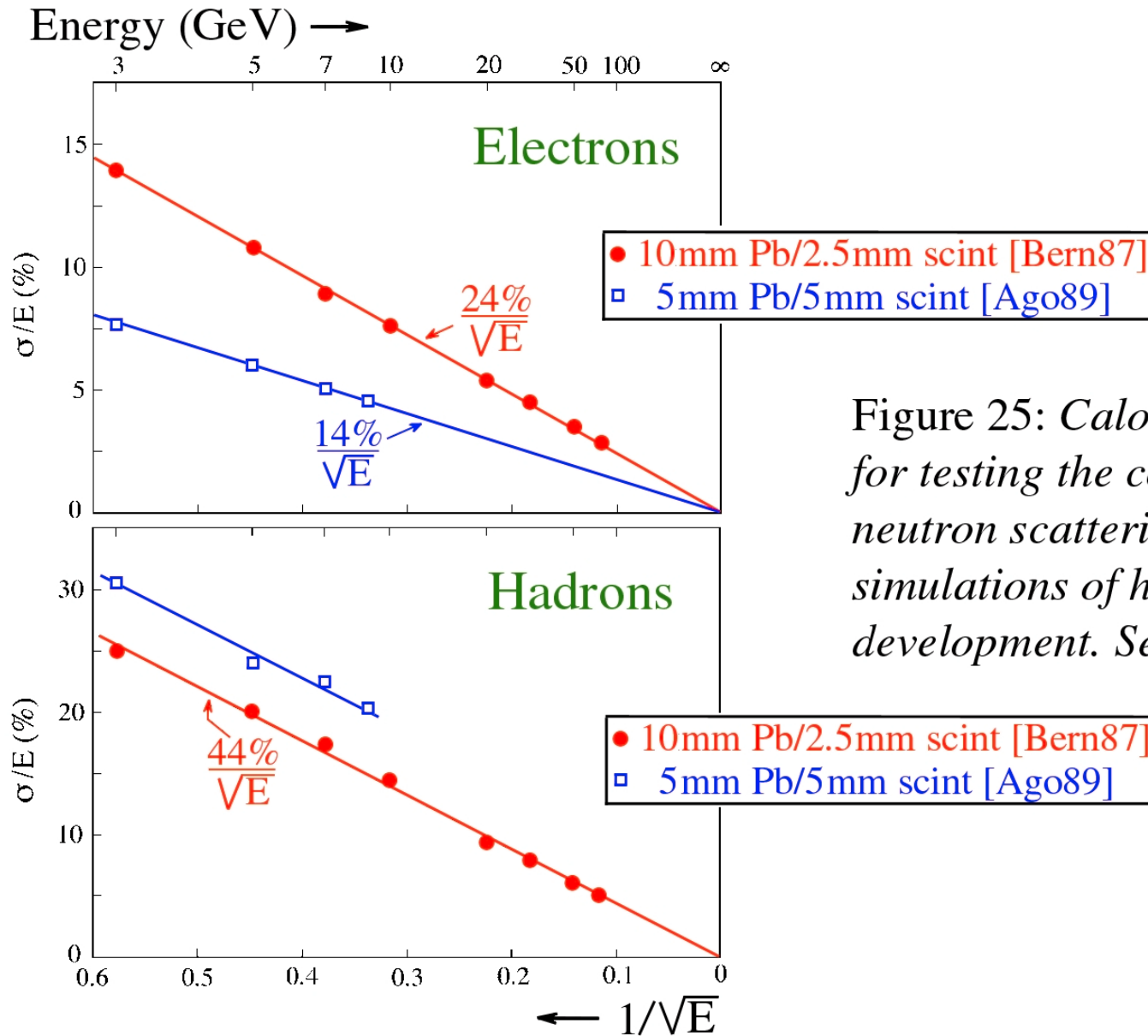


Figure 25: Calorimeter benchmark data for testing the correct implementation of neutron scattering data in Monte Carlo simulations of hadronic shower development. See text for details.